Titre: Title:	Biomechanical Response of the Epiphyseal Vertebral Growth Plate under Static and Cyclic Compression: A Finite Element Study
Auteur: Author:	Mojdeh Tireh Dast
Date:	2014
Type:	Mémoire ou thèse / Dissertation or Thesis
Référence: Citation:	Tireh Dast, M. (2014). Biomechanical Response of the Epiphyseal Vertebral Growth Plate under Static and Cyclic Compression: A Finite Element Study [Mémoire de maîtrise, École Polytechnique de Montréal]. PolyPublie. https://publications.polymtl.ca/1600/

URL de PolyPublie: PolyPublie URL:	https://publications.polymtl.ca/1600/
Directeurs de recherche: Advisors:	Isabelle Villemure, Carl-Éric Aubin, & Stefan Parent
Programme: Program:	Génie biomédical

UNIVERSITÉ DE MONTRÉAL

BIOMECHANICAL RESPONSE OF THE EPIPHYSEAL VERTEBRAL GROWTH PLATE UNDER STATIC AND CYCLIC COMPRESSION: A FINITE ELEMENT STUDY

MOJDEH TIREH DAST

INSTITUT DE GÉNIE BIOMÉDICAL
ÉCOLE POLYTECHNIQUE DE MONTRÉAL

MÉMOIRE PRÉSENTÉ EN VUE DE L'OBTENTION
DU DIPLÔME DE MAÎTRISE ÈS SCIENCES APPLIQUÉES
(GÉNIE BIOMÉDICAL)

DÉCEMBRE 2014

UNIVERSITÉ DE MONTRÉAL

ÉCOLE POLYTECHNIQUE DE MONTRÉAL

Ce mémoire intitulé:

BIOMECHANICAL RESPONSE OF THE EPIPHYSEAL VERTEBRAL GROWTH PLATE UNDER STATIC AND CYCLIC COMPRESSION: A FINITE ELEMENT STUDY

présenté par: TIREH DAST Mojdeh

en vue de l'obtention du diplôme de : Maîtrise ès sciences appliquées

a été dûment accepté par le jury d'examen constitué de :

M. SAVARD Pierre, Ph. D., président

Mme VILLEMURE Isabelle, Ph. D., membre et directrice de recherche

M. AUBIN Carl-Éric, Ph. D., membre et codirecteur de recherche

M. PARENT Stefan, M.D., Ph. D., membre et codirecteur de recherche

Mme NUÑO Natalia, Ph. D., membre

DEDICATION

To my mother, father and sister,

For their unconditional love.

ACKNOWLEDGEMENT

Foremost, I would like to sincerely thank my supervisors, Professors Isabelle Villemure and Carl-Éric Aubin for giving me the opportunity to work on this project. I wish to express my gratitude for their time and support during my research. Their assistance and guidance were essential to the organization, analysis and presentation of my work. I also thank Dr. Stefan Parent my co-director of research for his contribution to the clinical aspect of the project.

I would like to thank all my colleagues at École Polytechnique de Montreal and CHU Sainte Justine, especially Franck Le Naveaux for his great help and support during my research, Bahe Hachem for helping me in finite element modeling of spine, Amélie Chagnon the former Master student at École Polytechnique for transferring her model and knowledge to me for starting my work. I also express my gratitude to Anne-Laure Ménard for the French translation of the abstract.

I would like to thank my friends in Montreal who were with me in sad and happy moments and made my life joyful and pleasant. I do not acknowledge them individually because I am afraid that I may miss some of them, however, I cannot help mentioning Maryam Aramesh, who I shared my days with, for her decent support and encouragements during hard times.

I would like to thank Natural Science and Engineering Research Council of Canada, MÉDITIS and Medtronic for financially supporting this project.

Last but most importantly, I would like to express my gratitude to my family: to my sister for her genuine love and support in every single moment of my life; to my parents, who unconditionally devoted their all life to my sister and me. I wish I could find a word to thank them enough.

RÉSUMÉ

La scoliose idiopathique de l’adolescent (SIA), qui implique une déformation tridimensionnelle de la colonne vertébrale, affecte 1 à 3% des adolescents, principalement des filles. Les influences mécaniques sur la croissance du rachis jouent un rôle important dans la progression de la courbure chez les patients SIA, notamment pendant les périodes de croissance rapide comme l’adolescence. Les traitements sans fusion du rachis, via la modulation mécanique locale de la croissance osseuse, ont montré des avancées prometteuses pour le traitement précoce des déformations modérées de la colonne vertébrale. Des études *in vivo* récentes sur les plaques de croissance de rats, utilisant des chargements statiques et dynamiques équivalents au niveau de la contrainte moyenne appliquée, ont montré que les chargements dynamiques étaient aussi efficaces que les chargements statiques en termes de modulation de croissance, mais moins dommageables pour l’intégrité de la plaque de croissance en comparaison aux chargements statiques [1, 2]. Cependant, il a été montré que la combinaison de hautes fréquences et d’amplitudes d’oscillations conduit à des inflammations tissulaires.

Comme approche complémentaire à l’approche expérimentale pour investiguer la biomécanique du rachis, la modélisation numérique fournit une plateforme pour approfondir nos connaissances sur les structures du rachis et leurs comportements mécaniques [3]. En utilisant les simulations numériques, un paramètre peut aisément être modifié afin d’investiguer son effet spécifique en maintenant les autres paramètres constants. La modélisation par éléments finis constitue l’une des méthodes numériques couramment utilisées ; elle se base sur une méthode numérique rapide pour des analyses de contraintes et de déformations de problèmes complexes, en évitant les limites et difficultés associées aux études expérimentales. Bien que les modèles poroélastiques aient été développés pour investiguer la réponse dépendante du temps des tissus rachidiens, le comportement biomécanique comparatif de tissus cartilagineux, tels que les plaques de croissance sous chargements statiques vs. dynamiques, n’a pas encore été clairement déterminé [3, 4] et pourrait apporter des connaissances sur la compréhension de l’interaction entre les chargements mécaniques et le métabolisme tissulaire.

L’objectif principal de ce projet était d’étudier la réponse biomécanique de la plaque de croissance soumise à des compressions statique et dynamique, en utilisant des modèles par éléments finis. Afin d’atteindre cet objectif, un modèle axisymétrique poroélastique de la plaque

de croissance a d'abord été développé pour investiguer les composantes des contraintes et les déformations au sein du modèle pour différentes perméabilités transverses et pressions interstitielles périphériques (première partie). Ensuite, un modèle par éléments finis d'une unité fonctionnelle du rachis a été utilisé pour investiguer les mêmes paramètres à l'aide d'un modèle plus réaliste (seconde partie). Cette thèse visait à vérifier l'hypothèse suivante : *Les chargements en compressions statique et dynamique montrent une contrainte totale identique mais différentes pressions interstitielles (contraintes dans la phase fluide) et contrainte effective (contrainte dans la matrice solide), à l'intérieur des plaques de croissance*.

La première partie de cette thèse a inclus trois études ainsi que le développement d'un modèle axisymétrique de la plaque de croissance. La plaque de croissance a été modélisée comme une matrice solide isotrope transverse poreuse remplie de fluide. Des chargements en compression ont été appliqués selon cinq cas différents : statique 0.2 MPa, 0.2±30% MPa à 0.1 Hz (i), 0.2±70% MPa à 0.1 Hz (ii), 0.2±30% MPa à 1 Hz (iii), 0.2±70% MPa à 1 Hz (iv). En outre, des simulations ont été réalisées avec trois perméabilités transverses K, 10% K et 1% K (avec K=5×10^{-15} m^4/Ns), et deux pressions interstitielles périphériques 0.1 et 0 MPa. Dans la première étude, les effets de la fréquence et de l'amplitude de chargement sur les composantes des contraintes et la déformation dans le modèle ont été investigués. Les résultats n'ont montré aucune différence significative entre les compressions statique et dynamique avec différentes fréquences et amplitudes de chargement. Il a également été montré que la distribution de contraintes entre la matrice solide et la phase fluide variait dans le temps de façon à maintenir la contrainte compressive globale appliquée. Dans la seconde étude, l'influence de la perméabilité transverse sur les composantes de contrainte et la déformation a été étudiée. Les résultats ont indiqué que la déformation et la distribution de chargement entre les deux phases (matrice solide et phase fluide) étaient influencées par la perméabilité transverse. Des valeurs plus élevées de perméabilités transverses ont conduit à des contraintes effectives et des niveaux de déformation plus élevés, alors que les niveaux de pression interstitielle diminuaient et que la contrainte totale restait relativement inchangée. Dans la troisième étude, l'effet de la pression interstitielle périphérique a été investigué. Les résultats ont montré que l'effet d'une pression interstitielle périphérique non nulle est semblable à une réduction de la perméabilité transverse, toutes deux agissant comme une barrière contre le drainage de fluide.

Dans la seconde partie de cette thèse, un modèle 3D d'une unité fonctionnelle du rachis au niveau de L4-L5, incorporant le couplage entre la diffusion de fluide dans les pores et l'analyse de contraintes dans le disque et les plaques de croissance, a été utilisé pour les analyses de contraintes et de déformation dans les tissus cartilagineux. Le noyau, l'anneau, les plaques de croissance et l'os spongieux ont été modélisés comme des matériaux poroélastiques (les plaques de croissance comme isotropes transverses et les autres isotropes), alors que l'os cortical a été modélisé comme un matériau élastique linéaire. Les chargements en compression ont été appliqués selon cinq configurations identiques à celles du modèle axisymétrique. La pression interstitielle périphérique autour de l'anneau et des plaques de croissances a été fixée à 0.1 MPa. En utilisant ce modèle, les effets de la fréquence et de l'amplitude de chargement sur les composantes de contraintes, pertes de fluide et contraintes principales maximales et minimales ont été investigués au sein des plaques de croissance et du disque. Les simulations ont révélé des résultats similaires pour le chargement statique et les conditions de chargements dynamiques à basse fréquence. Cependant, les conditions à haute fréquence ont donné des réponses non fiables, qui résulteraient d'un drainage vers le haut qui a lieu dans les conditions à haute fréquence en l'absence de chargement gravitationnel dans cette étude.

Les résultats de simulation ont été comparés aux études expérimentales. Les résultats ont montré que la perméabilité du tissu ainsi que les frontières périphériques ont influencé la distribution de contraintes entre les deux phases du tissu. En outre, cette étude a révélé que les modèles poroélastiques actuels ne permettent pas de distinguer les compressions statique et dynamique. De plus, il a été conclu que la différence entre les compressions statique et dynamique dans les études expérimentales en termes de dommages et d'histomorphométrie de la plaque de croissance pourrait se rapporter aux niveaux d'activités cellulaires qui n'ont pas été intégrés dans notre modèle. L'hypothèse de ce projet a ainsi été réfutée car les chargements en compression statique et dynamique ont montré les mêmes composantes de contraintes.

Ce projet a permis d'investiguer l'influence des compressions statique et dynamique sur les composantes de contraintes, la déformation et la perte de fluide dans les plaques de croissance. Des améliorations pourraient être apportées afin d'obtenir davantage de connaissances sur la réponse biomécanique de la plaque de croissance soumise à des chargements mécaniques. Une géométrie plus réaliste pourrait aider à avoir une meilleure estimation de la distribution des

chargements dans le disque et les plaques de croissance. Par ailleurs, l’intégration des forces gravitationnelles dans les simulations pourrait améliorer les résultats en particulier à hautes fréquences. De plus, un stimulus mécanique correspondant aux réactions chimiques au sein des tissus devrait être intégré dans le modèle afin de possiblement mieux distinguer les compressions statique et dynamique avec les modèles.

ABSTRACT

Adolescent idiopathic scoliosis (AIS), a 3D deformity of the spine, affects 1-3% of adolescents, mainly females. Mechanical influences on spinal growth play an important role in AIS curve progression, mainly during the rapid growth periods such as adolescence. Fusionless corrective techniques of the spine, by means of local mechanical modulation of bone growth, have shown promising advances in the early treatment of moderate spinal deformities. Recent *in vivo* studies on rat growth plates using matched static and cyclic loadings in terms of average stress showed that cyclic loads were as efficient as static loads in terms of growth modulation but less detrimental to the growth plate integrity compared to static loads [1, 2]. However, it was shown that the combination of high frequency and oscillation amplitude resulted in infection in the rats.

As a complementary approach to investigate spinal biomechanics from experiments, computational modeling provides a platform to extend our knowledge about spinal structures and their mechanical behavior [3]. Using computational modeling, one parameter can be changed easily to investigate its effect while the other parameters are kept constant. Finite element modeling is one of the widely used computational methods; it provides a fast numerical method for stress and strain analysis in complex problems, while avoiding limitations and difficulties associated with experimental studies. Although poroelastic models have been developed to investigate the time-dependent response of the spinal tissues, the comparative biomechanical behavior of cartilaginous tissues such as growth plates under static vs. cyclic loads has yet to be fully understood [3, 4] and could provide insights on understanding of the interaction of mechanical loading and tissue metabolism.

The objective of this project was to study the biomechanical response of the growth plate to static and cyclic compressions using finite element models. To achieve this objective, an axisymmetric biphasic model of growth plate was first developed to investigate stress components and deformation within the model for different transversal permeabilities and peripheral pore pressures (part one). Then, a finite element model of a spinal functional unit was used to investigate the same parameters as well as fluid content using a more realistic model (part two). This thesis aimed at verifying the hypothesis that *Cyclic and static compressive loads show the same total stress but different pore pressure (stress in fluid phase) and effective stress (stress in solid matrix) within growth plates*.

Part one of the thesis included three studies together with the development of an axisymmetric model of a growth plate. The growth plate was modeled as transversely isotropic porous solid matrix filled with fluid. Compressive loads were applied in five cases: static 0.2 MPa, 0.2±30% MPa at 0.1 Hz (i), 0.2±70% MPa at 0.1 Hz (ii), 0.2±30% MPa at 1 Hz (iii), 0.2±70% MPa at 1 Hz (iv). Furthermore, simulations were done with three transversal permeabilities K, 10% K and 1% K (with $K=5\times 10^{-15}$ m^4/Ns) and two peripheral pore pressures 0.1 and 0 MPa. In the first study, the effects of loading frequency and amplitude on the stress components and deformation in the model were investigated. Results showed no significant difference between static loading and cyclic compressions at different loading frequency and amplitudes. It was also shown that the distribution of the stress between the solid matrix and fluid phase changed with time in a way to sustain the overall applied compressive stress. In the second study, the influence of the transversal permeability on the stress components and deformation was studied. Results indicated that deformation and load distribution between the two phases (solid matrix and fluid phase) were influenced by the transversal permeability. Higher transversal permeabilities resulted in higher effective stress and deformation levels, while the pore pressure levels decreased and the total stress remained relatively unchanged. In the third study, the effect of peripheral pore pressure was investigated. Results showed that the effect of non-zero peripheral pore pressure is similar to the reduction in transversal permeability because both acts as a barrier against fluid drainage.

In part two of the thesis, a 3-D model of a L4-L5 functional unit of the spine, incorporating the coupled pore fluid diffusion/stress analysis in the disc and growth plates, was used for stress and strain analyses in cartilaginous tissues. The nucleus, annulus, growth plates, and cancellous bone were modeled as poroelastic materials (growth plates as transversely isotropic and others as isotropic) whereas the cortical bone was modeled as a linear elastic material. The compressive loads were applied in five cases like the axisymmetric model. The peripheral pore pressure around the annulus and growth plates was set 0.1 MPa. Using this model, the effects of loading frequency and amplitude on the stress components, fluid loss and maximum and minimum principal strains were investigated in growth plates and disc. Simulations revealed similar results for the static and low frequency loading conditions. However, high frequency conditions resulted in unreliable responses, which were hypothesized to be a result of upward drainage happening in high frequency loading conditions in the absence of gravitational load in this study.

The simulation results were compared to experimental studies. The results showed that the permeability of the tissue as well as the peripheral boundaries influenced the stress distribution between the two phases in the tissue. Furthermore, this study revealed that current biphasic models cannot distinguish between static and cyclic compressions. In addition, it was concluded that the difference between the cyclic and static compressions in experimental studies in terms of damage and growth plate histomorphometry might refer to the cellular level activities which were not integrated in our model. The hypothesis of this project was refuted because the static and cyclic compressive loads showed the same stress components.

This project for the first time investigated the influence of the static and cyclic compressions on the stress components, deformation and fluid loss in growth plates. Some improvements can be done to provide more insights about the biomechanical response of the growth plate to the mechanical loads. More realistic geometry would help to have better estimation of the load distribution in the disc and growth plates. Furthermore, integration of gravitational load in the simulations would improve the results particularly at high frequencies. Moreover, mechanical equivalent stimuli for the chemical reactions in the tissue should be integrated to the model to be able to distinguish between static and cyclic compressions in FEM.

TABLE OF CONTENTS

LIST OF TABLES

LIST OF FIGURES

INTRODUCTION

Scoliosis is a three dimensional deformity of spine affecting 2-3% of the population [5]. Adolescent idiopathic scoliosis is the most common form of scoliosis with a prevalence between 70-80 % of all scoliotic cases [6]. Although its origin is still unknown, mechanical influences on spinal growth are thought to play an important role in the curve(s) progression [7, 8]. It is believed that once the deformity is established, its progression, mainly during growth spurt, is governed by Hueter-Volkmann principle [9, 10]. Under this mechanical growth modulation law, asymmetric loading over the vertebral growth plates leads to the vertebral wedging, which is promoted in a vicious cycle. This same principle is currently being exploited in the development of novel devices for the early treatment of moderate scoliotic curves.

Fusionless corrective techniques for scoliosis, by means of local mechanical modulation of bone growth, have shown certain advances in the early treatment of moderate spinal deformities [11-13], namely stainless steel staples, shape memory alloy staples and tethers. Fusionless implants aim at locally altering the stress distribution over the vertebral growth plate according to Hueter-Volkmann law leading to accelerated growth in the concave side of the curve and/or reduced growth in the convex side, with the purpose of inducing a global realignment of the spine.

There is strong experimental evidence that longitudinal bone growth is altered by static loads [14-16]. In addition, comparative *in vivo* studies have also investigated the effects of static versus cyclic compression on growth plates [17-20]. One recent comparative study between static and cyclic loads indicates that cyclic loads are as effective as static loads in growth modulation, but are less detrimental in terms of growth plate histomorphometry [1]. This result would be very promising in developing less detrimental growth modulating devices using cyclic loading. However, there are challenges in regard to elaborating this idea experimentally in terms of ethical issues and costs where finite element models can be helpful.

Nowadays, advanced computing power allows investigating a variety of treatments, deformities and spinal biomechanics through the use of finite element (FE) models. These models have been shown to be effective in simulating spinal biomechanics [21], growth modulation [22-24], deformities progression [25] and conventional treatments of AIS [26]. FE analyses provide detailed stress and strain distributions in different components of the model (vertebrae, discs, growth plates) which are difficult and sometimes impossible to measure in *in vivo* experiments. There are various FE models which can be used in development and assessment of new corrective methods based on their specific application. Nevertheless to date, none of them has addressed the biomechanical response of growth plates under different static and cyclic compressive loadings which is the target of interest in developing new cyclic growth modulation devices for the early treatment of scoliosis. This study will allow us to compare the developing stress, strain and fluid loss in different conditions and correlate them to the experimental results.

The objective of this project was to investigate stress and strain distributions within growth plates under both static and cyclic compressive loads using a biphasic finite element model. An axisymmetric model of the growth plate and a three dimensional spinal functional unit including L4/L5, intervertebral disc and growth plates were used to address this objective.

This thesis is divided into six chapters. The first chapter presents a literature review of relevant topics to the project. The second chapter explains the rationale of the project, the research question and specific project objectives. The third chapter presents the materials and methods to achieve the project objectives. Chapter four is devoted to the obtained results. Finally, Chapter five is analysis of results and discussion, followed by a conclusion and recommendations chapter for future studies.

CHAPTER 1: LITERATURE REVIEW

1.1 Spinal Anatomy

The normal anatomy of the spine is divided into four sections; the cervical, thoracic, lumbar and sacral segments as well as coccyx. The spine is composed of seven cervical vertebrae (C1-C7), twelve thoracic vertebrae (T1-T12), five lumbar vertebrae (L1-L5) and 5 sacral vertebrae (S1-S5) (Figure 1.1). The size of vertebrae gradually increases from the cervical to the lumbar segment in parallel with increasing spinal loadings. In the frontal plane, the spine is generally straight and symmetrical while there are four normal curvatures in the lateral plane. Curvatures of the cervical and lumbar segments are anteriorly convex (lordosis) while the thoracic and sacral segments are posteriorly convex (kyphosis) (Figure 1.1). The thoracic curve is built on the difference between anterior and posterior heights of vertebrae while curvatures in lumbar and cervical segments are based on the wedge shape of vertebrae and intervertebral discs [27]. These normal anatomic curvatures play a mechanical role in spine and increase its flexibility and shock absorbing capacity while maintain the stability and stiffness.

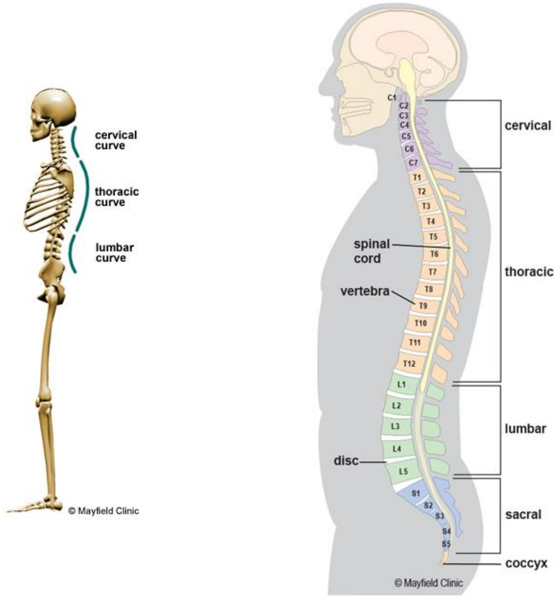

(a) (b)

Figure 1.1: a) Natural curves in the spine b) different regions in the spine (obtained on March 14th 2014 from http://www.mayfieldclinic.com/PE-AnatSpine.htm#.UyNLl_mwLTa)

The spine consists of different parts. The body of the vertebra is the main weight bearing part and provides the resting place for intervertebral discs. The lamina covers the spinal canal (the hole in the center of vertebra where the spinal cord passes through). Finally, the posterior elements provide additional stability to the spine and constrain the spinal range of motion while providing attachments for back muscles (Figure 1.2).

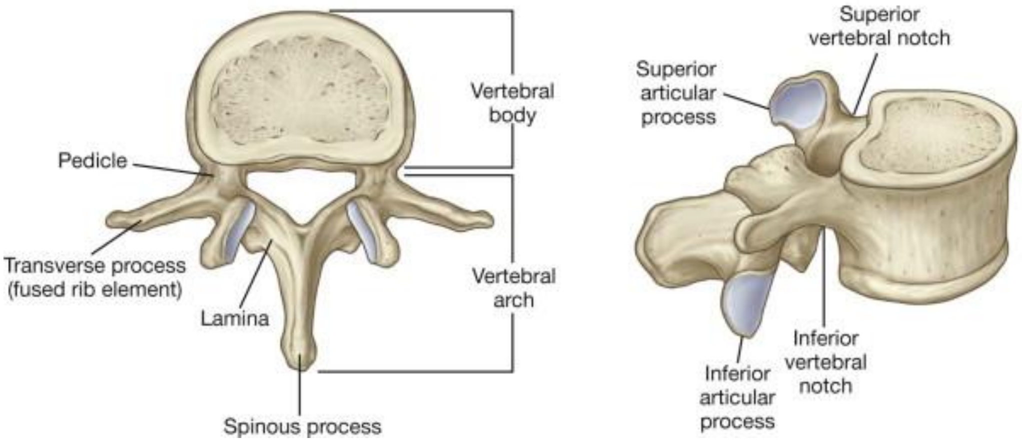

Figure 1.2: Typical vertebra [28]

1.1.1 Vertebrae

A vertebra is made of a bony anterior block, the vertebral body, and a posterior ring called neural arch which comprises articular, transverse and spinous processes. The vertebral body is made of cancellous bone surrounded by a thin layer of cortical bone. The superior and inferior surfaces are slightly concave and named endplates (formerly epiphyseal plates). The vertebral arch is composed of two pedicles and two laminae (Figure 1.2). The posterior elements vary in size and morphology based on their location and subsequently their function (Figure 1.3) [27].

(a) *(b)* *(c)*

Figure 1.3: Difference between vertebrae in different regions [28]

1.1.2 Epiphyseal plate

Epiphyseal plates, where the longitudinal vertebral growth occurs, are located on inferior and superior surfaces of vertebral bodies. As the skeleton matures, growth plates ossify and bone growth stops. In the spine, growth plates are located between vertebral bodies and intervertebral discs. The growth plate is an avascular, aneural cartilaginous tissue, which comprises chondrocytes embedded in an extracellular matrix. Three distinct zones can be distinguished based on the arrangement and size of chondrocytes: the reserve, proliferative and hypertrophic zones [29] (*Figure 1.4*). The reserve or resting zone includes randomly dispersed chondrocytes that do not highly proliferate. The high lipid and vacuole content might be linked to the nutritional function of this zone [30]. Chondrocytes of the proliferative zone are flattened compared to the reserve zone and aligned along the longitudinal columns. The flattened chondrocytes in the proliferative zone turn into spherical and enlarged ones in the hypertrophic zone. Chondrocytes in the proliferative zone are believed to be the only cells of the growth plate that divide [31]. The growth equals to the rate of newborn chondrocytes at the top of the proliferative zone multiplied by the maximum size of chondrocytes at the bottom of the hypertrophic zone. The matrix in proliferative zone is composed of randomly distributed collagen fibrils and matrix vesicles. The proliferative zone performs two functions: cellular proliferation and matrix production. The combination of these two functions results in longitudinal growth. The initial calcification happens at the bottom of the hypertrophic zone. This calcification results in impermeability of the intercellular matrix, which reduces the diffusion coefficient because of the high mineral content of the zone.

Longitudinal bone growth is a result of cell division, cell enlargement along with degradation and synthesis of extracellular matrix. The process starts from the pool of chondrocytes and it continues with the division of chondrocytes in the proliferative zone. This process would terminate by the apoptosis of the chondrocytes where the tissue is invaded by blood vessels and calcifies in the zone of provisional calcification. Synthesis and degradation of the matrix happen in both proliferative and hypertrophic zones [32, 33]. Regulation of the growth rate is not yet clearly understood and probably includes various parameters such as genetics, hormonal levels, nutrition and blood supply and mechanical loading [14, 34].

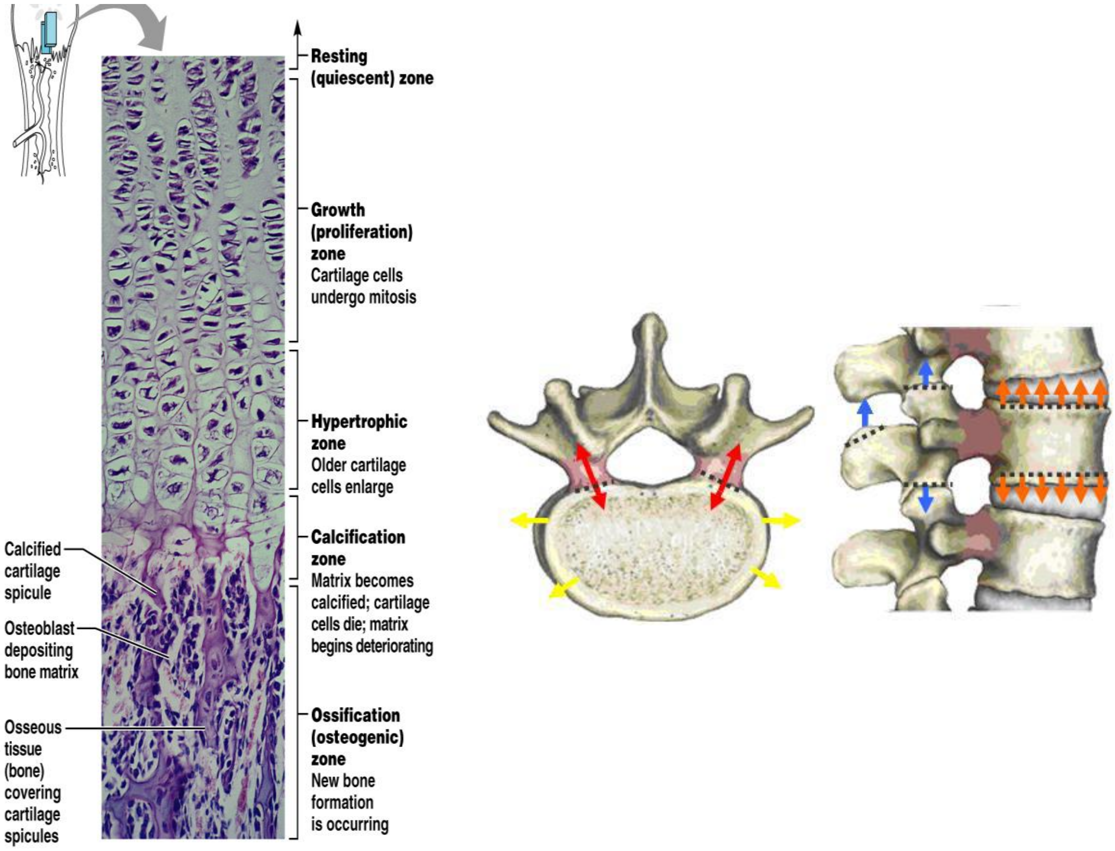

(a) *(b)*

Figure 1.4: a) Different zones in the growth plate b) growth plate location in vertebrae (red: neuro-central canal, bleu: vertebral processes, yellow: appositional growth, orange: epiphyseal plate)[35]

-

1.1.3 Intervertebral disc

Intervertebral discs have different functions in the spine and are subjected to a variety of forces and moments in the daily life. Along with facet joints, they are responsible for sustaining all compressive loads carried by the spine. Discs are also subjected to other types of loading such as tensile loads (in flexion, extension and lateral bending) and shear loads (in axial rotation with respect to the pelvis, and bending). Sustained loads by the discs can be divided into two main categories: short duration and high amplitude loads, as well as long duration and low magnitude loads. In short duration loads, damage and failure mechanisms are mostly related to the irreversible damage under loads higher than ultimate failure stress, while fatigue failure occurs under low magnitude loadings repeated for long durations [36].

The discs are composed of two distinct regions: the nucleus pulposus, located in the central area, and the annulus fibrosus, located in the outer boundary of the disc (Figure 1.5). The nucleus pulposus is made of a very loose and disorderedly distributed network of collagen fibers suspended in a mucoprotein gel. The nucleus acts as a shock absorber in physical daily activities and keeps the two vertebrae separated. In contrast, the annulus fibrosus is composed of structured dense layers of fibrocartilage containing the nucleus. The nucleus occupies about 40% of the whole disc [37]. The nucleus size and its swelling capacity are higher in the cervical and lumbar regions [36].

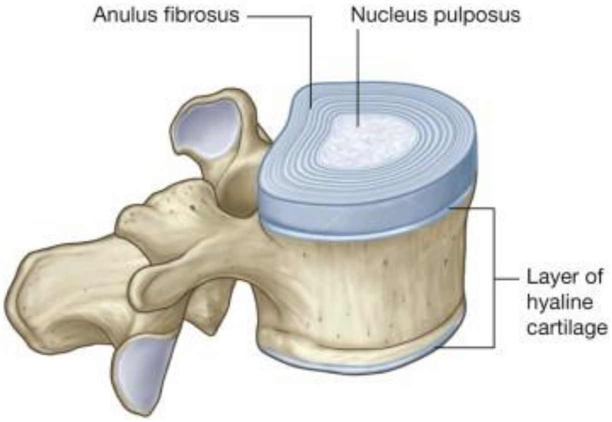

Figure 1.5: Intervertebral disc [28]

1.1.4 Ligaments

Ligaments are generally uniaxial structures and carry loads mostly along the direction of their fibers. They resist tensile forces and buckle under compression. In the spine, they provide tensile resistance against complex external loads. They have several functions in the spine. First, they allow physiologic motions with minimum energy loss by muscles. Second, they constrain ranges of motion in the spine and protect the spinal cord. Third, they help muscles in stabilizing the spine and, finally, they protect the spine in impact conditions by restricting vertebral displacement and absorbing the applied energy [36]. There are seven ligaments in the spine (Figure 1.6).

The posterior and anterior ligaments are located on the posterior and anterior surfaces of the vertebral body and extend along the spine. They are both connected superiorly to the base of the skull and extends to the sacrum. Along their length, they are connected to the vertebral bodies and intervertebral discs.

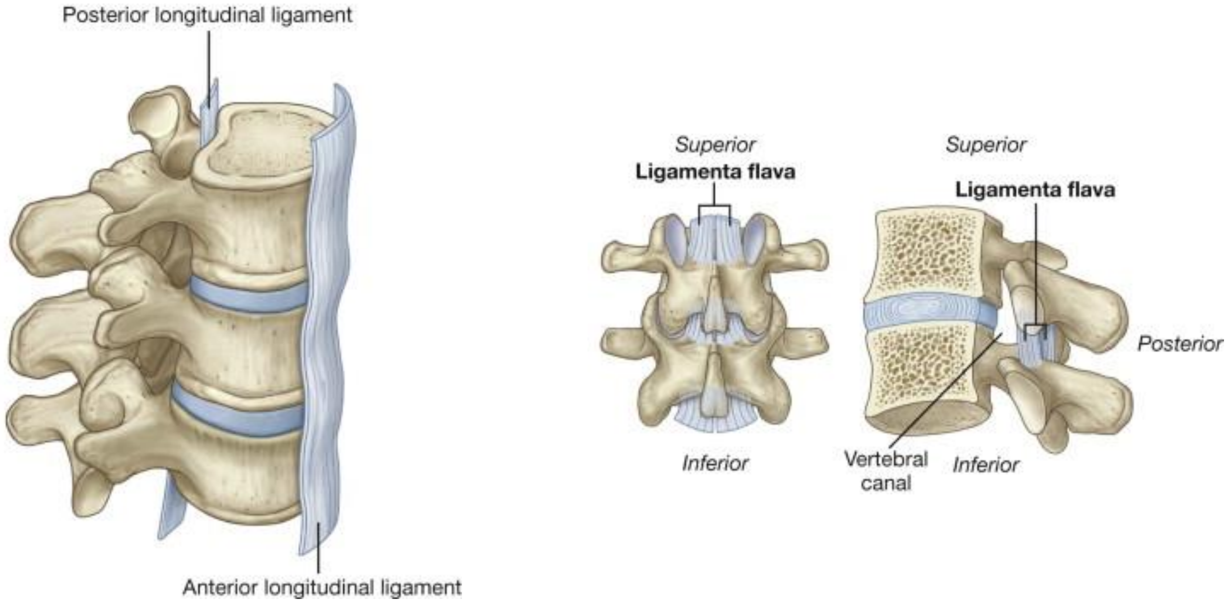

Figure 1.6: Ligaments in the spine [28]

The ligamenta flava pass through the laminae of the neighbouring vertebrae. This ligament is mainly made of elastic tissue and forms a part of posterior surface in the vertebral canal. The ligamenta flava keeps the laminae connected in flexion and helps in extension back to the anatomical position [28].

The intertransverse ligaments pass between the transverse processes in the thoracic segment and are considered rounded cords closely connected to the deep back muscles.

The capsular ligaments are connected beyond the margins of the adjacent articular processes. The fibers are arranged perpendicular to the facet joint planes. They are shorter in the thoracic and lumbar segments than cervical section.

The interspinous ligaments pass between adjacent vertebral spinous processes. Their attachment extends from the base to the apex of each process.

The supraspinous ligament originates from ligamentum nuchae and extends along the tips of the spinous processes. It is thicker and broader in the lumbar segment than in the thoracic segment.

1.2 Growth plate mechanics and mechanobiology

1.2.1 Growth plate mechanics

The biomechanical behavior of any tissue depends on its intrinsic material properties. The general approach to determine the material properties of the tissue is to perform experimental tests on the tissue, to describe its biomechanical behaviour with a mathematical function and fit the experimental tests results with the mathematical model. Confined and unconfined compression tests on growth plate along the growth direction are used to derive its material properties. The unconfined compression tests are done in two ways: creep and stress relaxation. In the creep test, the compressive load is kept constant and the deformation in the material is measured. However, in the stress relaxation test, the displacement is applied under a controlled rate then is kept constant and the stress in the tissue is recorded (Figure 1.7).

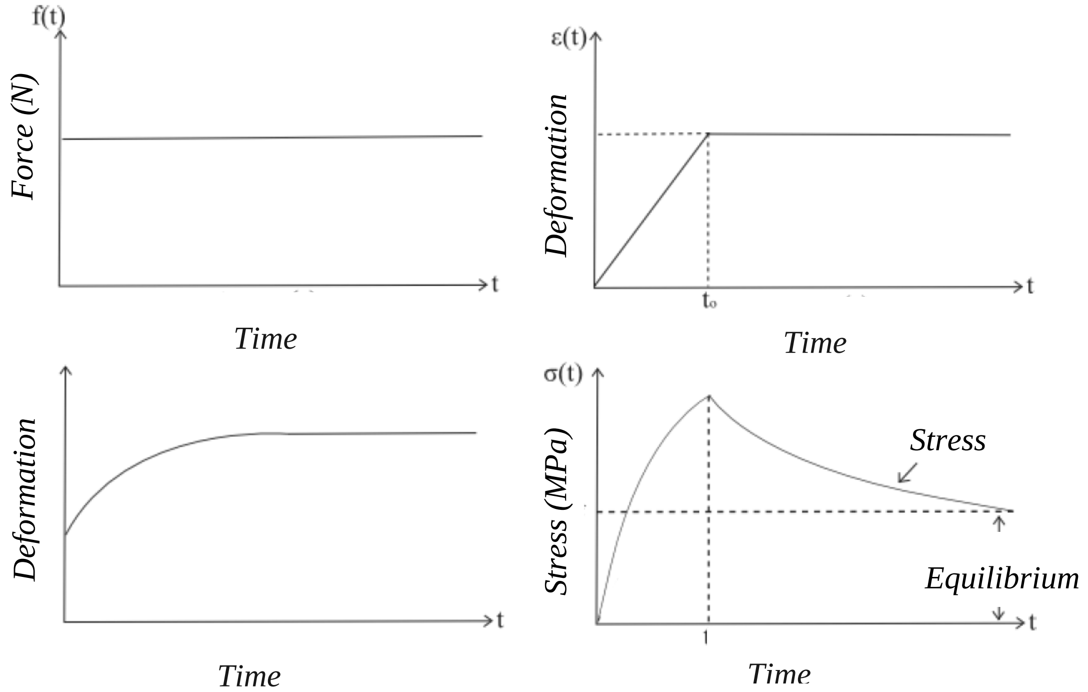

(a) (b)

Figure 1.7: a) Creep test b) stress relaxation test

Growth plate is a biphasic material which is composed of a fluid phase and a solid matrix. Based on the experimental results, this tissue shows viscoelastic properties signifying the time dependency of the biomechanical behaviour. The viscoelasticity can be either from an intrinsically viscous component of the material or the flow of interstitial fluid through the solid phase. In the case of cartilage, viscoelasticity can be explained largely by the frictional drag resulting from the movement of liquid through the porous extracellular matrix. The intrinsic viscosity of collagen and proteoglycans also plays a role, but of lesser importance [38-40].

The growth plate also shows orthotropic material properties which means that the measured stress is different in different directions in a certain point. Different biphasic models have been developed to better fit the experimental results with mathematical functions. Table 1.1 shows the different developed models as well as their characteristics and type of tests and tissue. Growth plate biomechanical behaviour can be fitted to transversely biphasic model better than isotropic biphasic model [41, 42]. Based on experimental results, the growth plate is about ten times stiffer in the radial (transverse) direction (4.6-10.6 MPa) than the axial direction (0.3-1.1 MPa). The comparison between radial (1.8-5 × 10^{-15} m^4/Ns) and axial (0.9-25 × 10^{-15} m^4/Ns) permeability is of similar range but with more variability in the axial direction. Furthermore, radial Poisson's ratio (0.24-0.3) is two or three times higher than the axial Poisson's ratio (≤0.1) [29, 42].

Growth plate mechanical properties probably change with the age, as ultimate strain and stress increase and the tensile moduli decreases [43].

Table 1.1: Biphasic models for biomechanical behaviour of cartilaginous tissue

Model	**Tissue**	**Biomechanical behaviour**	**Tests**
Biphasic poroelastic, Mow et al. (1980) [44]	Articular cartilage	Isotropic, elastic, linear	Indentation, confined and unconfined compression tests
Biphasic porovisco elastic, Mak et al. (1986) [38]	Articular cartilage	Viscoelastic, linear	Indentation, confined and unconfined

			compression tests
Biphasic nonlinear poroelastic, Cohen et al. (1994) [45]	Growth plate	Isotropic, elastic, non-linear	Confined compression test
Biphasic poroelastic transversely isotropic, Cohen et al. (1998) [41] Sergerie et al. (2009) [42] Wosu et al. (2012) [46]	Growth plate	Transversely isotropic, elastic, linear	Indentation, confined and unconfined compression tests
Biphasaic fibril reinforced, Soulhat et al. (1999) [47] Fortin et al. (2000) [48]	Articular cartilage	Elastic fibril reinforced, linear	Indentation unconfined compression test
Biphasic cone-wise linear elastic, quasilinear visco elastic Huang et al. (2001) [49]	Articular cartilage	Viscoelastic, linear	Confined and unconfined compression test
Biphasic porovisoelastic fibril reinforced Wilson et al. (2005) [50]	Articular cartilage	Viscoelatic fibril reinforced	Indentation unconfined compression test

1.2.2 Mechanical growth modulation

Clinical evidence shows that mechanical loads are vital for bone growth but the elevated loads can result in skeletal deformities or other pathological conditions in musculoskeletal system, namely adolescent idiopathic scoliosis, hyperkyphosis and tibia vara/valga [51, 52]. This relationship between bone growth and mechanical loadings, called mechanical growth modulation of bone growth, refers to Hueter-Volkmann principle, which states that an increased compression reduces the growth rate in growth plate while a decreased compression accelerates it. This principle has key implications in the progression of pediatric musculoskeletal deformities. In addition, it is exploited to develop new interventions in pediatric orthopaedics such as fusionless treatment approaches.

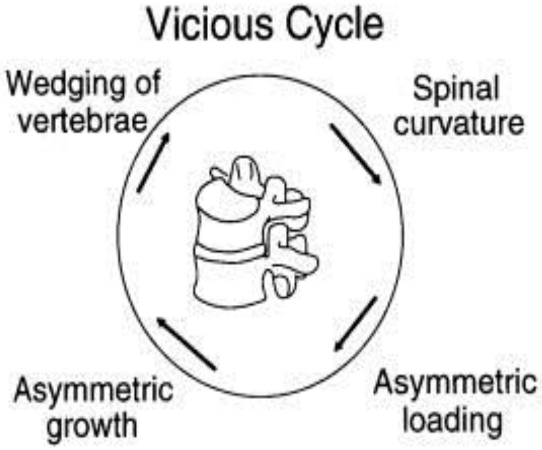

Figure 1.8: Vicious cycle in scoliotic curve progression [53]

For scoliosis, it is believed that once a deformity is established in the spine, its progression during growth is governed by Hueter-Volkman principle [9, 10]. Under this law, asymmetric loading over the vertebral growth plates leads to the vertebral wedging that is promoted in a vicious cycle (Figure 1.8). In this cycle the greater growth reduction in the compressed side of vertebra coupled with accelerated growth in the distracted side induce more progression in scoliotic curve specially during the adolescent growth spurt [13].

This law is qualitative and does not include the load history, growth plate dimensions and the level of the maturity in the growth plates [29]. *In vivo* experiments which apply the load on the immature animal growth plates have been used to formulate the relationship between growth rate and applied load. The numerical correlation expresses the growth rate as a linear function of altered stress as:

$$G = G_m\left[1 + \beta(\sigma - \sigma_{m)}\right] \quad , \tag{1-1}$$

Where G is the actual growth rate (mm/year), G_m is the mean baseline growth, σ expresses the actual stress on the growth plate, and σ_m is the mean stress on the growth plate. β is called the scaled parameter and is between [0.4 – 1.7 MPa^{-1}] depending on the species and growth plate location [14].

1.2.3 Dynamic vs. static loading for growth modulation

There is a strong experimental evidence showing longitudinal bone growth alteration by static loads, as an increased compression slows down bone growth, and conversely a reduced pressure accelerates it [14-16]. Comparisons between *in vivo* and *in vitro* studies provide the opportunity to include all the parameters that are intrinsically involved, however there are some difficulties regarding the control of applied loads on the growth plate. Static compression leads to growth plate thinning; also, the growth is even more slowed when the compressive load is sustained for a longer time [15, 54].

Comparative *in vivo* studies investigated the difference between static and dynamic compression and tension applied on growth plates [18-20, 55]. Their results show either the same, or more slowed growth under compressive loads for the dynamic group compared to the static group while under tensile loads the growth was more accelerated in the dynamic group. However it should be noted that in this comparison either the loading magnitude is not well defined [55], either the average loading in static and dynamic groups is not matched [19, 20, 55], or the loading parameters are not normalized [18-20, 55], which makes the evaluation of comparative static/dynamic studies difficult. The most recent study, which investigated matched static and dynamic loading with the same average compressive stress, indicates that dynamic loads are as effective as static loads in growth modulation, but are less detrimental in terms of growth plate histomorphometry [1]. In this study a compressive load of 0.2 MPa was applied perpendicularly on the rat caudal growth plates.

1.3 Scoliosis

Scoliosis is a (3-D) deformity of the spine affecting the orientation, position and shape of vertebrae with a prevalence between 2-3 % among adolescents based on a Cobb angle criterion of 20 degrees in the coronal plane. There are different categories to better classify the etiology of scoliosis such as congenital, functional, neurological and idiopathic. The origin of the idiopathic scoliosis, as the name signifies, is not known; it is the most common type of scoliosis. The primary clinical measure of scoliosis deformity is the Cobb angle [56] (Figure 1.9). Another measure is the Risser grade (0-5) which gives a useful estimate of how much skeletal growth remains by grading the progress of bony fusion of the iliac apophysis.

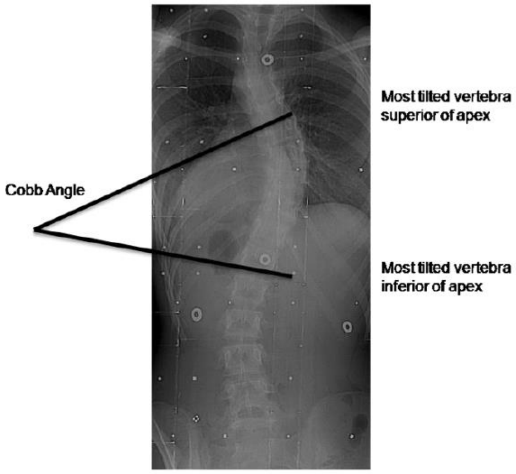

Figure 1.9: Measurement of Cobb angle

1.3.1 Adolescent idiopathic scoliosis

Adolescent idiopathic scoliosis has a prevalence between 70-80% among scoliotic patients affecting 1-3% of adolescents mainly females [5]. Despite all theories, which have been developed to explain the etiology of the AIS, the causative factors are not yet well understood. Genetics, thrombocytes, connective tissue, neurological influences, melatonin, skeletal muscle influences and biomechanical factors are among considered factors [57-61]. The progression of scoliosis mostly occurs during puberty when the growth has its peak velocity between the ages of 11-13 years old in girls and 13-15 years old in boys. The difference between pressure over growth plates in convex versus concave sides induces vertebral wedging that adds to the deformity of spine within a vicious cycle (Figure 1.8). Gender, curve pattern, curve degree before the puberty and the curve progression rate are risk factors in curve progression [62].

1.3.2 Conventional treatments

Conventional treatments for AIS include observation, bracing and surgery based on the scoliotic curve degree and skeletal maturity of the patient. Observation is mostly recommended for the patients with Cobb angles of 20 or less; it includes regular checkups on the curve progression.

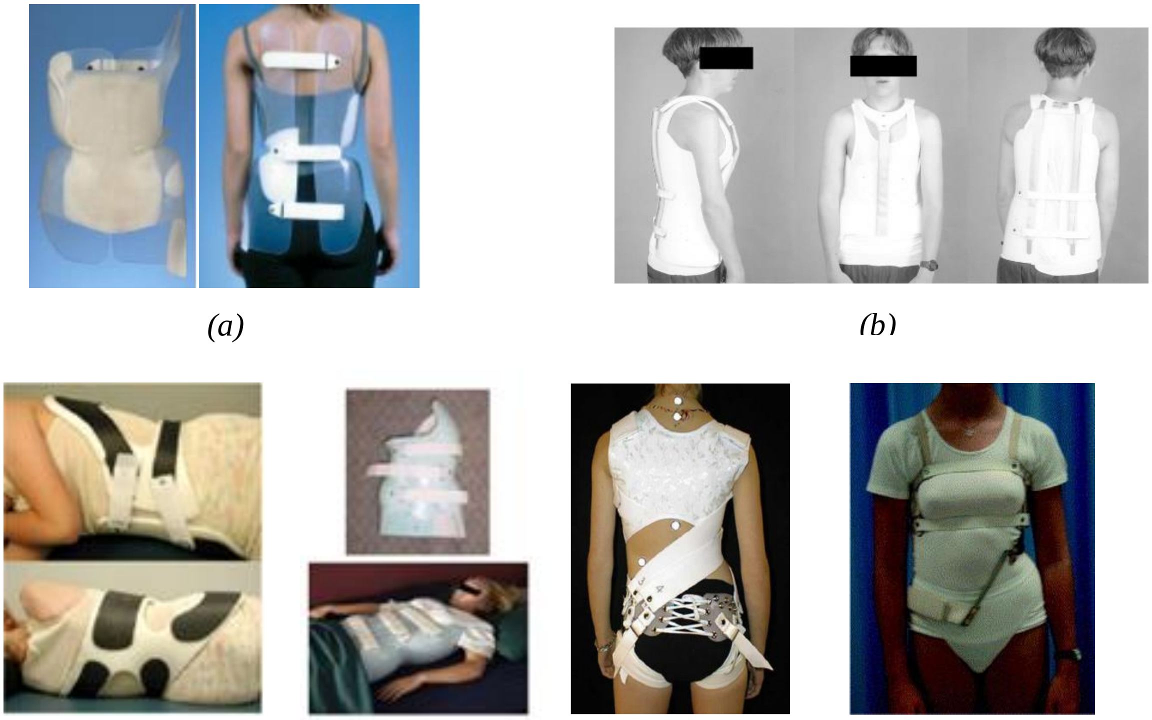

(a) (b)

(c) (d) (e) (f)

Figure 1.10: a)Boston brace [63] B) Milwaki Brace [64] c) Providence [65] d) Charleston [66] e) SpineCor [67] f) TriaC [68]

Braces are recommended for mild curves (Cobb angles between 20 and 40 degrees). They can be categorized in three main groups: full time bracing (Boston, Milwaukee), night-time bending bracing (Charleston, Providence) and non-rigid braces (Spine-Cor, TriaC) (Figure 1.10). The objective of all these braces is to apply external forces on the trunk to prevent curve progression. In the last decades, a lot of efforts have been made to develop the best possible braces using clinical studies and finite element simulations. Studies have shown that braces are more effective in girls, patients with lower BMI, younger patients and more flexible curves [69-71]. This treatment can however cause heavy psychological impacts on the young patients [72]. Furthermore, there are other studies showing that the incidence of the surgery in braced patients remains the same as patients without bracing [73]. Despite all these limitations, studies on the design and optimization of the braces provide promising perspectives for this treatment [26, 74-77].

Surgical treatment is the ultimate solution for scoliotic patients. In this approach, rods combined with fusion are used to apply required forces to correct the spinal curvature(s). For the spinal fusion, supplementary bone tissue is used to join two or more vertebrae together so they will turn into a solidified structure (Figure 1.11). This treatment is postponed until skeletal maturity of the spine unless the risk factors for curve progression are high. In this case, the spinal growth will be arrested to avoid the complication due to the spinal growth [78]. Surgical intervention helps to improve the appearance of the patients and provides a permanent correction by preventing the curve progression. However, it is an invasive surgery with long healing time which could reduce the spinal mobility and have an elevated rate of complications [79].

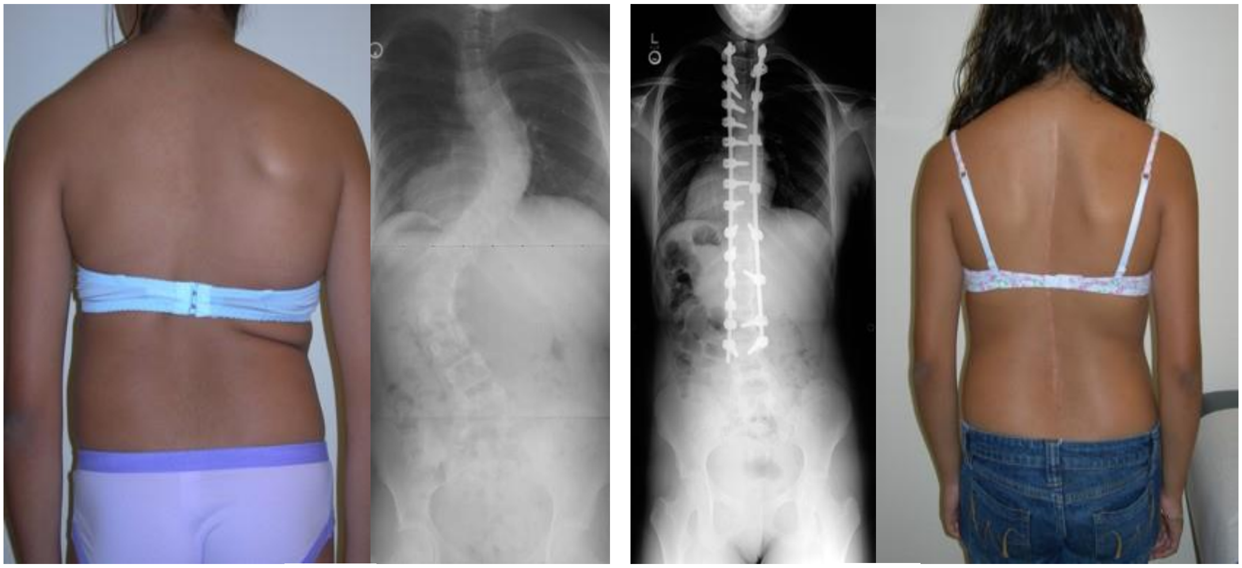

(a) *(b)*

Figure 1.11: Surgical treatment, a) before surgery b) after surgery

1.3.3 Fusionless growth modulation treatments

Fusionless growth modulation approaches are an alternative to the conventional treatments of scoliosis. They use residual growth of the vertebrae to realign the spine. Their objective is to avoid fusion, and if possible, treat the moderate curves prior to the end of the growth spurt through minimally invasive surgeries.

There are three main groups of fusionless corrective approaches: distraction based devices (i.e. growing rods [80, 81], vertical expandable prosthetic titanium rib [VEPTR] [82]) (Figure 1.12), guided growth implants (i.e. Luqué trolley [83], Shilla [84]) (Figure 1.13) and compression based devices (i.e. tethers [85], staples [86], mini staples [24] and shape memory alloys [87]) (Figure 1.14).

Distraction based devices increase the growth rate over concave side by reducing its compressive loads. In first versions of this method, repetitive surgeries were required to increase the length of the expanding rod, consistent with growth and realignment of spine but some newer versions are now controlled magnetically from outside of the patient’s body. The length of the rod is increased in regular time intervals depending on the growth rate and scoliotic curve degree (Figure 1.12).

(a) *(b)* *(c)*

Figure 1.12: Distraction based devices a)magnetically controlled growing rod [88] b) growing rod [89] c) Vertical expandable prosthetic titanium rib [90]

In Luque trolley technique, U or L shape rods were fixed to the spine in a segmental fashion using sublaminar wires (trombone like posterior instrumentation). It uses a passive self-lengthening technique (no repetitive surgery) with non-locking screws (

Figure 1.13a) [91]. In the Shilla method, the apex of the curve is fused and fixed using pedicle screws to dual rods. Rods slide through gliding pedicle screws at either end of the curve as spine grows. It has a self-lengthening system (no repetitive surgery) by non-locking screws too (

Figure 1.13b) [84, 92].

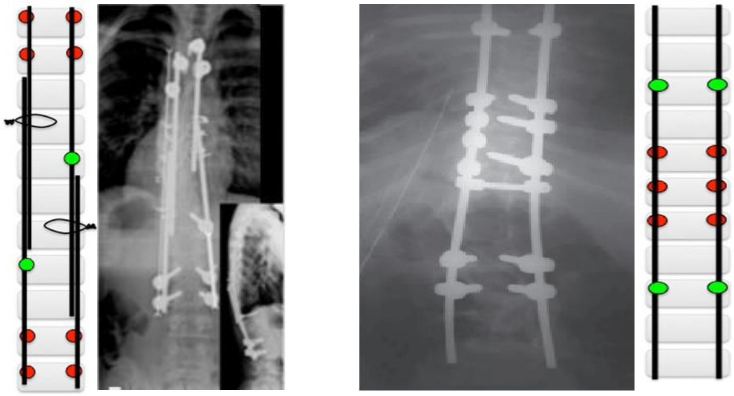

(a) (b)

Figure 1.13: Guided growth device a) Luqué trolley Technique [91] b) Shilla Technique[92]

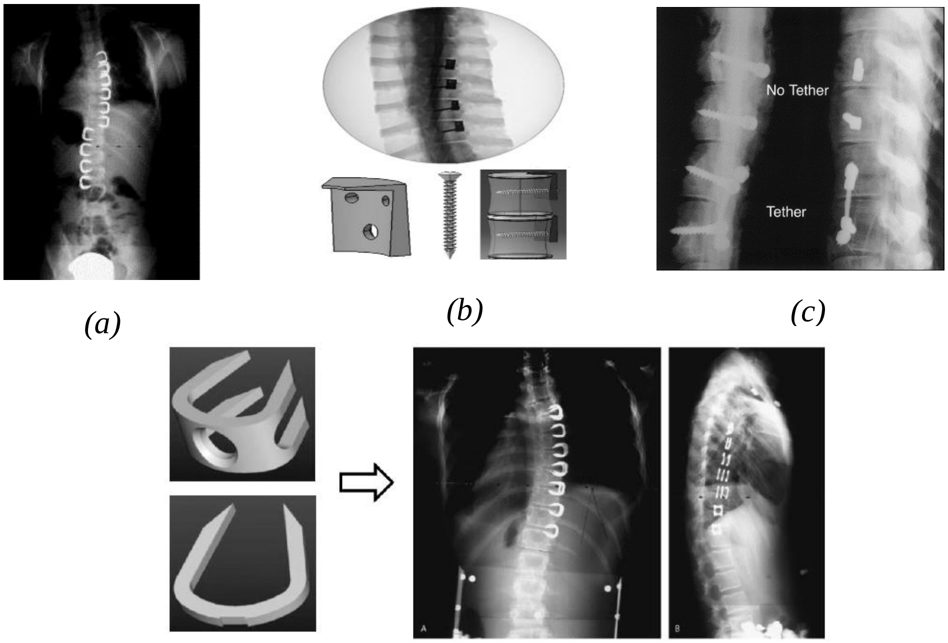

(a) (b) (c)

(d)

Figure 1.14: Compression based devices a) staples [86] b) mini staples [24] c) flexible tether [85] d) shape memory alloy staples [86]

In compression based methods, an applied compression over convex side reduces the growth rate and leads to correcting the vertebral wedging and realigning the spine (Figure 1.14). All these methods follow the same principles, i.e. changing loading over growth plates and using the mechanical growth modulation phenomenon and residual growth to realign the spine. However, some of them are thoroughly static such as staples and mini staples by applying a constant force in all condition while there are fusionless devices such as tethers and expandable rods in which the applied pressure on the growth plates varies during time or in different postures which provides a dynamic nature for them.

Despite all promising results in animal and human studies, it should be taken into account that these devices focus on coronal correction and the current consensus amongst authors is that a restriction of coronal plane progression would succeed in limiting additional vertebral axial derotation; however this hypothesis has yet to be verified.

In fusionless modulating devices, the impact on sagittal spinal alignment is not well controlled and the axial direction on bone deposition restricts the possibilities for pressure or tension application through mechanical devices. The other challenge in design of fusionless devices is in regard to maintain a minimal level of surgical invasiveness, which limits the target of corrective instrumentation to the anterior portion of the vertebral bodies

As these devices target adolescents, there is still a residing uncertainty on their long term influence on intervertebral disc health.

1.4 FEM of spine

Finite element modeling (FEM) is a numerical method for modeling the mechanical behavior of complex systems. It provides a detailed stress and strain analysis with lower costs and ethical issues associated with experimental studies. In the finite element method, the complex geometry is divided into a large number of subdomains, which are simply called elements. Then, the problem is solved for each element and results are assembled based on the connecting nodes between elements. In the musculoskeletal system, the FEM can be implemented to analyze the strain and stress distribution within different parts in the spine particularly: growth plates and discs. Furthermore, it helps to test the theories for spinal disorder pathomechanism. More above, disc degeneration, bone remodeling, growth modulation and impact analysis are other fields in which FEM is helpful.

1.4.1 Geometry

There are different finite element models in terms of geometry. The model can be representative of the whole spine or just a particular segments of the spine. They can also just include vertebrae and discs or more parts like posterior elements, ligaments and rib cage. Furthermore, the geometry can be simplified or be realistically reconstructed. In the simplified model, a simple but representative model is constructed based on the *in vitro* studies and image processing. This type of models provides the possibility of structured meshing and parametric sensitivity analysis and can be adjusted to the other patients. In contrast, realistic models include the actual geometry of the tissue or group of tissues and are more difficult to develop. In this type of models, there is less control over the meshing but the interaction between different tissues is considered (Figure 1.15).

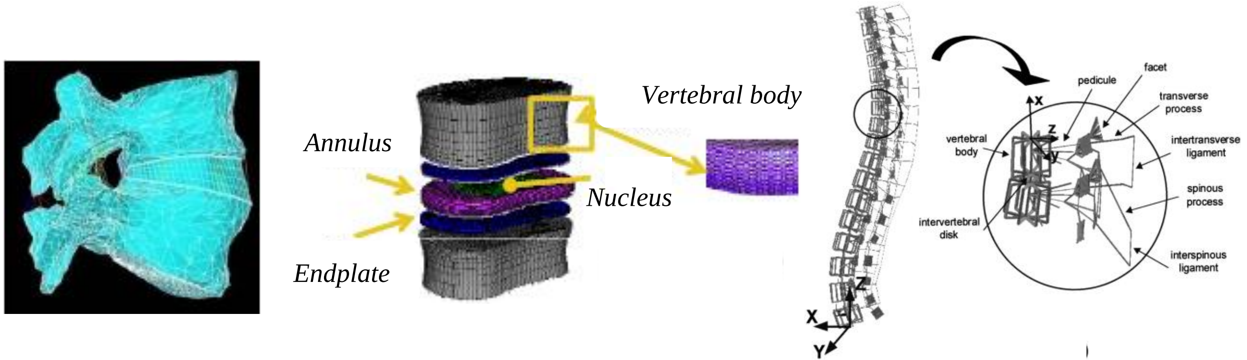

(a) *(b)* *(c)*

Figure 1.15: a) Realistic geometry [93] b,c) Simplified geometry [21, 94]

In FEM of spine, the soft tissues, such as cartilaginous growth plate, ligaments, intervertebral discs, etc., are usually additionally modeled since geometries of these tissues are not included in the reconstruction from images.

There are different types of elements for meshing the model. They can generally be divided in two groups; volumetric (solid) elements and beam elements. The implementation of beam or solid elements depends on the model specific application; the solid elements provide a detailed analysis of stress and strain in corresponding elements (growth plates, discs, vertebrae, etc.) and they can be exploited in implant models, growth modulation simulation, disc degeneration and etc. (Figure 1.16a) [21, 95].

However, beam element models simulate the overall behavior of the model without considering the stress distribution in a vertebra or disc level. They can be exploited in problems that need fast processing and immediate effects like bracing. Because of the simplicity of the beam element models in comparison with volumetric element, more organs can be added to the model (Figure 1.16b) [96].

Consequently, hybrid models simulate the detailed stress analysis in the areas of interest while they implement beam elements for other parts to keep computational cost as low as possible (Figure 1.16c) [97].

a) b) c)

Figure 1.16: a) volumetric element model [98] b) beam element model [26] c) hybrid model [97]

1.4.2 Mechanical properties (vertebrae, growth plate, disc)

The spine shows a complex biomechanical behavior due to its complex geometry and mechanical properties of its composing tissues. Most tissues of the spine have an anisotropic behaviour, which means that they have different properties in different directions in a particular location (e.g. bone and cartilaginous tissue). They are also mostly heterogenous, with different material properties in different locations (e.g. cancellous bone in the vertebrae). In addition, certain tissues are considered to be hyper elastic representing a nonlinear relationship between applied stress and resulting strain (e.g. discs and growth plates). Finally, some tissues are viscoelastic which means their response is dependent on the rate and history of applied loads (e.g. discs and endplates). In numerical modeling of spine, simplifications are commonly justified and used to avoid the above mentioned complexities and corresponding computational costs.

The vertebral body is composed of cortical and cancellous bone, which have different texture and material properties. The cortical bone is denser with less water content comparing to cancellous bone which has a porous structure. In finite element modeling of the spine, these types of bones are usually considered as linear elastic materials because their nonlinear properties is negligible compared to the cartilaginous tissues such as intervertebral discs and growth plates [21, 77, 95].

Intervertebral discs and growth plates are composed of a porous solid matrix with high fluid content. There are two general approaches to model these cartilaginous tissues: continuous and biphasic medium. In the continuous approach, the cartilaginous tissue is regarded as a single phase material, which can be modeled as a linear elastic, hyperelastic, viscoelastic or visco-hyperelastic. In the biphasic theory, the material is composed of two phases: a solid and a fluid phases. More parameters are required to describe a poroelastic medium, such as the elastic modulus 0.2 - 2 MPa, the Poisson's ratio $\nu \approx 0 - 0.45$ and the permeability $k \approx (0.4 - 5) \times 10^{-15}$ m^4/Ns.

The appropriate model of material is chosen depending on the nature of problem. In impact analysis, considering the time dependent properties is unavoidable so that viscoelasticity should be taken into account. In validation of spinal disorder pathomechanisms, bone remodeling and growth modulation, most often using a linear elastic model saves a lot of time in simulations while the results are still valid. Because, in growth modulation and bone remodeling, problem turns into an iterative analysis in which the geometry is updated based on the applied forces. Including the viscoelasticity to this type of problems would increase the simulation times enormously (Figure 1.17).

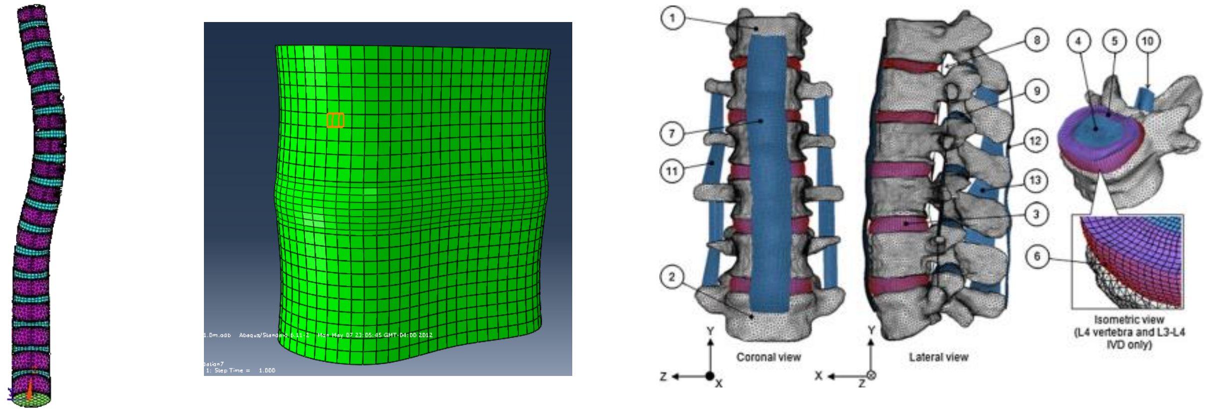

(a) *(b)* *(c)*

Figure 1.17: a) linear elastic [99] b) biphasic model [21] c) nonlinear elastic [100]

Another type of problems in finite element modeling of musculoskeletal system refers to disc degeneration. The common type of models in this type of problems is biphasic models. Biphasic models provide the stress distribution in solid and fluid phases and correlate the stress component in the solid phase to the damage in the tissue.

1.4.3 Loading and boundary conditions

The spine operates under different types of loadings. The gravity, combined to another important loading source, the muscles form a part of spinal loading. There are also other forces transferred from adjacent joints and segments.

Gravitational loading has been estimated from anatomical studies [101] and *in vivo* measurements of intradiscal pressure. It should be noted that the intradiscal pressure also include the muscle loads [102]. There are different ways to integrate spinal loadings in numerical models of the spine. The first way is to place a percentage of body weight on T1 and to add an additional percentage on the successive vertebrae [22, 103]. This method does not include muscle forces. In another study, weight ratios were applied with a lateral offset in the sagittal plan to better define the geometric center of mass of the patient. In this study, the rib cage and soft tissues were integrated which helped providing more stability for the spine [26].

In aforementioned studies, the muscle forces are not considered. Experimental *ex-vivo* studies showed that lumbar spine can support a tangential force up to 1200 N before buckling while this force reduces to 80-100 N when it is applied perpendicularly [104]. As our spine can support up to 1000 N under physiologic conditions, the tangential force seems to provide more realistic results. It was suggested that the presence of muscle forces results in a net force vector which remains tangential to the spinal curvature (follower type load) [105]. This method was further adopted and modified by Shirazi-Adl et al. [106].

Some finite element studies have adopted this method in their models. Driscoll et al. used a follower type load [95] in one study and a combination of the follower and vertical gravitational loadings in another study. In his combined method, spinal load vectors in the coronal plane respected gravitational direction (z-axis of global coordinate system) while loading in the sagittal plane was maintained tangential to the curve of the spine to ensure spinal stability as displayed by the resultant load vectors at each level (Figure 1.18) [98].

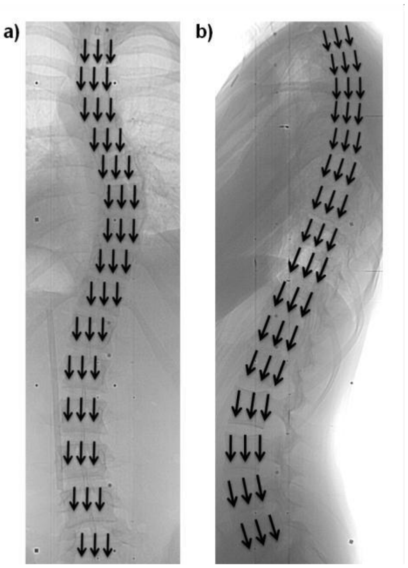

Figure 1.18: a)Vertical force in the coronal plane and b) tangential force in the sagittal plane [98]

Furthermore, Clin et al. developed an optimization process to find the appropriate zero-gravity and gravity geometry to consider the effect of gravity in the initial geometry in reconstructed images [107].

In addition to spinal loadings, boundary conditions need to be applied to the spine to constrain the model. The role of constraints is to prevent rigid body motion and represent the symmetry condition, whenever relevant. The general objective is to do the modeling as close as possible to the real system.

The boundary condition depends directly on the model. In whole spine models [76, 97, 98], the pelvis (or L5) is usually completely constrained and T1 vertebra is constrained in vertical direction but can move in transversal plane. For segment models, the inferior surface of the inferior vertebra is usually fully constrained in the vertical direction [21] while other loads are applied on the top surface of the superior vertebra.

CHAPTER 2: RESEARCH RATIONALE, OBJECTIVES AND HYPOTHESIS

Based on literature review in chapter 1, the rationale of this project can be described in following points:

- Fusionless methods have shown promising results in the early treatment of moderate scoliosis, as shown by numerous published studies and growing number of registered patents. These devices use residual vertebral growth to realign the spine and correct the scoliotic deformity. Their current mode of action is mainly based on static compression on the convex side of the curvature. The corresponding reduced growth rate on the convex side will gradually correct the wedged vertebral shape and hence reduce the Cobb angle (Heuter-Volkmann principle).
- Recent studies have proposed that cyclic compressions are as effective as static ones in modulating bone growth and they are moreover less detrimental to growth plates than static compressions. A cyclic loading approach could then be of great interest to develop new fusionless corrective approaches for the early treatment of moderate scoliotic curves.
- Fusionless approaches have their own limitations, such as a lack of information about their long term effect on the intervertebral discs and growth plates health as well as restriction of uni-lateral correction of 3-D deformity of scoliotic spine. Improvements in the understanding of the corresponding corrective biomechanics would lead to a significant contribution into the development of new fusionless approaches for the early treatment of AIS.
- After reviewing the literature relevant to the fusionless methods, it is recognized that there is a lack of knowledge about the developing stress and strain within the growth plate under cyclic and static compressive loadings. Experimental approaches in this case would be technically challenging and may not provide all the desired information. Finite element method, however, allows to analyze stress and strain within the tissue and study the effect of different parameters with less cost and restrictions. Hence, a finite element study, which would investigate stress components, strain and fluid content within growth plates under different loading regimes, could be of high interest and importance. Finite element

studies could help comparing stress profiles from static and cyclic loadings. Furthermore, they could help us to find the effective components corresponding to the growth modulation and damage in growth plates. These results could be further used to develop new design concepts in this era.

The research hypothesis of this thesis is:

Cyclic and static compressive loads show the same total stress but different pore pressure (stress in fluid phase) and effective stress (stress in solid matrix) within growth plates

From the experimental studies, cyclic and static compressions have the same growth modulating effects while cyclic loads cause less damage to the growth plates compared to the static loads. Furthermore, in biphasic materials, the total stress is the summation of the effective stress and pore pressure. Hence, it was hypothesized that cyclic and static compressions have the same total stress since the equilibrium between applied load and resultant stress should be satisfied. It was also suggested that cyclic loads cause less effective stress and consequently damage in the growth plates.

The general objective of this project is to computationally study the biomechanical response of the growth plate under static and cyclic compressive loads using finite element method.

To address this general objective two specific objectives are defined;

Objective 1: To study the effect of compressive loading frequency (0.1 and 1 Hz), oscillation amplitude (±30% and ±70%), peripheral pore pressure (0 and 0.1 MPa) and transversal permeability (K, 10% K and 1% K) on the developing stress (pore pressure, effective stress and total stress) and vertical deformation within a biphasic axisymmetric finite element model of growth plate.

Objective 2: To compare static and cyclic compressions in terms of stress components (pore pressure, effective stress and total stress), maximum and minimum principal strains and fluid loss in growth plates and disc (nucleus and annulus) using a finite element model of functional spinal unit.

CHAPTER 3 : MATERIAL AND METHODS

The developed methodology pursues the two specific objectives of this thesis. The organization of the project can be summarized by the following diagram (Figure 3.1).

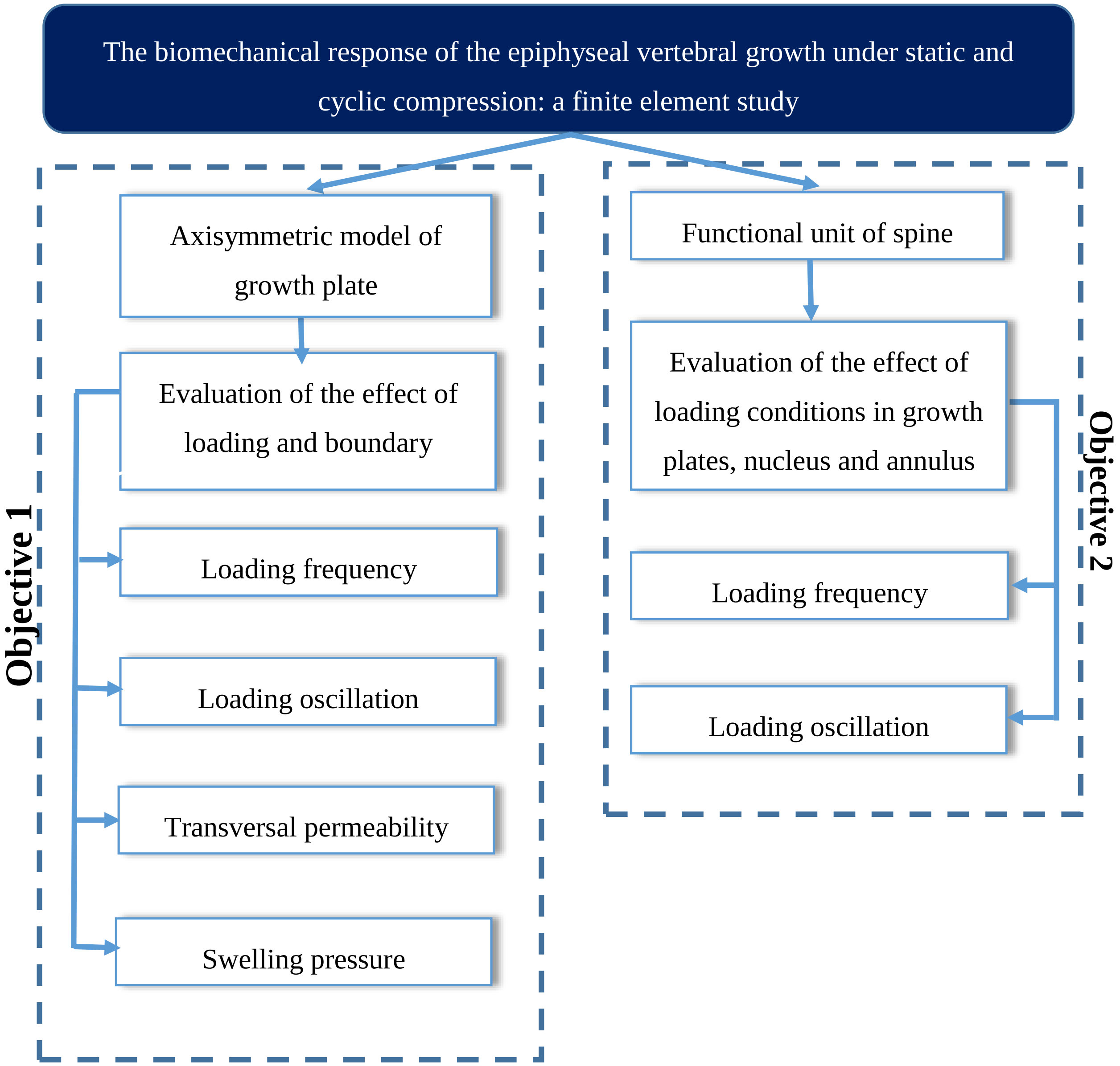

Figure 3.1: Schematic organization of the methodology

3.1 Objective 1: Study of the developing stress and deformation in the growth plate using a biphasic axisymmetric finite element model: effects of material properties, loading and boundary conditions

A commercial finite element package (ABAQUS v6.12-3, Dassault Systèmes, Providence, RI, USA) was used to develop an axisymmetric poro-elastic finite element model of a growth plate tissue. Uniaxial unconfined compression was simulated by placing a rigid surface above the growth plate under static and cyclic loadings. Material properties, geometry, loading and boundary conditions are explained in detail in the following sections:

3.1.1 Material properties

The growth plate is a highly anisotropic, nonhomogeneous and multiphase material. In this study, simplifying assumptions were made to avoid computational burden and modeling difficulties. Therefore, the growth plate was modeled as a transversely isotropic porous solid matrix filled with fluid. This is justified by the fact that Cohen et al. showed that a transversely isotropic model for growth plate fits the experimental data much better than an isotropic model (Figure 3.2) [41]. The required material properties to define biphasic materials in ABAQUS are: the drained Young’s modulus *E*, the Poisson ratio υ, the porosity n, the void ratio e, and the permeability *K* [41].

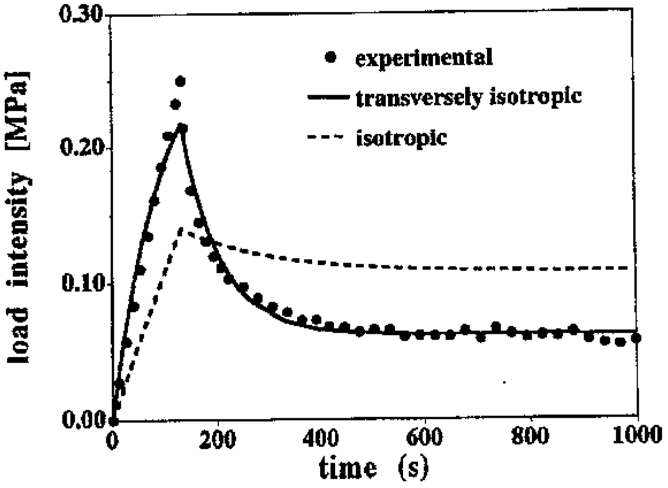

Figure 3.2: Stress relaxation diagram in response to a ramped displacement for both isotropic and transversely isotropic biphasic model fits [41]

A strain dependant permeability was used in this study, since it has been shown that permeability is highly strain dependant when soft tissues undergo finite deformations [108-110]. To include the reduced permeability as a result of increasing deformation under compressive load, the permeability was defined as a function of void ratio e:

$$k = k_0 \left[\frac{e(1+e_0)}{e_0(1+e)}\right]^2 exp\left[M\left(\frac{1+e}{1+e_0} - 1\right)\right], \tag{3-1}$$

where $e=n/(1-n)$ and the subscript 0 indicates corresponding initial values. M is a constant defined by Argoubi and Shirazi-Adl based on the experimental results [111].

The material properties were taken from unconfined compression experimental results derived by Cohen et al. (Table 3.1). Subscript t and a stand for transversal and axial coordinates respectively. The biphasic theory was used for hydrated soft tissues and a transversely isotropic model was exploited to derive an analytical solution for unconfined compression test of cylindrical samples of growth plate tissues compressed between two rigid surfaces with a frictionless interface. The plane of transverse isotropy was considered to be perpendicular to the cylindrical axis and the stress relaxation response to the step and ramp loadings was solved. The solution then was used to derive the biphasic material properties of bovine distal ulnar growth plate from unconfined compression stress relaxation tests [41]. In our study, the initial void ratio and M were estimated by matching Cohen's stress relaxation experimental results to the simulation results obtained from our ABAQUS FE model. After trying different values, for initial void ratio (2-5) and for M (8-18), these parameters were set to the value of 4 and 12 respectively for e_0 and M. It should be mentioned that the exponential component in equation (3-1) simplifies to $exp\ [M\varepsilon_{ij}]$ in the case of small deformations where ε_{ij} stands for dilatation [111]. The simulations were done with the assumption of fully saturated incompressible phases.

Table 3.1: Material properties for the transversely isotropic poroelastic model of growth plate [41]

E_a (MPa)	**E_t (MPa)**	**K_t ($\times 10^{-15}$ m^4/N-s)**	**K_a ($\times 10^{-15}$ m^4/N-s)**	**v_t**	**v_{at}**
0.47±0.11	4.55±1.21	5±1.8	3.4±1.6	0.3±0.2	0

Three different transversal permeabilities; K_t, 10% K_t, 1% K_t were used in the simulations in order to investigate the effect of this parameter on the biomechanical response of the growth plate to the cyclic and static loadings. The axial permeability K_a was kept constant because the upper and lower boundary surfaces were impermeable and, hence, the variation of permeability would have a negligible effect on results compared to the transversal permeability. Figure 3.3 visualizes the permeability factor and impermeable boundary condition. The material properties are different from one species to another and considering three different levels of transversal permeability would help to cover a wide range of this parameter in the simulations.

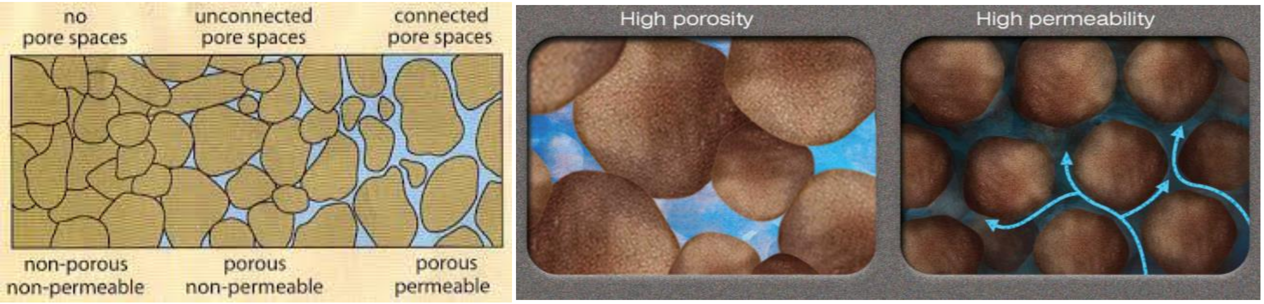

Figure 3.3 : Schematic representation of porosity, permeability and impermeability (obtained on December 19th 2014 from http://petroleum101.com/what-is-a-petroleum-reservoir/ and http://syntropolis.net/knowledgehub/encyclopedia/suitability-of-a-reservoir-for-its-conversion-into-ugs/)

In the poro-elastic constitutive law, the total stress developed in the material is a combination of its effective stress (stress in the solid matrix) and of its pore pressure (pressure in the fluid phase) (equation 3-2). The consolidation theory, which is based on this principle, is widely used for biomechanical modeling of cartilage [112, 113]. In our ABAQUS model, a specific formulation was used in which pores were filled with saturated fluid and temperature was not involved. In addition, the solid matrix and fluid phase were both considered to be incompressible.

$$\sigma^{porous} = \sigma^{effective} - P \tag{3-2}$$

3.1.2 Geometry

An axisymmetric model of the cylindrical sample was developed in ABAQUS. The radius R and height h of the specimen was chosen 2 mm and 3.5 mm respectively based on the Sergerie et al. unconfined compression experiments (Figure 3.4) [42].

In this study, the mesh was done using 180 8-node axisymmetric elements (CAX8P). This type of elements uses quadratic interpolations for the displacement and linear interpolation for the pore pressure.

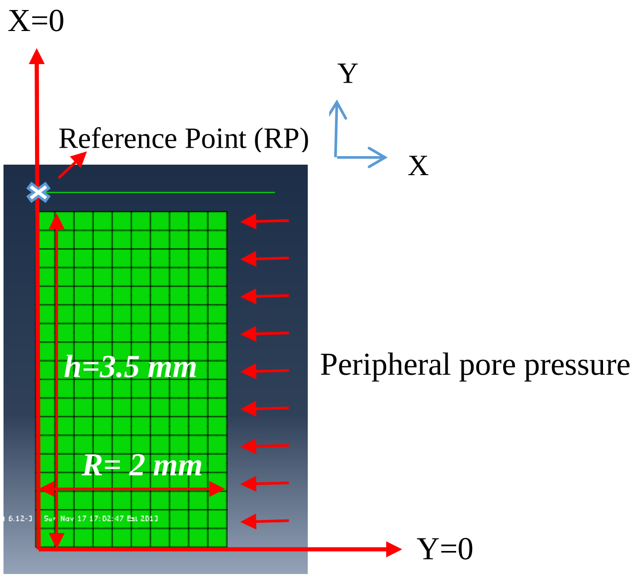

Figure 3.4: Axisymmetric model of growth plate

3.1.3 Boundary and loading conditions

In the axisymmetric model, boundary conditions were modeled as follows: the surface at y=0 was confined in y direction but could expand frictionlessly in the x direction. Both surfaces at y=0 and y=h were assumed to be impermeable. At axis x=0, no fluid flow and displacement along x direction were allowed because of the axisymmetry. Exchange of fluid was allowed only at the peripheral regions of the growth plate. At x=R, two different boundary conditions were investigated. In one condition, a pore pressure of 0.1 MPa was applied to approximate the resistance of the flow by the swelling pressure of the growth plate. This value was believed to be in the reported range for the epidural and intramuscular pressure during activity [114, 115]. In the second condition, it was assumed that there was no resistance to the permeating fluid, resulting in zero peripheral pore pressure. These boundary conditions were prescribed to approximate the possible pathways of fluid transport at the peripheral regions around the growth plates via the ingrowth of blood vessel (Figure 3.5). A rigid surface was placed above the growth plate to apply the uniform compressive loading over the superior surface of the growth plate. A small gap of 2 mm was considered between the rigid surface and the growth plate to facilitate the contact recognition in ABAQUS. The interaction between the rigid surface and the specimen was considered frictionless so that the specimen can freely expand in lateral direction.

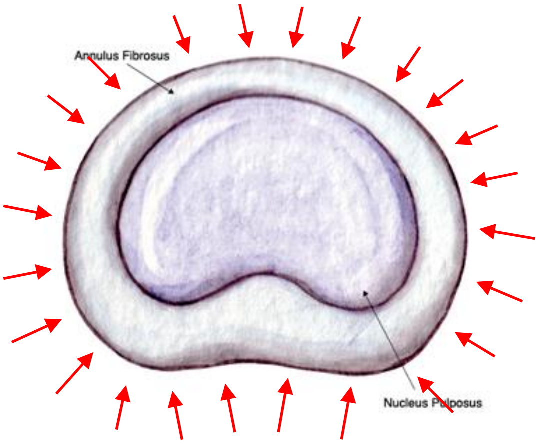

Figure 3.5 : Schematic representation of peripheral pore pressure around disc

A cyclic compressive stress with the average of 0.2 MPa was applied at two different frequencies (0.1 and 1 Hz) and amplitudes (0.2 ±30% and 0.2±70% MPa) for a total of four different conditions, based on a parallel experimental study (Table 3.2, Figure 3.6) [2]. The results were compared to the corresponding sustained static compressive stress of 0.2 MPa.

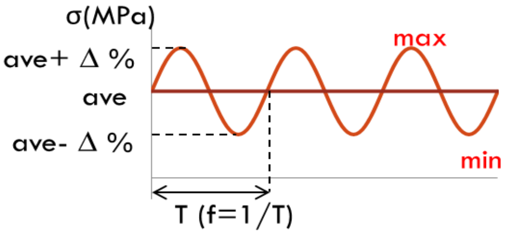

Figure 3.6: Schematic representation of the sinusoidal oscillating compressive loading

The summary of material properties and boundary conditions that were investigated in this study are presented in Table 3.3. The loading conditions were chosen based on an experimental study where the effect of compressive loading frequency and amplitude on the growth rate and growth plate histomorphometry was investigated. The mean value (0.2 MPa) represents a wide physiological stress range that still reduces growth rate but does not arrest it (stress value over 0.6

MPa). The frequency of loading is either low (0.1 Hz) or close to the frequency of physical activities such as walking (1 Hz) [2].

Table 3.2: Summary of compressive loading conditions

Condition	**Average compressive load (MPa)**	**Loading frequency (Hz)**	**Oscillation amplitude (%)**
static	0.2	-	-
(i)	0.2	0.1	30
(ii)	0.2	0.1	70
(iii)	0.2	1	30
(iv)	0.2	1	70

Table 3.3: Summary of investigated material properties and boundary conditions

Condition	**Transversal permeability**	**Peripheral pore pressure**
A	K	0.1 MPa
B	$0.1 \times K$	0.1 MPa
C	$0.01 \times K$	0.1 MPa
D	K	0
E	$0.1 \times K$	0
F	$0.01 \times K$	0

3.1.4 Study 1: Influence of the frequency and amplitude of compressive loading on the stress components and deformation within the growth plate

In the first study, the effects of loading frequency and amplitude were investigated on three stress components (pore pressure, effective stress and total stress) and deformation within the growth plate. Furthermore, the results were compared to the experimental results so one could find the corresponding effective components in the context of growth modulation and growth plate damage.

3.1.5 Study 2: Effect of the peripheral pore pressure on the stress components and deformation within the growth plate

In the second study, the effect of peripheral pore pressure was investigated. Two conditions were examined: peripheral pore pressure of 0.1 MPa and no pore pressure. Then, the stress components in addition to deformation within the growth plate were compared together to conclude about the effect of the presence of peripheral pore pressure. The compressive loads were applied at different frequencies and amplitudes as well as under the static condition.

3.1.6 Study 3: Influence of the transversal permeability on the stress components and deformation within the growth plate

In the third study, a sensitivity study was conducted to analyze the effect of three different transversal permeabilities on the biomechanical response of the growth plate under cyclic and static loadings. The results would be helpful in interpreting experimental results as the poroelastic properties are different from one species to another one.

3.2 Objective 2: Study of the effects of loading conditions on the stress components, principal strains and fluid loss in a finite element model of the functional spinal unit

A 3-D model of a L4-L5 functional unit of the spine, incorporating the coupled pore fluid diffusion/stress analysis in the disc and growth plates, was used for stress and strain analyses in cartilaginous tissues. The details regarding the geometry, material properties, loading and boundary conditions are presented in following sections:

3.2.1 Material properties:

The nucleus, annulus, growth plates, and cancellous bone were modeled as poroelastic materials whereas the cortical bone was modeled as a linear elastic material [21]. The material properties were the same as Argoubi et al. study [111] and are listed in the Table 3.4.

Table 3.4: Material properties for the L4/L5 motion segment [111]

Component	**Drained Young modulus *E* (MPa)**	**Poisson ratio v**	**Initial void ratio e_0**	**Initial permeability K_0 ($\times 10^{-15}$ m^4/Ns)**	***M***
Nucleus	1.5	0.1	4.00	0.3	12
Annulus matrix	2.5	0.1	2.33	0.11	10
Cancellous bone	100	0.2	0.4	100	18
Cortical bone	12000	0.3	-	-	-
Annulus fibers	500	0.3	-	-	-
Growth plates	E_t=4.5 E_a=0.47	v_t=0.3 v_{at}=0	4	K_t=5 K_a=3.4	12

3.2.2 Geometry

This model developed in another project [21] using a commercially available FE software (ABAQUS v6.12-3, Dassault Systèmes, Providence, RI, USA) was used. The original model consisted of vertebral bodies (cortical and cancellous bones), disc (nucleus and annulus) and endplates. In this study, the growth plates were integrated to the model and the linear biphasic elements were substituted by nonlinear elements. A primary transverse geometry of the disc was created using CT scans of the Visible Human Project database in combination with parametric equations developed by Little et al. [116]. The cross-sectional area of the disc was set to be 2000 mm^2 in the resulting geometry using a scaling factor [117]. A percentage of 40% of the cross sectional area was devoted to the nucleus pulposus and positioned with the posterior offset of 3 mm from its original centered position [118]. Hypermesh (version 12.0, Altair HyperWorks Inc., Minnesota) was used to generate mapped mesh in the model. The volumetric parts of the model (the annulus, nucleus, growth plates, and cancellous bone) were modeled using three-dimensional twenty node elements (C3D20RP). This type of elements uses quadratic interpolations for the displacement and linear interpolation for the pore pressure and adopts reduced integration method as well. Four-node shell elements were used for modeling of the cortical bone with a thickness of 1 mm [118, 119]. The large displacement feature was activated to take into the account the geometric nonlinearities since the lumbar segments even under moderate loads undergo large displacements and strains [21]. The axial geometry of the disc was assumed with an initial bulge and height of 1 mm and 8 mm respectively [118, 120]. The annulus fibrosus was considered as a matrix of homogenous ground material reinforced by fibers, which took up 15% of the volume [121, 122]. Collagen fibers were oriented at ±30° with respect to the transversal plane in eight annular layers [123]. They were represented with a quasi-linear viscoelastic theory developed by Lu et al. and Lee et al. [121, 123]. The stress relaxation function in fibers was presented as $\sigma(\varepsilon, t) = G\,(t) \times E_0\varepsilon_0$ where E_0 is the instantaneous elastic modulus and ε_0 is the applied strain. G(t) is the reduced relaxation function developed from experimental results by Yahia et al. [124];

$$G(t) = G_0\left[1 - \sum_{i=1}^{N} g_i\left(1 - e^{-t/\tau_i}\right)\right] \qquad 3\text{-}3$$

where G_0 is the instantaneous stress relaxation modulus and g_i and τ_i are the Prony series constants. The thickness of the growth plates was set to 2 mm. The growth plates were assumed to be parallel to each other to minimize the effect of combined loads, which would be generated if the disc was wedged. The height of the vertebral bodies (L4 and L5) were assumed to be 25 mm (Figure 3.7) [125].

3.2.3 Boundary and loading conditions

In all simulations, the inferior surface of L5 was completely constrained and a uniform pressure was applied on the superior surface of L4 with the constant average amplitude of 0.2 MPa. The simulations were done for both static and cyclic loadings. In cyclic simulations, a sinusoidally oscillating compressive stress (0.2 ±30% MPa and 0.2 ±70% MPa) was applied at two different frequencies (0.01 and 1 Hz) (Table 3.2, Figure 3.6). The loading parameters, frequency and amplitude, were chosen based on a parallel experimental study [1].

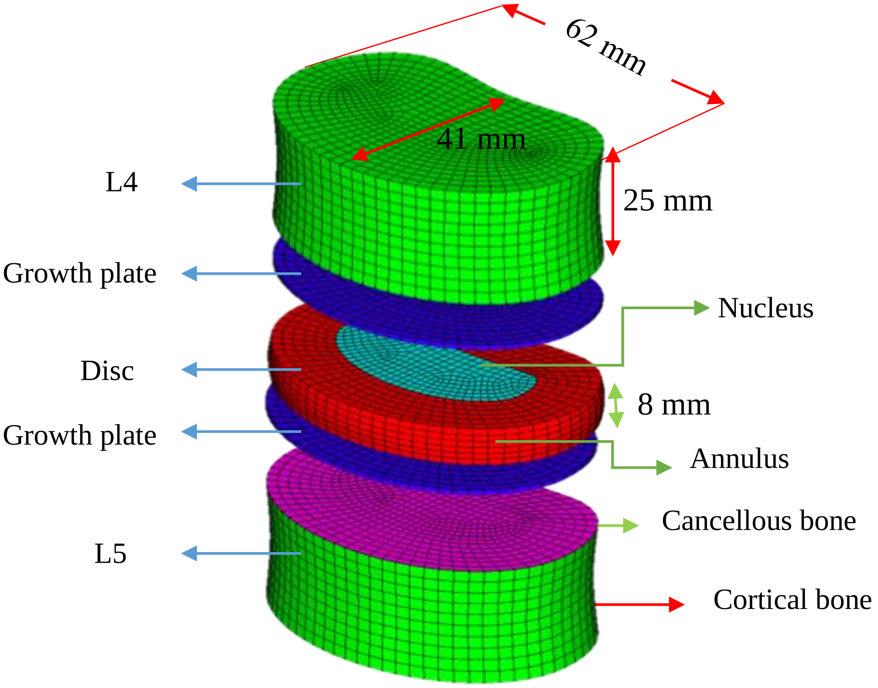

Figure 3.7: Detailed geometry of the spinal functional

Fluid exchange was only allowed through the peripheral regions of the annulus fibrosus and growth plates as well as the interface between the growth plates and the disc. The boundary pore pressure at the peripheral regions of the disc and growth plates was assumed to be 0.1 MPa to approximate the resistance of the flow by the epidural and swelling pressure of the disc [115, 126, 127].

3.2.4 Study of the influence of the frequency and amplitude of compressive loading on the stress components, principal strains and fluid loss within the growth plates, nucleus and annulus

This study was done to provide more insights about developing stress components, principal strains and fluid loss in the growth plates, nucleus and annulus using the developed functional spinal unit under cyclic vs. static compressive loadings. In this section, the effect of cyclic loading frequency and amplitude on the aforementioned parameters were studied and results were compared to the static loading. The boundary conditions were more realistically modeled compared to the axisymmetric models so the results helped to find out how accurately the geometrically simplified axisymmetric models can predict the desired information. In this model, the exchange of fluid between the different parts (disc, growth plates, and vertebral bodies) was incorporated and its effect on the results were investigated.

CHAPTER 4: RESULTS

This chapter presents the results of this research project. The first section is devoted to the results of the first objective, where the effects of loading and boundary conditions as well as material properties on the stress components and deformation were studied using an axisymmetric model of the growth plate. The second section of Chapter 4 presents the results of simulations for the functional unit of the spine, where developed stress components and principal strains as well as fluid loss in growth plates and disc (nucleus and annulus) were analyzed.

4.1 Effects of material properties, loading and boundary conditions on the developing stress and deformation using a biphasic axisymmetric finite element model of growth plate (Objective 1)

4.1.1 Influence of the frequency and amplitude of compressive loading on the stress components and deformation within the growth plate

In this study, stress components and deformation within the growth plate were investigated for five cases of different frequencies and amplitudes of compressive loading. As presented in Chapter 3, simulations were also done for six different combinations of boundary conditions and material properties (Table 3.3).

Results can be seen in Figure 4.2 to Figure 4.8, with curves smoothed with the moving average method to facilitate the analyses. For comparison, a sample of original results (without smoothing) can be seen in Figure 4.1, which shows the effective stress curves between times 1500 and 1530 s in condition A for the static case and four cyclic cases. The influence of the loading frequency and amplitude on the aforementioned parameters is discussed for each condition separately in the following sections.

4.1.1.1 Condition A

In condition A, the transversal permeability was K (5×10^{-15} m^4/N-s) and the peripheral pore pressure was set at 0.1 MPa while the loading conditions were according to Table 3.2. Figure 4.2 shows time histories of the stress components and displacement in the growth plate. The simulations were aimed to be done for a duration of one hour but combined high frequency and amplitude loading conditions encountered convergence problem. It was tried to solve the problem by mesh refinement but convergence could not be improved. Hence, results for condition A are presented for the duration of 2500 s instead of 3600 s.

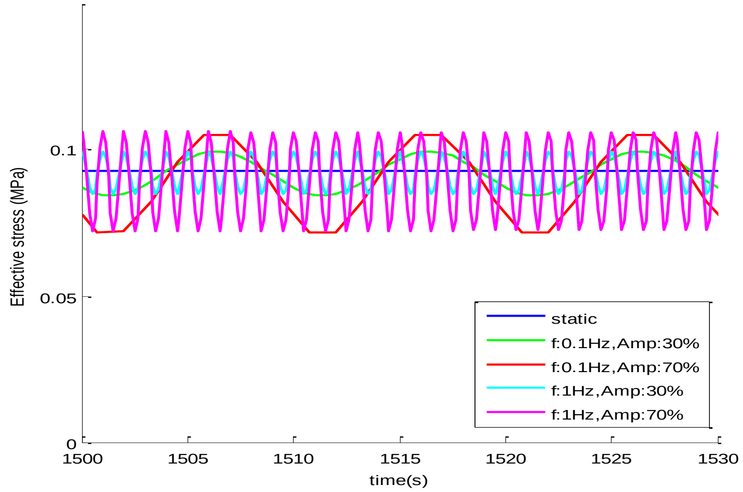

Figure 4.1: Original sinusoidal results for effective stress diagrams between times 1500 and 1530 s for condition A for the static case and four dynamic cases

The pore pressure increased up to 0.175 MPa and then took a declining trend until it stabilized around 0.1 MPa (Figure 4.2a). The effective stress showed an overall increasing trend from 0.025 MPa to ~0.08 MPa (Figure 4.2b). The positive effective stress corresponded to a compressive stress in the tissue. The total stress, which is the summation of effective stress and pore pressure, increased to reach a peak value of (~ 0.21 MPa) and then decreased to eventually stabilize at around 0.18 MPa (Figure 4.2c). The displacement showed an increasing trend indicating more compression of the tissue with time (Figure 4.2d). It reached the displacement of 0.6 mm at the end of the loading period. All curves showed very similar trend for the five loading conditions, except locally around the peak values for the pore pressure and total stress. These differences can be observed in the magnified subfigures.

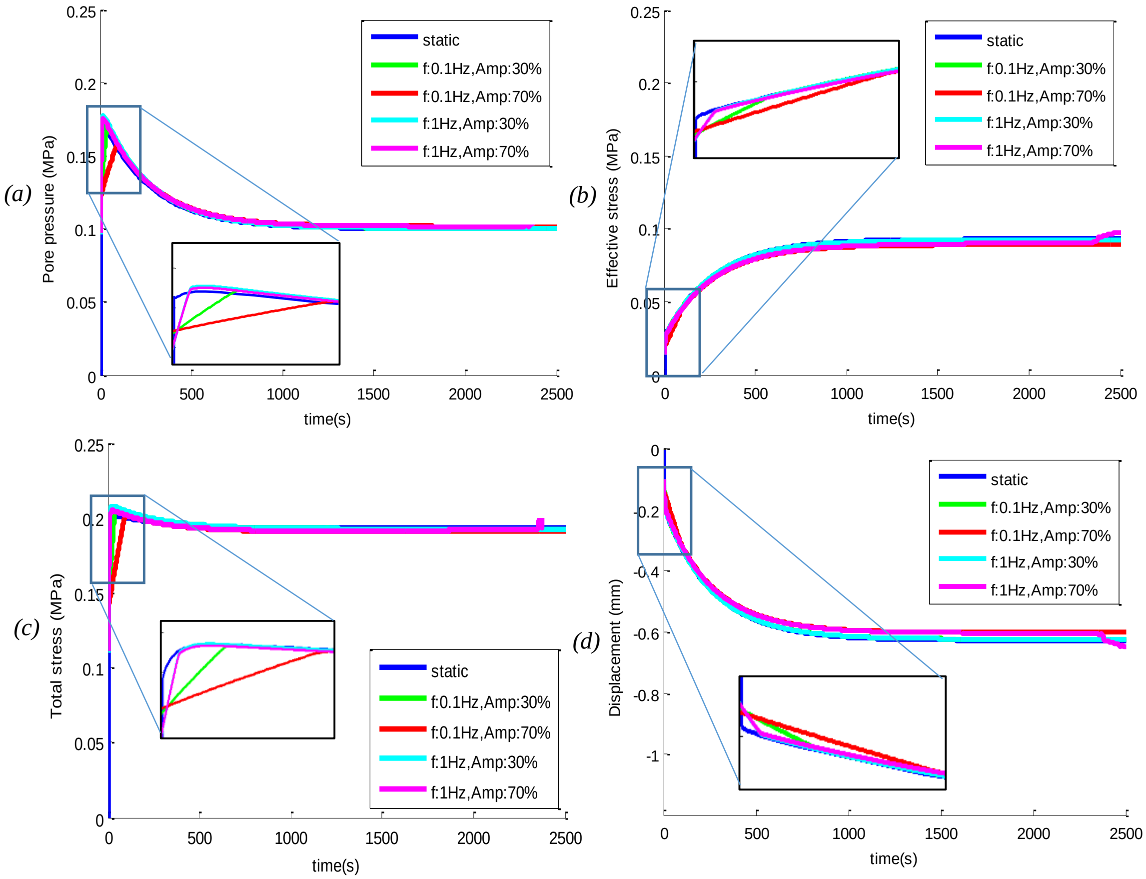

Figure 4.2: Time histories of a) pore pressure b) effective stress c) total stress d) displacement in the growth plate for condition A

Figure 4.3 shows the pore pressure, effective stress, fluid volume ratio and the deformation magnitude within the growth plate. As it can be seen, the pore pressure was higher at the central area compared to the peripheral area at the beginning. The pressure reduced with time and the distribution unifies at the end of loading period (Figure 4.3a). The effective stress showed a uniform distribution and a stress concentration was seen close to the rigid surface and peripheral area. The effective stress level increased with time (Figure 4.3b). The upper surface of growth plate underwent more deformation compared to the lower surface, which increased with time (Figure 4.3c)

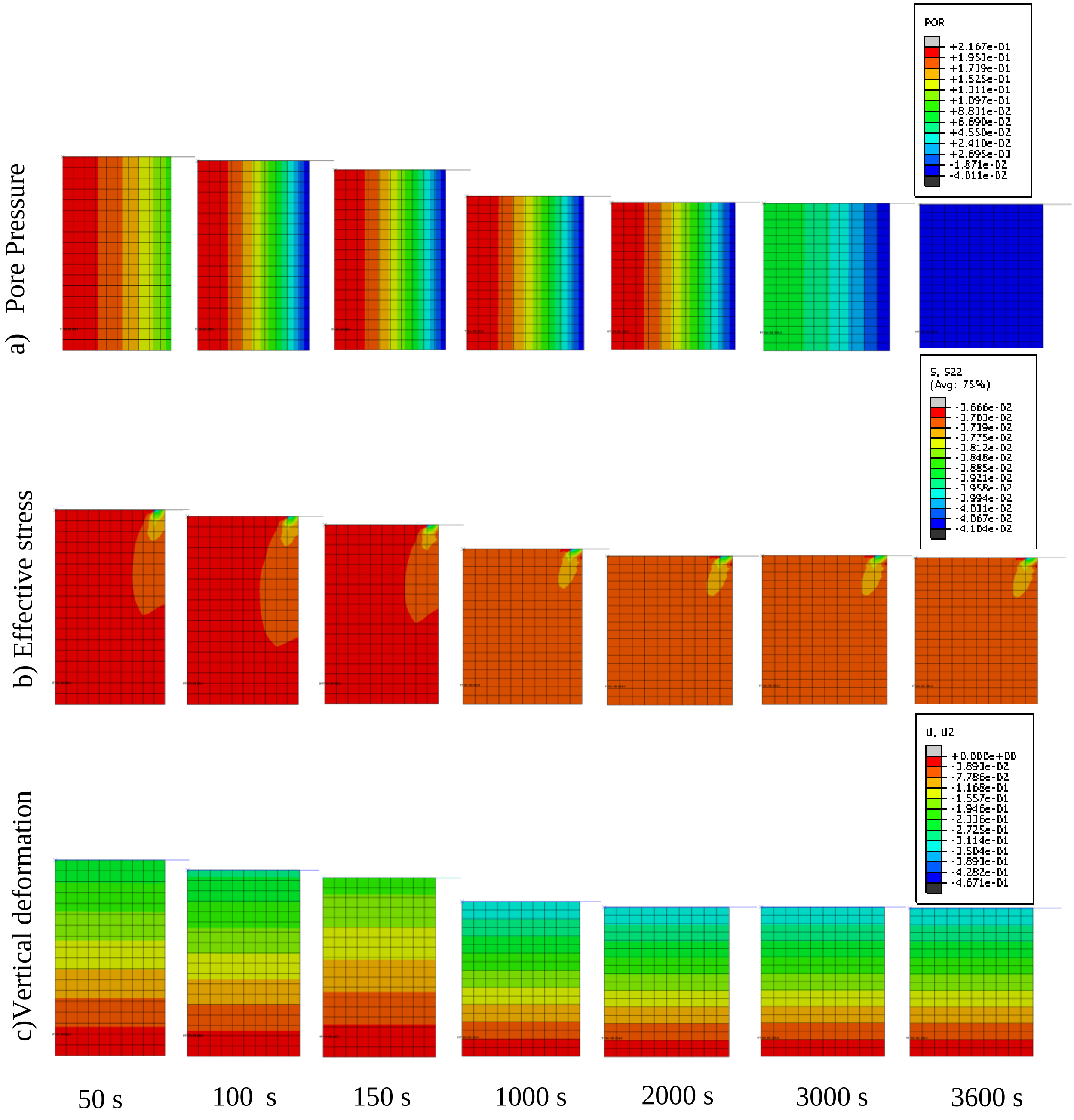

Figure 4.3 : a) Pore pressure b) effective stress c) vertical deformation within the growth plate at 50, 100, 150, 1000, 2000, 3000 and 3600 s

4.1.1.2 Condition B

In condition B, the transversal permeability was reduced to 10% K (with K=5×10^{-15} m^{4}/N-s) while the other conditions were kept like in condition A (peripheral pore pressure of 0.1 MPa).

Loading conditions were as listed in Table 3.2. Stress components (pore pressure, effective stress and total stress) as well as displacement graphs can be seen in Figure 4.4.

Both static and cyclic loadings showed the same decreasing trend for pore pressure (Figure 4.4a). Cyclic conditions developed slightly less pore pressure at the beginning of the loading but they converged to the amount of 0.12 MPa like with the static condition at the end of the loading period. The effective stress was almost the same for static and cyclic loading conditions (Figure 4.4b). After the first initial spike, the effective stress gradually increased to reach the value of 0.75 MPa at the end of the loading period. The total stress followed the same trend in all loading conditions, however, its magnitude was slightly different (Figure 4.4c). The total stress gradually decreased over time from 0.22 MPa to 0.2 MPa with a very slow rate. The displacement gradually increased under compressive loading from 0.2 to 0.5 mm over the time (Figure 4.4d). All loading conditions had their ultimate displacement at -0.5 mm.

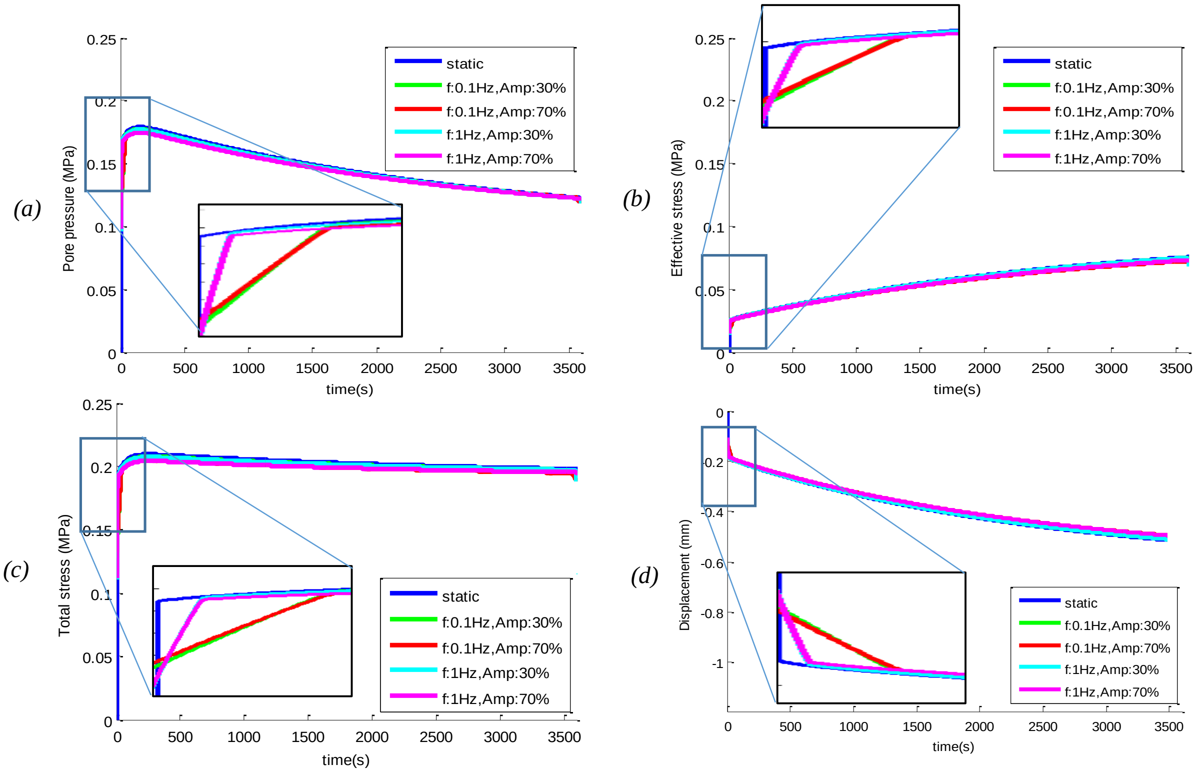

Figure 4.4: Time histories of a) pore pressure b) effective stress c) total stress d) displacement within growth plate for condition B

4.1.1.3 Condition C

In condition C, the transversal permeability was reduced to 1 % of the experimentally measured value *K* (with K=5×10^{-15} m^4/N-s) and other conditions remained unchanged (peripheral pore pressure of 0.1 MPa). The same five loading conditions listed in Table 3.2 were simulated. Stress components as well as displacement graphs are shown in Figure 4.5.

The rate of change in stresses and displacement was very slow. In addition, different loading conditions showed very close curves, which made it difficult to distinguish them. In this condition, the pore pressure had an almost constant level at ~ 0.17 MPa (Figure 4.5a) while the effective stress increased with a very slow rate from 0.025 MPa to 0.03 MPa (Figure 4.5b). The total stress increased at the beginning of compression to 0.22 MPa and then reduced to 0.18 MPa at the end of loading (Figure 4.5c).

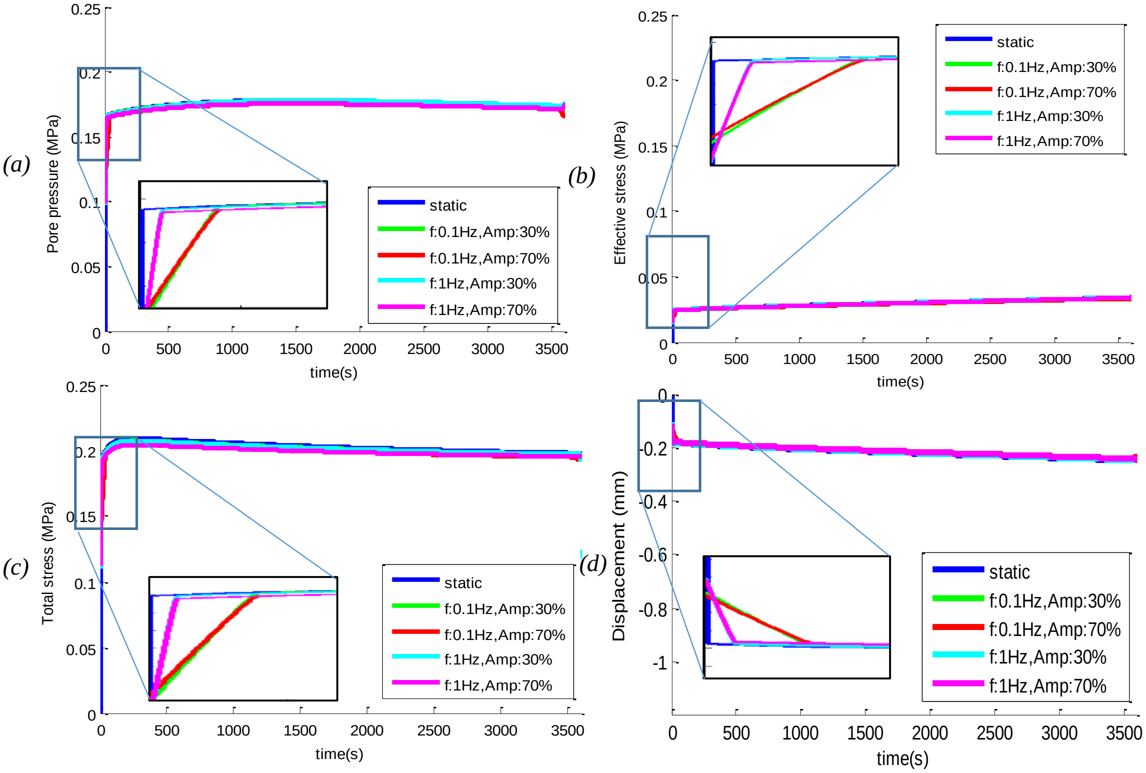

Figure 4.5: Time histories of a) pore pressure b) effective stress c) total stress d) displacement within growth plate for condition C

Furthermore, the height of the growth plate decreased with a slow rate from 0.19 mm to 0.21 mm (Figure 4.5d). In spite of similar trends and values for the five loading conditions, they showed slightly different behavior at the beginning of the compressive loading (magnified subfigures).

4.1.1.4 Condition D

Results for condition D are presented in Figure 4.6. In this condition, the material properties were applied as reported in the literature (transversal permeability of K=5×10^{-15} m^4/N-s). The peripheral pore pressure was set to zero, which means there was no resistance against the fluid flow in the peripheral direction. Furthermore, the simulations were done for the same five loading conditions (Table 3.2).

The pore pressure increased quickly up to 0.2 MPa and then took a descending trend to reach 0.02 MPa at the end of the loading period. The rate of change was high at first and slowed down afterwards (Figure 4.6a). The effective stress kept increasing gradually shortly after the initial spike with a fast rate in the first 500 s (Figure 4.6b). It reached 0.18 MPa at the end of the loading time. The total stress showed an initial spike where the stress went up to 0.225 MPa and then gradually decreased to reach 0.2 MPa (Figure 4.6c).

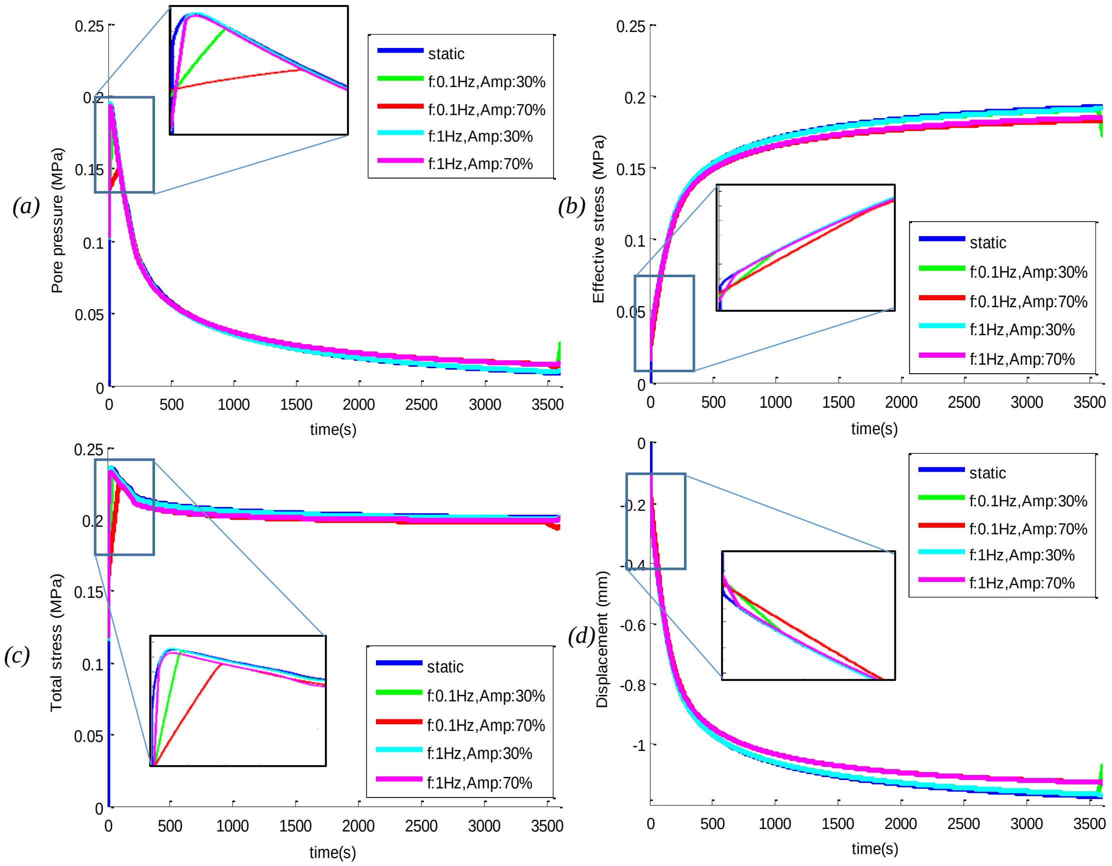

Figure 4.6: Time histories of a) pore pressure b) effective stress c) total stress d) displacement within growth plate for condition D

Displacement curves had a fast rate of decrease at the beginning and the rate of change slowed down afterwards (Figure 4.6d). The ultimate displacement was around 1.2 mm for all loading conditions. Results were not sensitive to the loading frequency and amplitude. The only difference appeared in the first 200 s, which was shown in the magnified subfigures.

4.1.1.5 Condition E

The results for condition E are shown in Figure 4.7. In this condition, the transversal permeability was reduced to 10 % of the measured values reported in the literature *K* (with $K=5\times10^{-15}$ m^4/N-s) and there was no pore pressure on the peripheral surface, which allowed fluid to expel out freely. Loading conditions remained the same and were summarized in Table 3.2.

Pore pressure graphs can be seen in Figure 4.7a. They quickly ascended to reach the peak pressure of 0.2 MPa and then gradually descended to the level of 0.075 MPa at the end of the loading period.

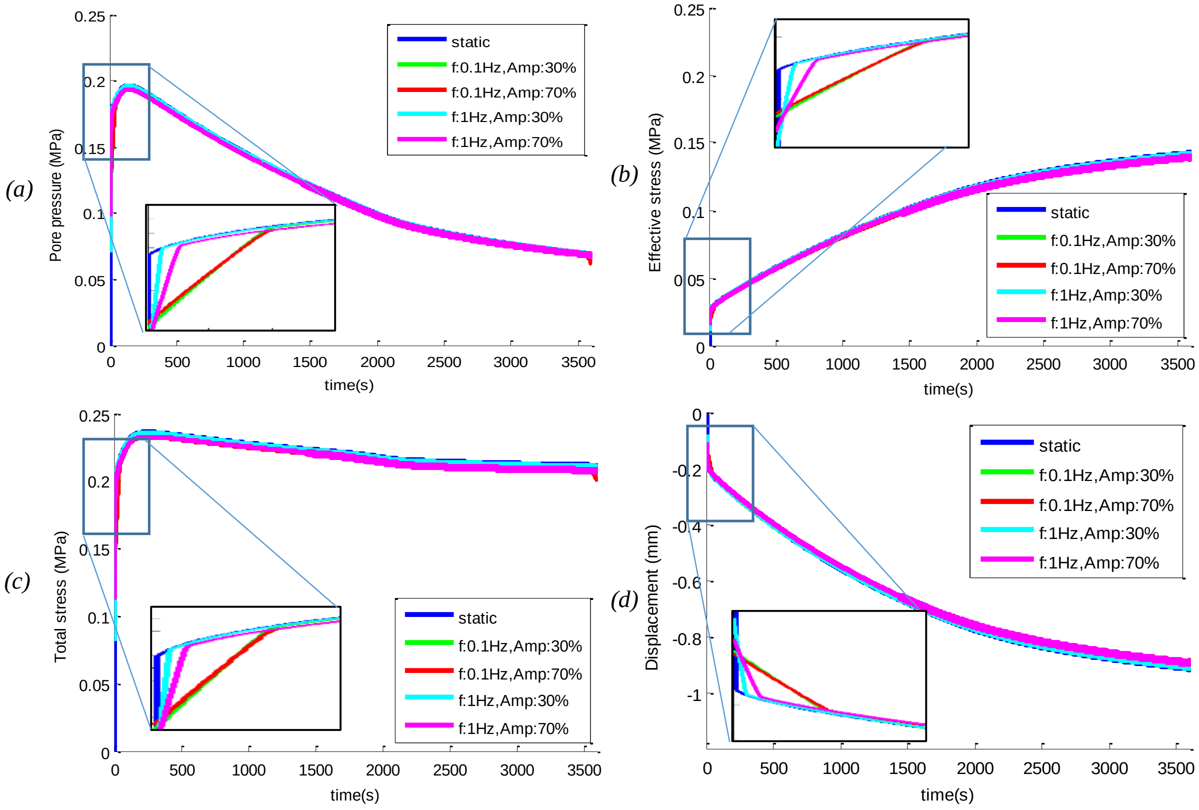

Figure 4.7: Time histories of a) pore pressure b) effective stress c) total stress d) displacement within growth plate for condition E

Effective stress curves increased progressively over time to reach their max value of 0.13 MPa at the end of the loading period (Figure 4.7b). The total stress increased over a short period of time to attain the peak value (0.23 MPa) and then gradually decreased to the level of 0.22 MPa (Figure 4.7c). Displacement graph followed a descending trend over time from 0.2 mm to 0.98 mm (Figure 4.7d). In general, the stress components and displacement showed no sensitivity to the loading frequency and amplitude. The only observed difference was related to their sequence in reaching the peak point at the beginning of the loading, which can be seen from magnified subfigures.

4.1.1.6 Condition F

Figure 4.8 shows the stress components and displacement graphs in condition F. In this condition, the transversal permeability was reduced to 1 % of the experimentally measured permeability *K* (with $K=5\times10^{-15}$ m^4/N-s) and the peripheral pore pressure was set to zero. The five loading conditions listed in Table 3.2 were simulated.

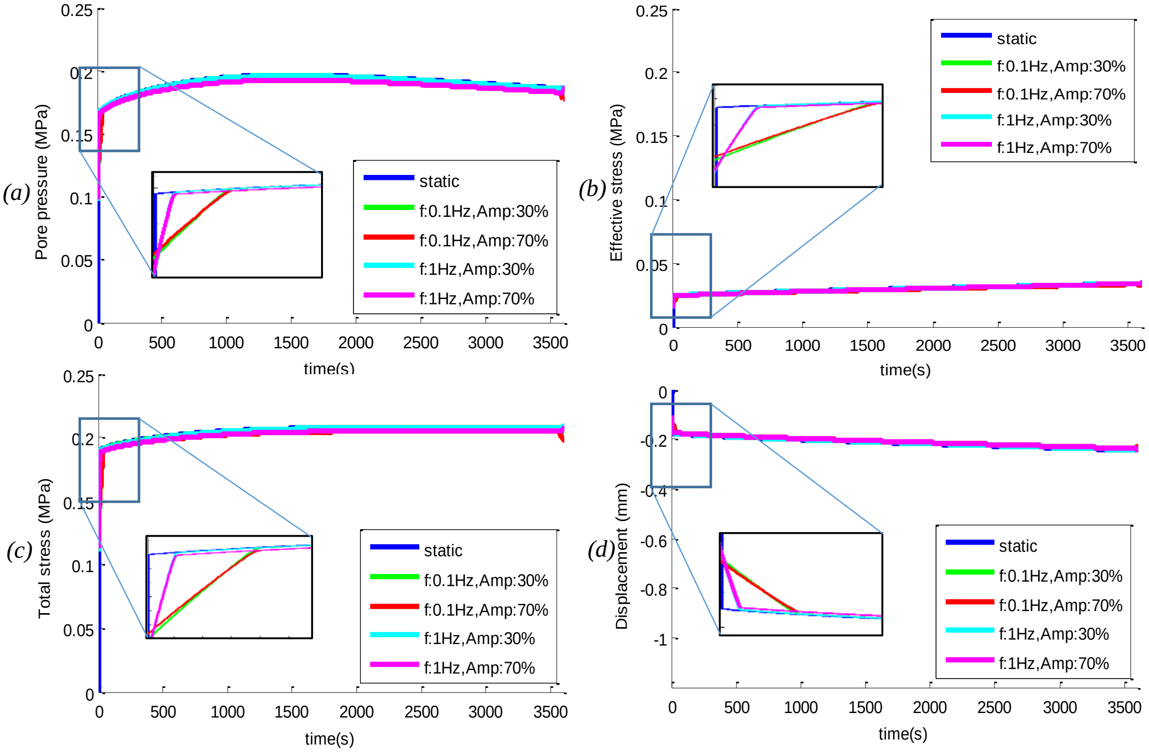

Figure 4.8: Time histories of a) pore pressure b) effective stress c) total stress d) displacement within growth plate for condition F

As it can be seen in Figure 4.8, no relaxation behavior could be seen. All loading conditions showed very close stress components and deformation curves with almost no sensitivity to the loading frequency and amplitude. In addition, the rate of change was very slow in both stresses and displacement graphs. The pore pressure first had an increasing trend and then eventually stabilized at ~ 0.18 MPa. The effective stress had an almost constant level around 0.025 MPa. The total stress first increased to reach the maximum value and then stabilized at 0.2 MPa. The displacement had an increasing trend with a very slow rate from 0.18 mm to 0.22 mm. Different loading conditions showed different behavior at the beginning of the loading, which can be seen in the magnified subfigures.

4.1.2 Effect of the peripheral pore pressure on the stress components and deformation within the growth plate

4.1.2.1 Comparison between conditions A and D

In this section, conditions A and D were compared in terms of the pore pressure, effective stress, total stress and displacement. In these conditions, the transversal permeability was set to K (5×10^{-15} m^4/N-s) and was combined with a peripheral pore pressure of 0.1 (condition A) or no pore peripheral pore pressure (condition D). The pore pressure showed higher peak stress in the absence of peripheral pore pressure (0.2 MPa vs. 0.175 MPa). Furthermore, the pore pressure decreased faster when no pressure was applied on the boundary surface as it reached the value of 0.02 MPa comparing to 0.1 MPa in presence of peripheral pore pressure at the end of the loading period (Figure 4.9a).

The tissue experienced a higher level of effective stress when there was no resistance against fluid to drain out. It reached the value of 0.18 and 0.08 MPa respectively in the absence and presence of the peripheral pore pressure at the end of the loading period (Figure 4.9b). The total stress was similar for both conditions. However, the condition with a peripheral pore pressure of 0.1 MPa showed a slightly lower peak stress (0.2 MPa vs. 0.23 MPa). In addition, the total stress was 0.18 and 0.2 MPa respectively in the presence and absence of peripheral pore pressure at the end of the loading period (Figure 4.9c). When there was no pressure on the boundary surface, the height of the tissue decreased more than the other condition. The displacement at the end of loading was 0.6 and 1.1 mm respectively for the condition with the pore pressure of 0.1 and 0 MPa (Figure 4.9d).

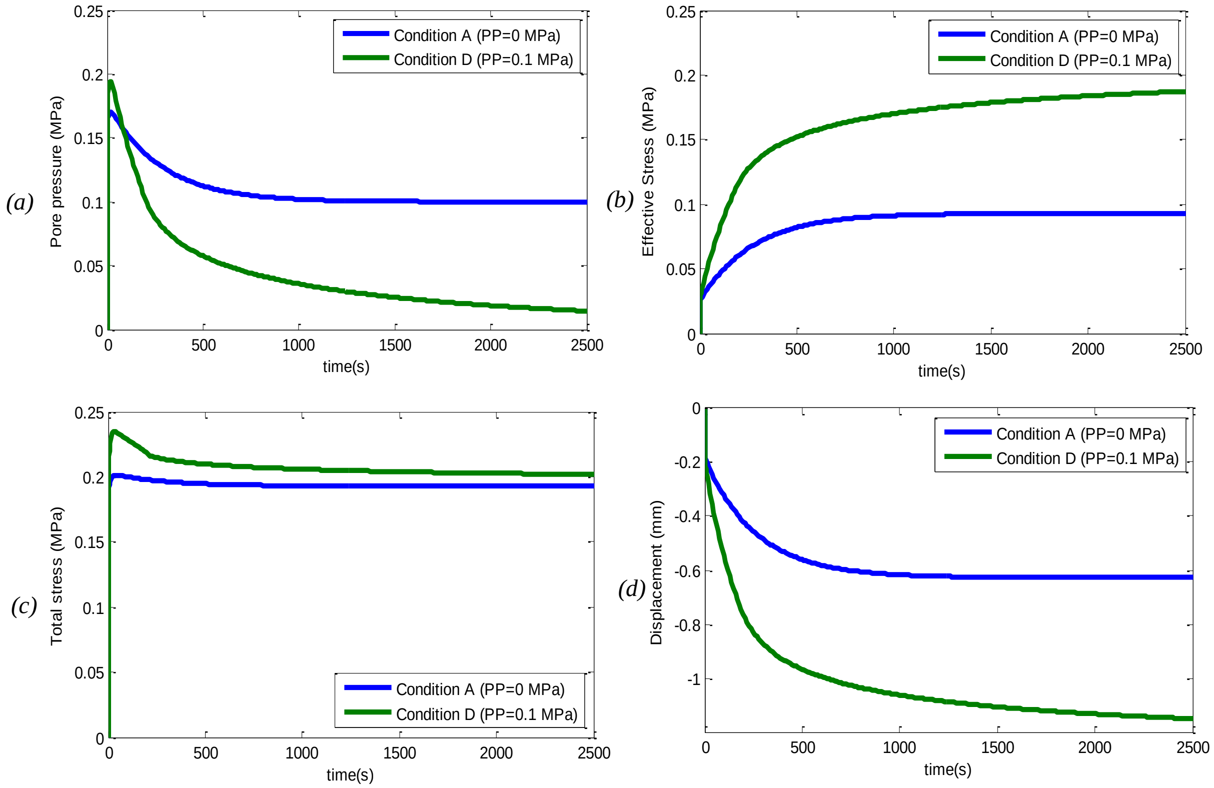

Figure 4.9: Comparison between conditions A and D: a) pore pressure b) effective stress c) total stress d) displacement

4.1.2.2 **Comparison between conditions B and E**

In this section, conditions B and E were compared in terms of pore pressure, effective stress, total stress and displacement. In both conditions, the transversal permeability was reduced to 10 % *K* (with $K=5\times10^{-15}$ m^4/N-s) while peripheral pore pressure was set to 0.1 MPa for condition B and to 0 MPa for condition E. The pore pressure showed a lower peak and higher relaxed stress levels in the presence of peripheral pore pressure, 0.18 vs. 0.2 MPa and 0.125 vs. 0.07 MPa respectively for the peripheral pore pressure of 0.1 and 0 MPa (Figure 4.10a). In the absence of peripheral pore pressure, the contribution of the solid matrix in sustaining the load was more important (64% vs. 37.5 %) (Figure 4.10b). The initial peak in the total stress was more pronounced in the absence of the peripheral pore pressure and the total stress was slightly higher than the condition with peripheral pore pressure of 0.1 MPa at the end of the loading period (0.21 vs. 0.19 MPa) (Figure 4.10c). In the absence of peripheral pore pressure, the tissue underwent a higher level of deformation, -0.9 vs. -0.5 mm respectively with peripheral pore pressure of 0 and 0.1 MPa, at the end of the loading (Figure 4.10d).

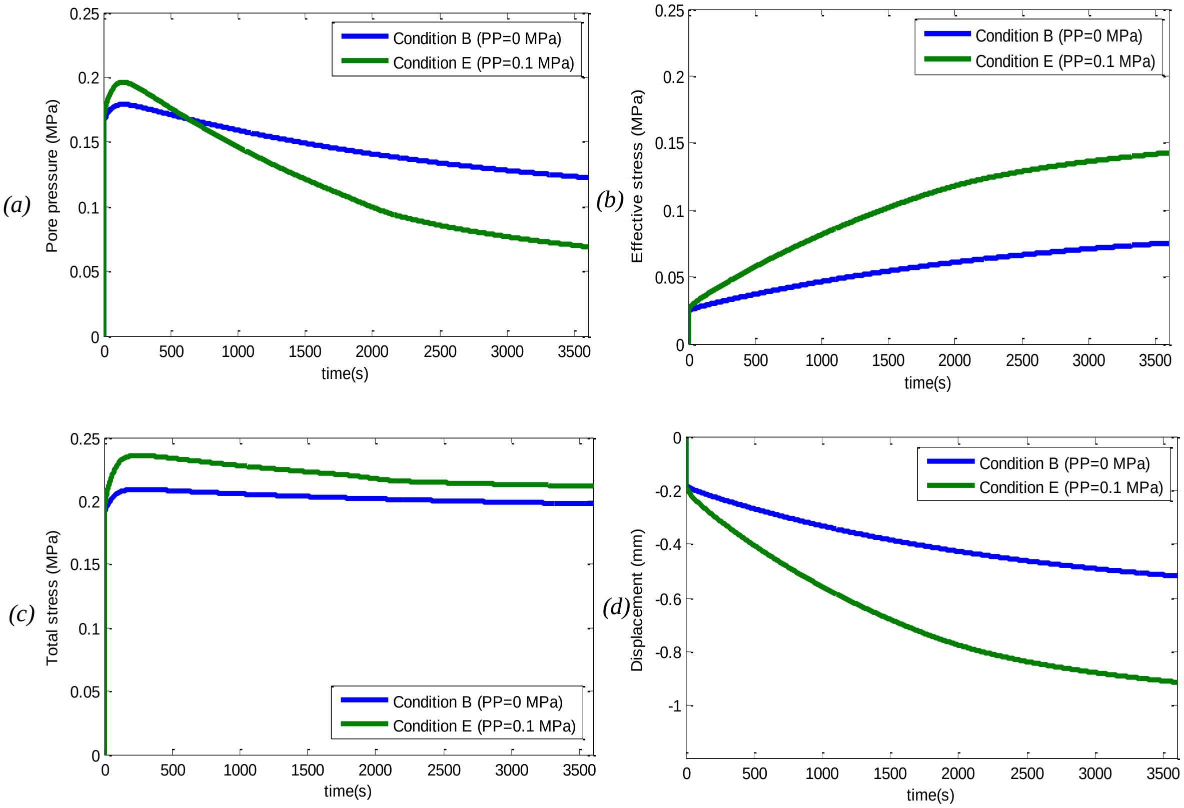

Figure 4.10: Comparison between conditions B and E: a) pore pressure b) effective stress c) total stress d) displacement

4.1.2.3 Comparison between conditions C and F

In this section, conditions C and F were compared. In these conditions the transversal permeability was reduced to the 1 % K (with K=5×10^{-15} m^{4}/N-s) while the peripheral pore pressure was set to 0.1 MPa for condition C and to 0 MPa for condition F. The pore pressure trends were similar with the peripheral pore pressure of 0 or 0.1 MPa. The pore pressure was however a little higher in the absence of peripheral pore pressure (0.185 MPa vs. 0.175 MPa)(Figure 4.11a). The effective stress at the end of the loading period was 0.03 vs. 0.05 MPa respectively in the presence and absence of boundary pore pressure (Figure 4.11b). The total stress was almost the same in the presence and absence of the pressure on the boundary surface. It showed the stress of 0.21 MPa vs. 0.23 MPa at the end of loading period (Figure 4.11c). The tissue experienced more deformation when there was no peripheral pore pressure and hence the height of tissue decreased more (-0.35 mm) in that condition compared to the one with pore pressure (-0.25 mm) (Figure 4.11d).

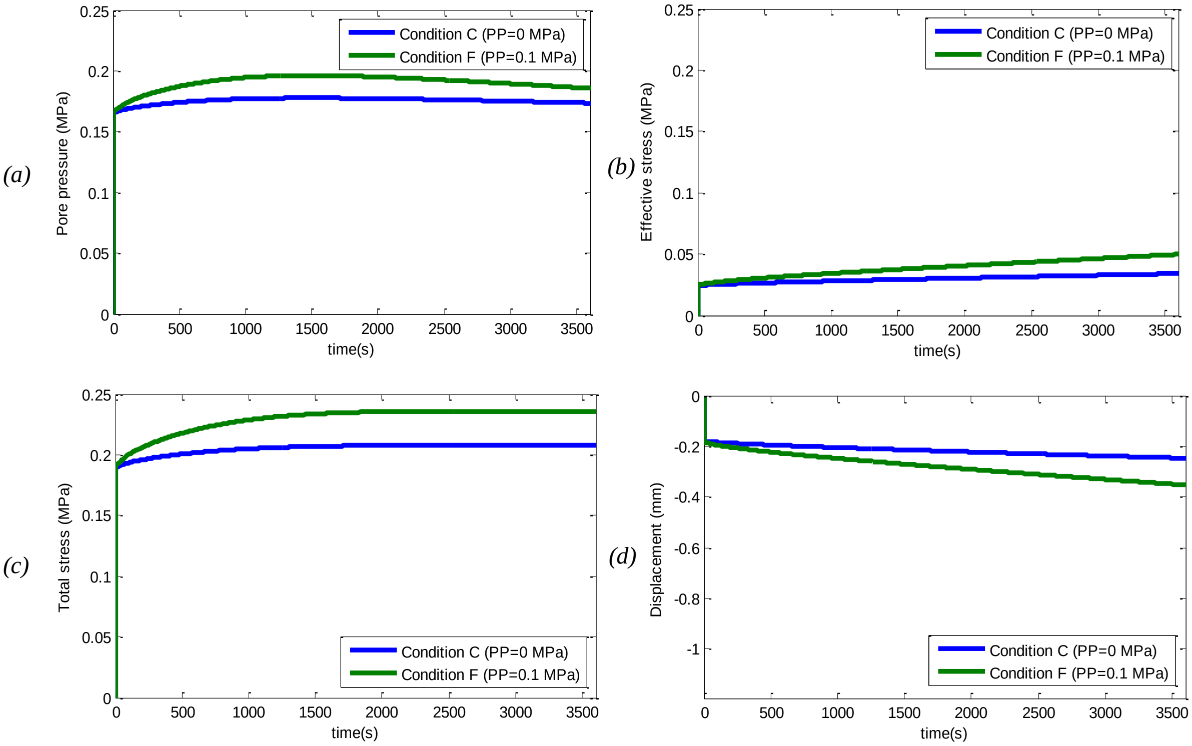

Figure 4.11: Comparison between conditions C and F: a) pore pressure b) effective stress c) total stress d) displacement

4.1.3 Influence of the transversal permeability on the stress components and deformation within the growth plate

4.1.3.1 Comparison among conditions A, B and C

In this section, the effect of the transversal permeability on the pore pressure, effective stress, total stress and displacement was studied. The transversal permeability was set to *K*, 10% *K*, 1% *K* (with *K*=5×10^{-15} m^4/N-s) respectively in conditions A, B and C with the peripheral pore pressure of 0.1 MPa. The pore pressure at the end of loading (relaxed pore pressure) was increased with the reduction in the transversal permeability to reach 0.1, 0.125 and 0.175 MPa respectively for permeability of *K*, 10% *K* and 1% *K*. (Figure 4.12a). In the transversal permeability of 1% *K*, the pore pressure had an increasing trend while it was decreasing in the two other conditions. The effective stress showed increasing trends for all three conditions.

However, reduced equilibrium values were observed with reduced transversal permeability, respectively 0.09, 0.075 and 0.03 MPa for the permeability of *K*, 10% *K* and 1% *K* (Figure 4.12b). The total stress was not much influenced by transversal permeability compared to the two other stress components. The total stress at the end of loading was 0.19, 0.2 and 0.21 MPa for the permeability of *K*, 10% *K* and 1 % *K* respectively (Figure 4.12c). The tissue deformation showed decreasing trends over time and reduced equilibrium values with reduced transversal permeability (-0.6, -0.5 and -0.25 mm respectively for the highest to the lowest permeability) (Figure 4.12d).

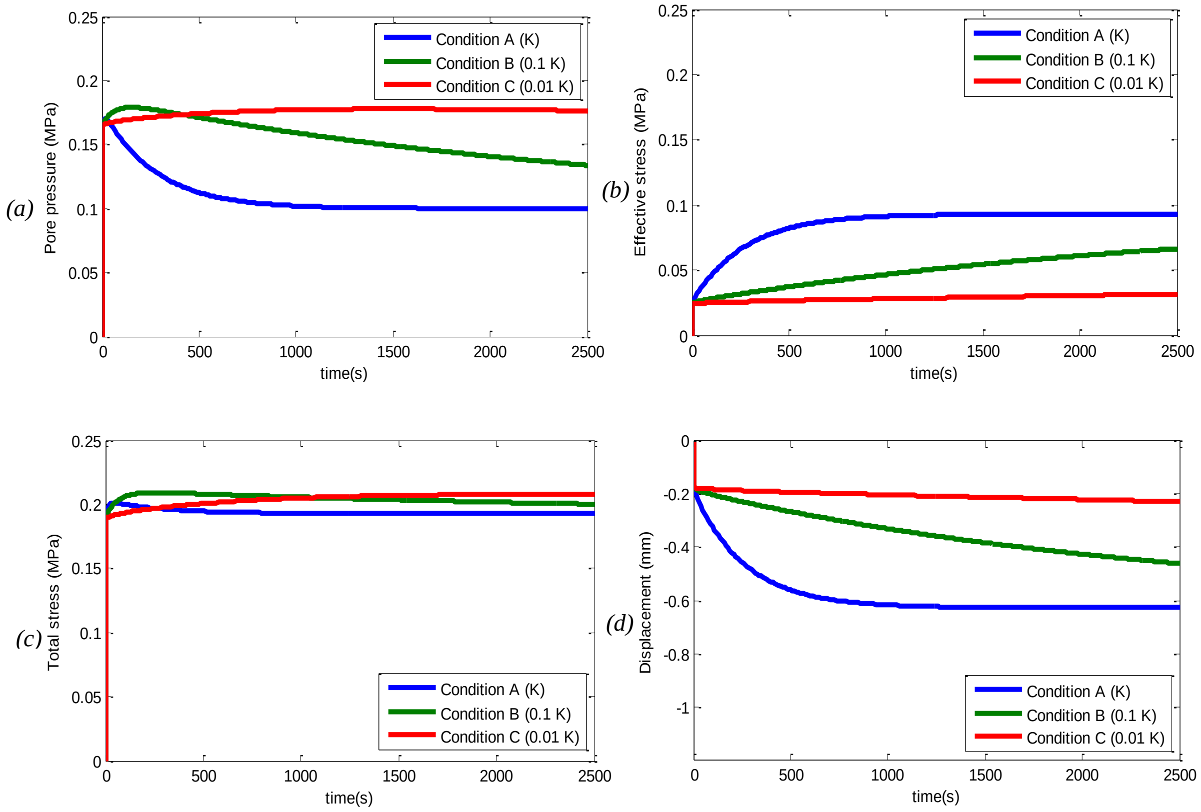

Figure 4.12: Comparison among conditions A, B and C: a) pore pressure b) effective stress c) total stress d) displacement

4.1.3.2 **Comparison among conditions D, E and F**

In this section, the effect of transversal permeability was studied in the absence of the peripheral pore pressure. The transversal permeability was set to *K*, 10% *K* and 1% *K* (with $K=5\times10^{-15}$ m^4/N-s) respectively in conditions D, E and F with no peripheral pore pressure for all three conditions. The pore pressure showed a pressure of 0.02, 0.07 and 0.18 MPa respectively for the highest to the lowest transversal permeability (Figure 4.13a). Condition F (1 % *K*) had an increasing trend while conditions E and F had decreasing trends. The effective stress decreased with reduced transversal permeability; 0.18, 0.13 and 0.05 MPa were respectively the stress levels for the permeability of *K*, 10% *K* and 1% *K* at the end of the loading (Figure 4.13b). The total stress was 0.23, 0.21 and 0.2 MPa respectively for the transversal permeability of *K*, 10% *K* and 1% *K* (Figure 4.13c). The deformation of tissue decreased with reducing the permeability (-1.18, -0.9 and -0.35 mm respectively for the lowest to highest permeability) (Figure 4.13d).

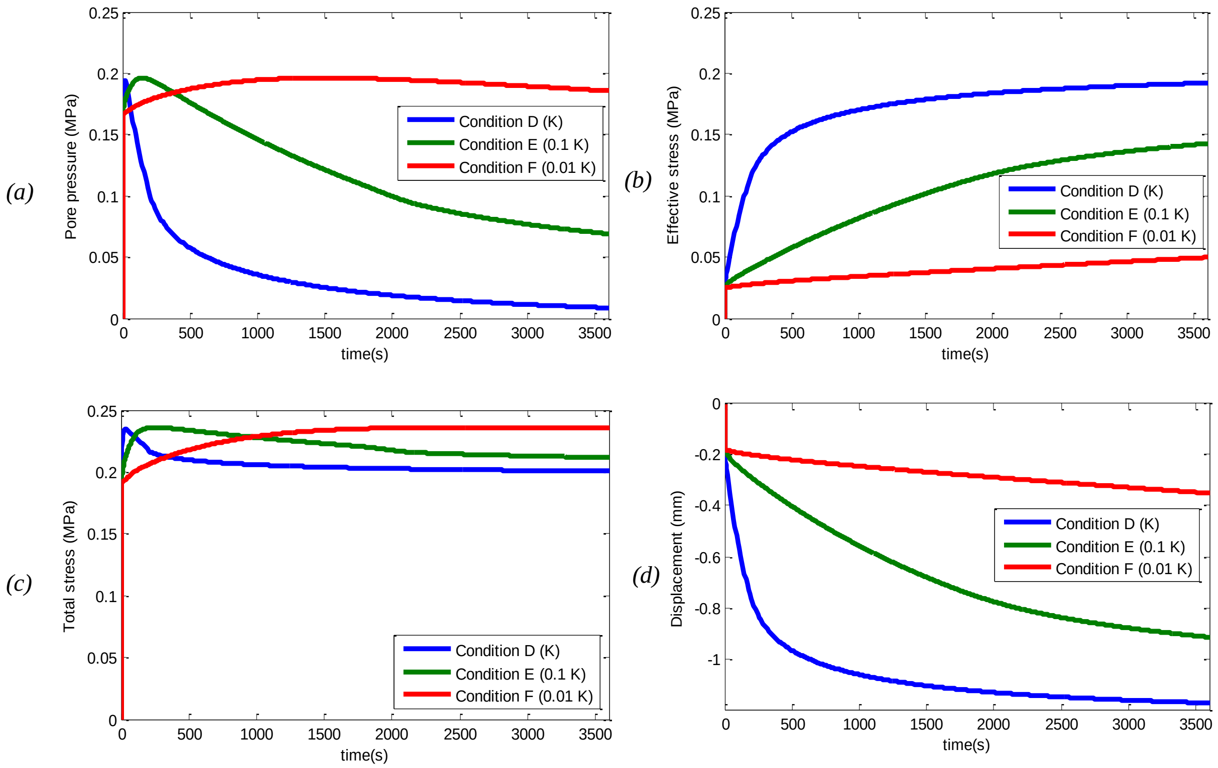

Figure 4.13: Comparison among conditions D, E and F a) pore pressure b) effective stress c) total stress d) displacement

4.2 Effects of loading conditions on the stress components, principal strains and fluid loss in a finite element model of the spinal functional unit (Objective 2)

In this section, stress components, deformation and fluid loss within the cartilaginous tissues (growth plates and intervertebral disc) under compressive loading were investigated using a functional unit of the spine. Five compressive loadings were studied: static (0.2 MPa), 0.2±30% MPa at 0.1 Hz (i), 0.2±70% MPa at 0.1 Hz (ii), 0.2±30% MPa at 1 Hz (iii) and 0.2±70% MPa at 1 Hz (iv) (Table 3.2). The simulations were initially aimed to be done for a duration of 1000 s. However, the preliminary simulations were done using linear elements, which did not converge for the desired loading period. The convergence problem was more severe at high frequency and high amplitude loading conditions. To improve the convergence, nonlinear elements were used, which helped to solve the problem. However, the simulation time became very long and the simulations were forced to stop after about three weeks. The results were reported for the time period that the simulations were completed. Considering the results (Figure 4.14 to Figure 4.18), it can be seen that high frequency conditions (iii and iv) showed a distinct behavior. In particular, the total stress in these conditions exceeded 0.2 MPa, which is the applied compressive load. This phenomenon can be addressed to a critical condition which was happening in high frequency loading conditions (iii,iv) and will be discussed in the discussion chapter in detail. Accordingly, the results for these two conditions will not be investigated in the following sections.

4.2.1 Influence of the frequency and amplitude of compressive loading on the stress components, principal strains and fluid loss within the growth plates

Stress components (pore pressure, effective stress and total stress), fluid volume as well as minimum and maximum principal strains were investigated in the upper and lower growth plates. Stress components and principal strains were reported as the average value over all elements in the growth plate. The fluid volume is the summation of the individual element fluid contents (the fluid volume ratio measured at element centroid multiplied by the element volume). The results were the same for both upper and lower growth plates as the effect of gravity was not considered in this study. Figure 4.14 shows the results for the growth plate. The results were smoothed with the moving average method to make the comparison easier.

Pore pressure curves can be seen in Figure 4.14a. The pore pressure gradually decreased in static and low frequency loading conditions (i, ii) to reach the value of 0.18 MPa at the loading time of 500 s. Figure 4.14b shows the curves for the effective stress for different loading conditions. The growth plates sustained compressive stress (negative values indicate a compressive stress). The effective stress magnitude for static and low frequency loading conditions (i, ii) gradually increased over time and reached the level of 0.04 MPa at the time of 500 s. The total stress showed a stable stress level of 0.2 MPa for the static and low frequency loading conditions (i, ii) (Figure 4.14c).

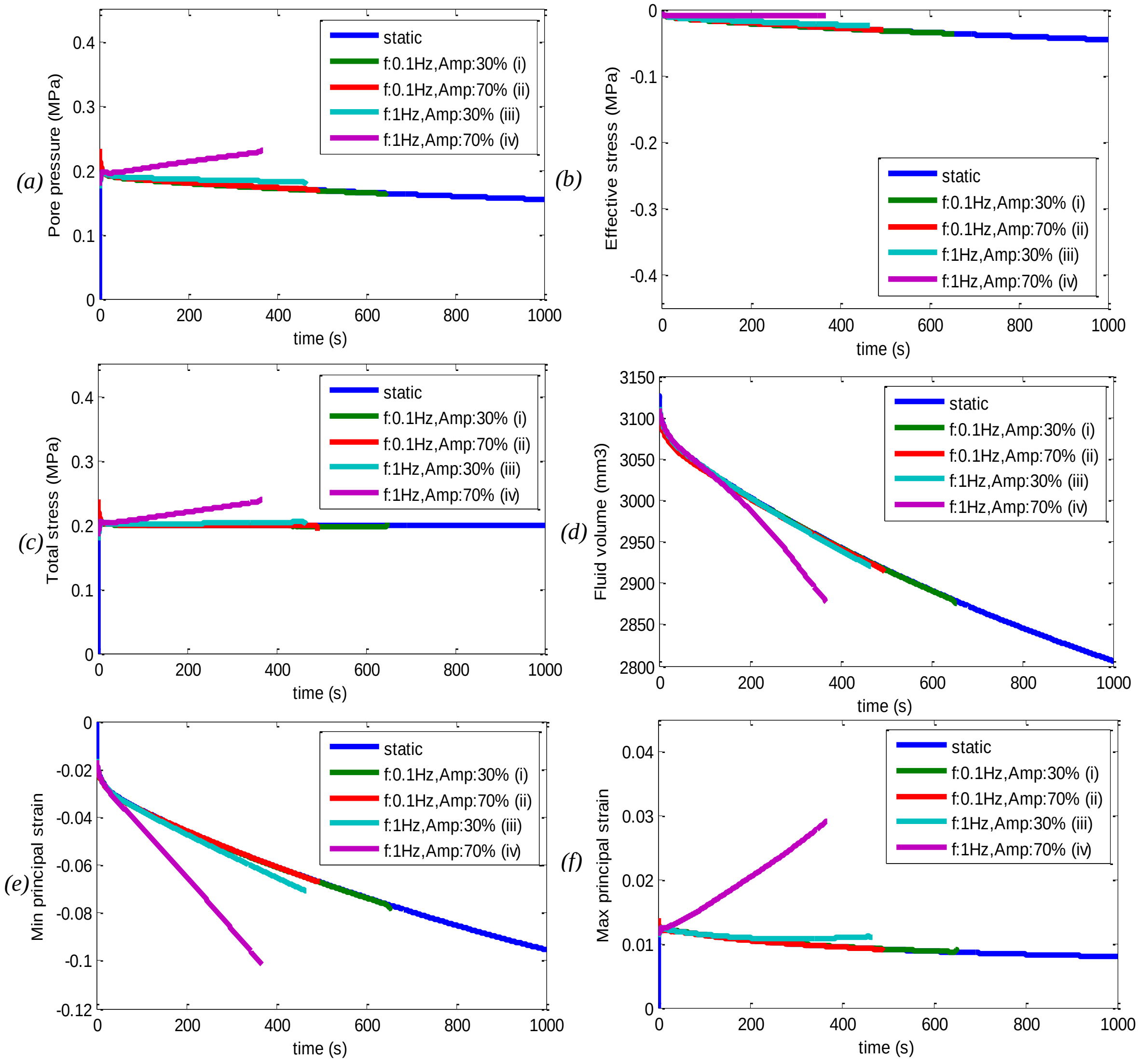

Figure 4.14: Time histories of a) pore pressure b) effective stress c) total stress d) fluid content e) min principal strain and f) max principal strain in the growth plate

Fluid content in the growth plate decreased with time (Figure 4.14d). The fluid loss for the static and low frequency loading conditions (i, ii) was the same, with the value of 2920 mm^3 at the time of 500 s. To investigate the developing strain in the tissue, minimum and maximum principal strains were considered (Figure 4.14e and Figure 4.14f). They were derived for each element centroid and then averaged over all elements in the growth plate. Minimum principal strain showed negative values, which stood for a compressive strain (Figure 4.14e). It also showed a declining trend, which means the compressive deformation was increasing over time. Static and low frequency loading conditions (i, ii) showed a similar curve and reached the compressive strain of 0.07 at the time of 500 s. Maximum principal strain had positive values, which signified the tensile strain (Figure 4.14f). The curves slowly diminished for the static and low frequency loading conditions (i, ii) from 0.012 at the beginning of the loading to 0.009 at the time of 500 s. Figure 4.15 shows the pore pressure, effective stress, fluid volume ratio and deformation magnitude contours within the growth plate. The pore pressure showed higher values at the central region, which unified at the end of loading period (Figure 1.15a). The effective stress showed a rather uniform distribution while the stress level increased with time (Figure 1.15b). The fluid content was higher at the central area compared to the peripheral region. Its intensity first increased and then decreased with time (Figure 1.15c). The deformation distribution was uniform at first however, the upper surface experienced more deformation compared to the lower surface at the end of loading period (Figure 1.15d).

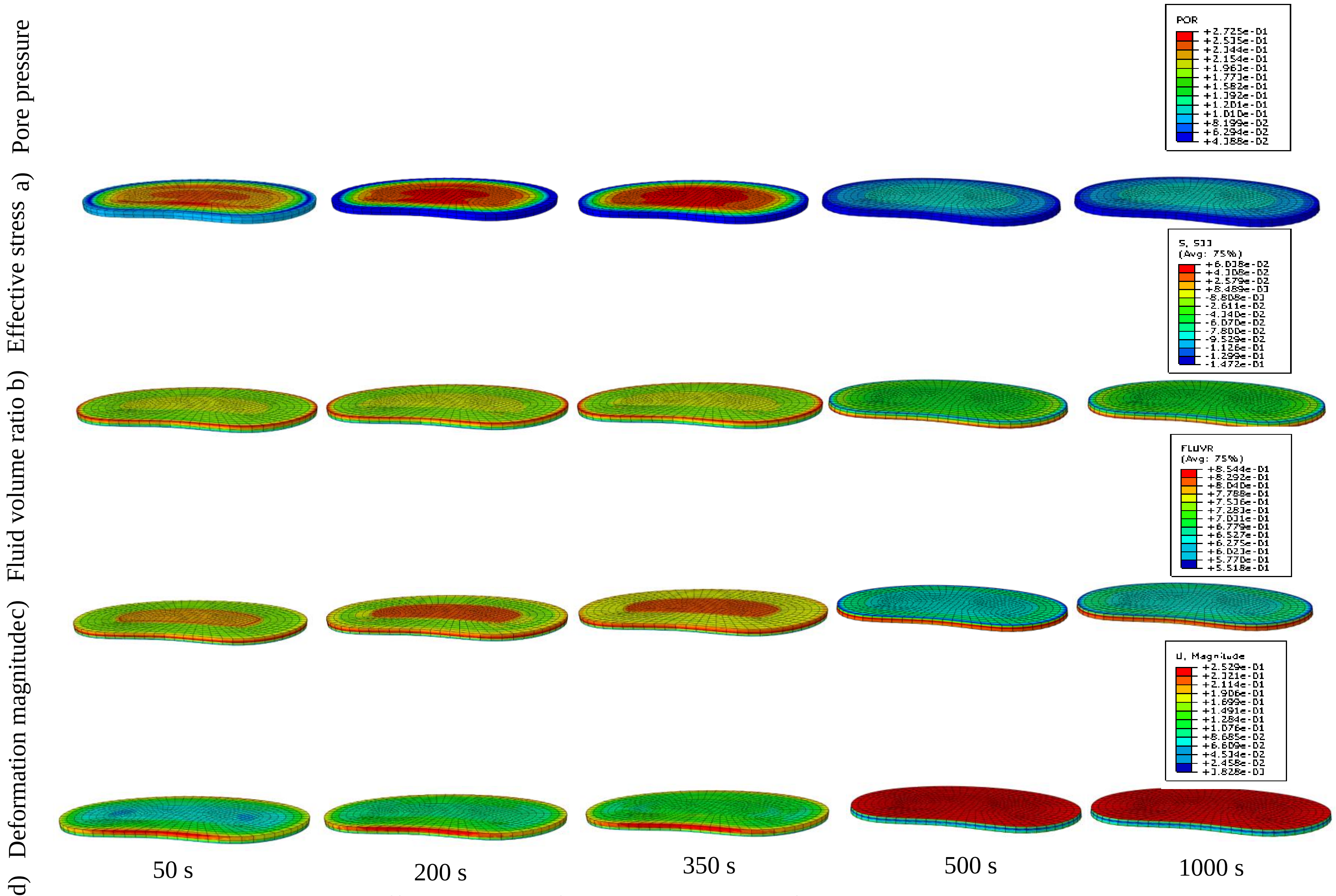

Figure 4.15 : a) Pore pressure b) effective stress c) fluid volume ratio d) deformation magnitude contours within the growth plate at times of 50, 200, 350, 500 and 1000 s

4.2.2 Influence of the frequency and amplitude of compressive loading on the stress components, principal strains and fluid loss within the nucleus

Figure 4.16 presents stress components, fluid volume, minimum and maximum principal strain in the nucleus. The results were averaged over all elements in the nucleus and smoothed by the moving average method to make the comparison easier. The pore pressure curves descended very slowly for static and condition (i) and reached the value of 0.21 MPa at the time of 500 s (Figure 4.16a). The decreasing rate was even slower in condition (ii) and it reached the level of 0.22 MPa at the time of 500 s. Figure 4.16b showed the effective stress curves in the nucleus. The effective stresses were reported as they were (it means that negative values showed the compressive stress and positive values stood for tensile stress). For static condition and condition (i), absolute values of effective stress slowly decreased and stabilized at the level of ~0.022 MPa at the time of 500 s. For these conditions, the effective stress had a negative value, which meant that the tissue was under compressive stress. Condition (ii) showed a lower level of compressive stress but it also stabilized at ~ 0.019 MPa after an initial ascending trend. The total stress curves are shown in Figure 4.16c. The total stress decreased with a very slow rate for static and low frequency loading conditions (i, ii). They reached the value of 0.22 MPa at the time of 500 s. Figure 4.16d shows the fluid content in the nucleus part for the different loading conditions. The initial volume content was 3992 mm^3. The fluid volume in the nucleus initially rose up to 3994 mm^3 and then decreased with a slow rate for static loading and condition (i) to reach 3992 mm^3 at the time of 500 s. In addition, condition (ii) took an increasing trend with a very slow rate and reached the value of 3995 mm^3 at the time of 500 s. Minimum principal strain had negative values, which stood for compressive strain (Figure 4.16e). Static and low frequency loading conditions (i, ii) showed similar behavior and had an almost constant level of -0.02. Maximum principal strain had positive values, which meant that the strain was tensile (Figure 4.16f). Condition (i) and static condition showed similar results. Their curve descended with a very slow rate to reach the value of 0.016. Condition (ii) had slightly lower values and moved close to the static condition as it descended to the value of 0.015 at the time of 500 s. Figure 1.17 shows the pore pressure, effective stress, fluid volume ratio and deformation magnitude within the nucleus.

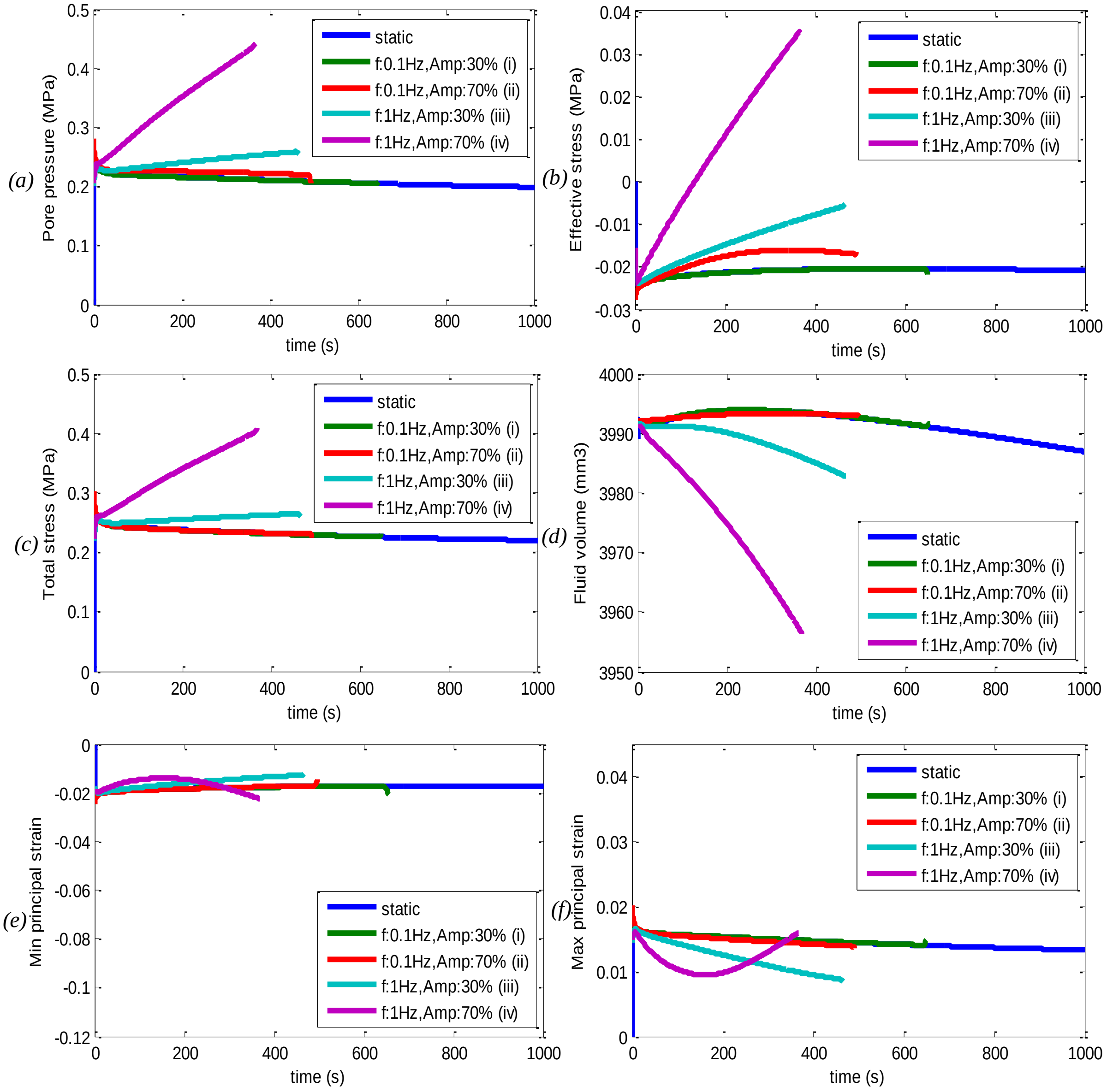

Figure 4.16: Time histories of a) pore pressure b) effective stress c) total stress d) fluid content e) min principal strain and f) max principal strain in the nucleus

As it can be seen, the pore pressure was higher in the central region compared to the peripheral area. Its intensity increased first and then decreased (Figure 1.17a).The effective stress had a uniform distribution with slightly higher stress levels in the peripheral area (Figure 1.17b). The fluid volume ratio was uniform within the nucleus and decreased with time (Figure 1.17 c). The upper surface of the nucleus experienced more deformation compared to the lower surface. The distribution of deformation was more uniform at the end of the loading period (Figure 1.17d).

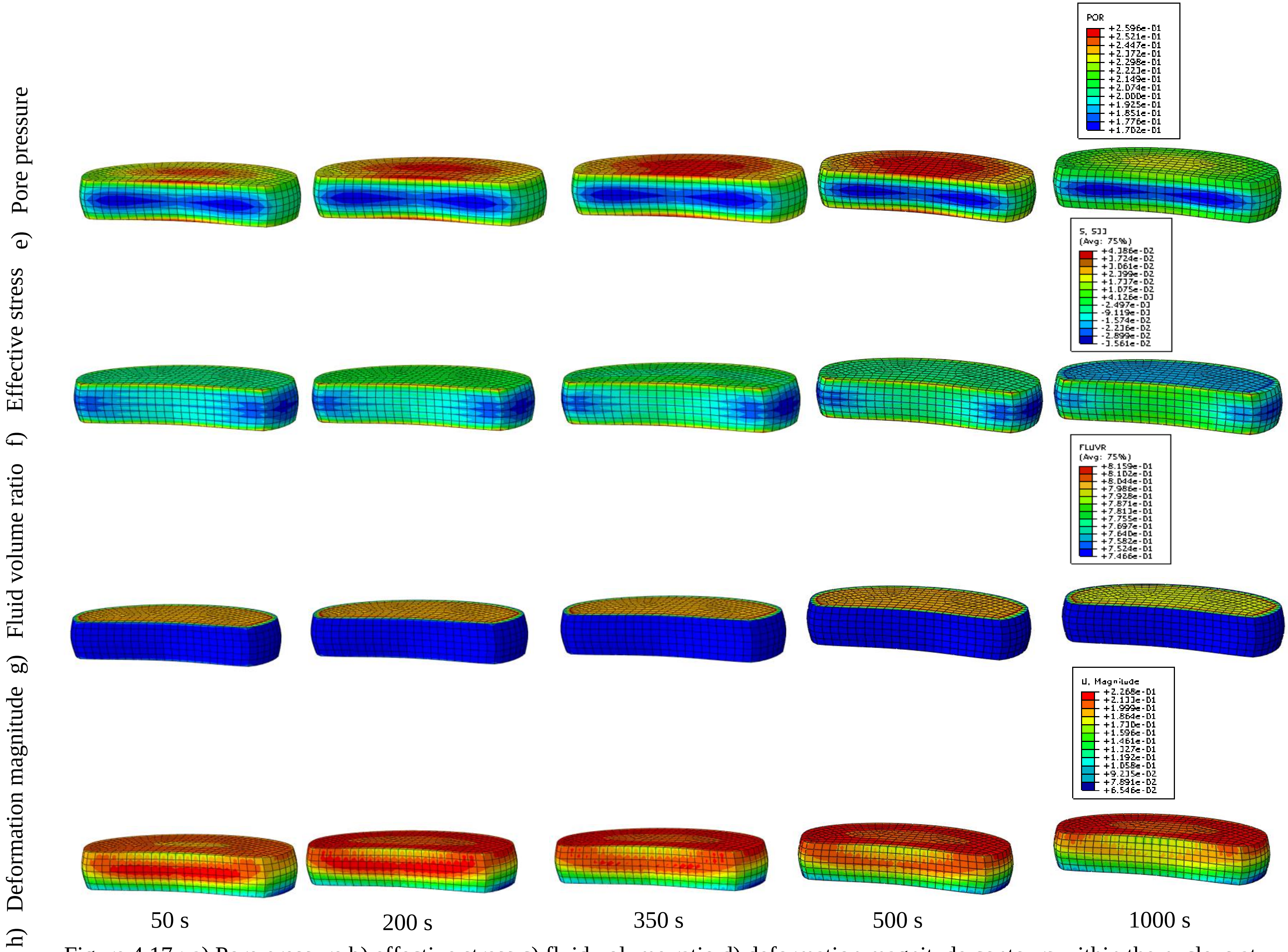

Figure 4.17 : a) Pore pressure b) effective stress c) fluid volume ratio d) deformation magnitude contours within the nucleus at times of 50, 200, 350, 500 and 1000 s

4.2.3 Influence of the frequency and amplitude of compressive loading on the stress components, principal strains and fluid loss within the annulus

Stress components, principal strains and fluid content in the annulus part are presented in Figure 4.18. The results were derived from the annulus elements in the disc. Pore pressure curves are shown in Figure 4.18a. The pore pressure had almost a constant level for all conditions. Static and condition (i) showed similar results with a stress level of 0.15 MPa at 500 s. Condition (ii) had slightly more pore pressure (0.16 MPa). Figure 4.18b shows effective stress curves over time in the annulus part. Static loading and condition (i and ii) experienced a more or less constant level of compressive effective stress. The stress level was slightly higher for the static and condition (i) (0.42 MPa) compared to condition (ii) (0.4 MPa).

The total stress was the same for static and low frequency conditions (i, ii) and had a constant level at ~ 0.2 MPa (Figure 4.18c). Figure 4.18d shows the fluid volume in the annulus part over time. Fluid volume increased in all conditions, which meant that the tissue was taking in fluid. Condition (ii) had the slowest rate of fluid intake (fluid content of 8096 mm^3 at the time of 500 s) while condition (i) and static loading showed the same result (fluid content of 8102 mm^3 at the time of 500 s) (Figure 4.18d). Figure 4.18e showed minimum principal strain in the annulus over time. Minimum principal strain had negative values in all conditions, which was correlated to compressive strain. Conditions (i, ii) had very similar curves; they showed relatively constant levels of strain and their values were very close to each other (-.022 at the time of 500 s). Maximum principal strain was positive in all conditions, which was correlated to the tensile strain (Figure 4.18f). Conditions (i, ii) and static loading had very slowly increasing curves which were very close to each other. They moved from 0.02 to 0.022 over the loading period of 500 s. Figure 4.19 shows the pore pressure, effective stress, fluid volume ratio and deformation magnitude contours within the growth plate. The pore pressure showed a higher intensity in the vicinity of the nucleus which increased with time (Figure 4.19a). Furthermore, the effective stress intensity in posterior area decreased with time (Figure 4.19b). Fluid volume ratio was the highest in the posterior area and the lowest in the vicinity of the nucleus. The intensity of the fluid volume decreased with time in the posterior area (Figure 4.19c). The deformation distribution was not even too. The posterior and peripheral areas experienced more deformation compared to other regions that increased with time (Figure 4.19d)

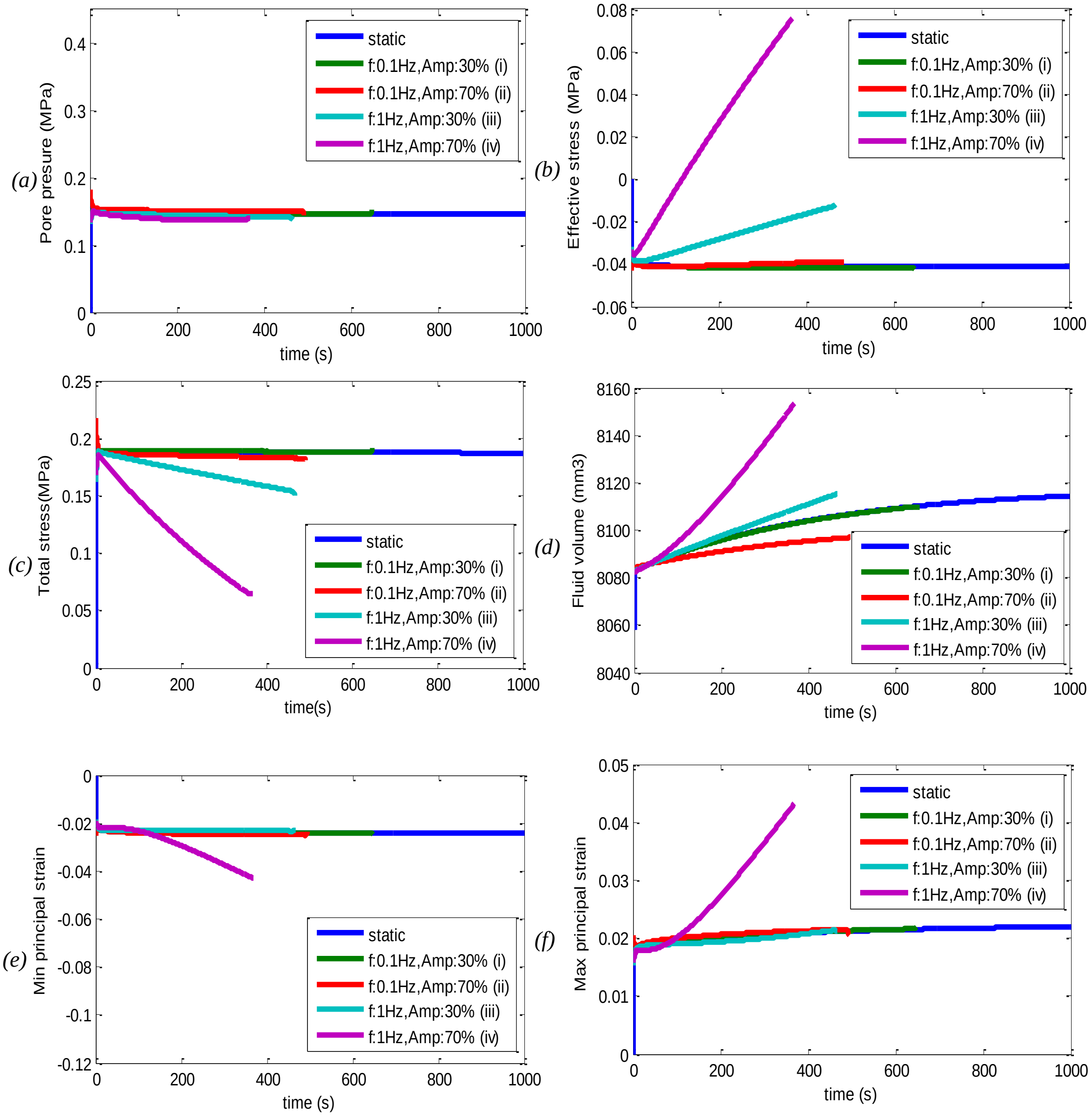

Figure 4.18: Time histories of a) pore pressure b) effective stress) total stress d) fluid content e) min principal strain and f) max principal strain in the annulus

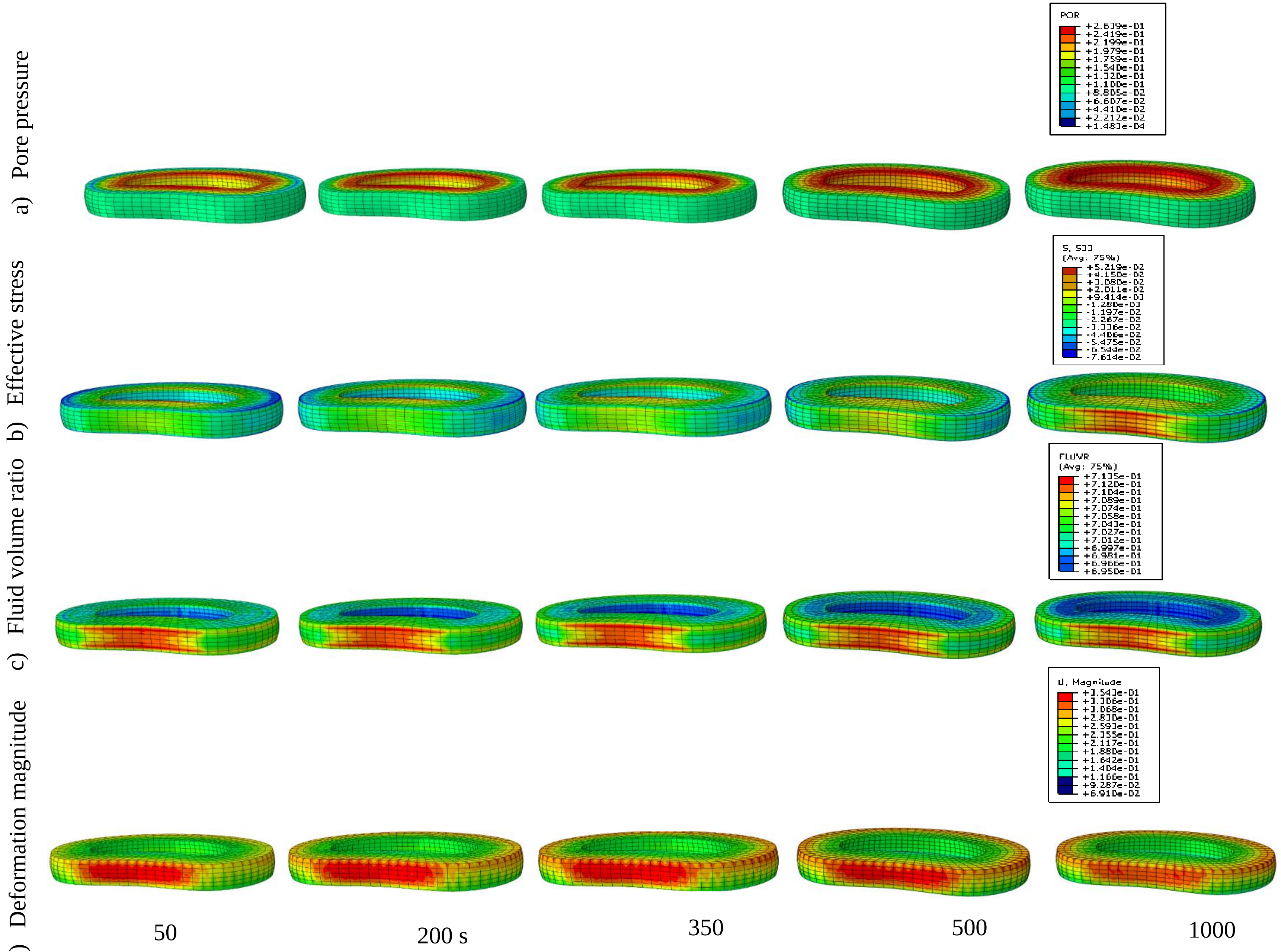

Figure 4.19 : a) Pore pressure b) effective stress c) fluid volume ratio d) deformation magnitude contours within the annulus at times of 50, 200, 350, 500 and 1000 s

CHAPTER 5: DISCUSSION

In this project, the biomechanical response of the growth plate to cyclic and static compressive loadings was investigated using the finite element method. Experimental results reported that cyclic compressive loads are as effective as static compressive loads in terms of growth modulation but they result in less damage in growth plates [1]. Furthermore, in the biphasic theory, the total applied stress is split between fluid phase (pore pressure) and solid matrix (effective stress). The project hypothesis projected the idea that cyclic and static compressive loads show the same total stress to satisfy the equilibrium between applied load and resultant stress. However, the load distribution between the fluid and solid phases is different.

This study was done in two parts. In the first part, the effects of boundary conditions (peripheral pore pressure), transversal permeability and loading conditions (frequency and amplitude of oscillation) on the developing stress components and deformation were investigated using an axisymmetric biphasic model of the growth plate. In the second part, simulations were done using a 3-D biphasic model of a spinal functional unit and the stress components, principal strains and fluid content were analyzed in the growth plates and intervertebral disc.

4.3 Effects of material properties, loading and boundary conditions on the developing stress and deformation using a biphasic axisymmetric finite element model of the growth plate (Objective 1)

For the growth plate modeled as a poroelastic material, the distribution of the stress between solid matrix and fluid phase changed with time in a way to sustain the overall applied compressive stress. The applied compressive load was first mainly taken by the fluid phase and, as a result, the pore pressure increased. Then, the load was gradually transferred to the solid matrix phase, which was translated by an increase in the effective stress. The height of the growth plate then decreased with time, as fluid was expelling from the tissue and as the solid matrix contribution to support the applied load was increasing. The total stress, representing the summation of the effective stress and pore pressure, maintained a relatively constant level, in order to ensure equilibrium under the applied external compression.

None of the pore pressure, effective stress, total stress and deformation variables were influenced by the loading frequency and/or amplitude. Indeed, only very slight differences were observed for higher transversal permeabilities or when no peripheral pore pressure was applied. However, a distinction in their behavior occurred in the transient response stage at the beginning of the compression (first 200 s), where the viscoelastic material properties of growth plates made them sensitive to the loading frequency. As a result, the time to reach the peak point and the value of the peak point were different for different loading frequencies. Unfortunately, there is no other analytical study reporting the stress distribution between two phases in growth plates, which makes the comparison to ground truth impossible. Furthermore, reported experimental studies investigated the effect of loading on the growth plate height (after growth) or cellular level contents such as solute transport, collagen content, proteoglycan and etc. which were not addressed in the finite element model and thereby could not be compared to the analytical results.

A reduction in transversal permeability was associated with an increased pore pressure and with a reduction in effective stress and deformation. However, the total stress was not influenced by the loading condition as much as other stress components. Differences between loading conditions (frequency and oscillation amplitude), although non-significant, were more pronounced in higher transversal permeabilities. In this study, the inferior and superior surfaces of the sample were impermeable so the peripheral area was the only path along which the fluid could drain. When reducing the transversal permeability, the fluid faced more resistance on its way to the peripheral surface. As a result, fluid loss in the tissue decreased, and pore pressure maintained a higher level because of the greater fluid content trapped in the tissue, and the growth plate underwent less vertical deformation. As the structure deformed the fluid expelled from the tissue and the applied load was transmitted to the solid skeleton, thereby, in lower permeabilities, the load transfer to the effective stress did not happen as much as in high transversal permeabilities.

When applying a peripheral pore pressure of 0.1 MPa instead of a free peripheral boundary, the pore pressure level in the tissue increased while the effective stress and deformation level decreased. However, the total stress showed very low sensitivity to the peripheral pore pressure so that the overall stress equilibrium was maintained. An increased peripheral pore pressure means more resistance against the fluid to go out of the tissue. This prevents the fluid to flow through the tissue and expel, which then prevents deformation of the tissue. Since less fluid expelled out, the pore pressure trapped in the tissue continues to sustain the pore pressure and the solid matrix did not take over the load as much, which was translated by a decrease in effective stress.

When increasing the transversal permeability, the delay in the response to the applied load, initial spike and then relaxation got more noticeable. As an important part of tissue viscoelastic properties refers to the frictional drag resulting from the movement of the liquid phase through the porous extracellular matrix, the fluid flow increased the viscoelastic response of the tissue. Therefore, the viscoelastic effects were more pronounced with higher transversal permeabilities and lower peripheral pore pressures.

In this study, the superior and inferior surfaces of the growth plate were modeled as impermeable, which is not representing the real physiological boundaries around the vertebral growth plates. Indeed, the growth plate does exchange fluid with both its adjacent vertebral body and disc, and hence its superior and inferior boundaries are not fully impermeable. Representing more appropriate boundary conditions on the superior and inferior surfaces could provide a more realistic biomechanical behavior of the growth plate under different compressive loading conditions. Furthermore, the axial permeability effects, which were then not considered in the model, would have to be taken into the account for superior and inferior surfaces modeled as partially permeable. This would particularly change the stress distribution between two phases by enhancing the fluid flow in the tissue, similarly to peripheral pore pressure and transversal permeability, which have been discussed before.

4.4 Effect of loading conditions on the stress components, principal strains and fluid loss in a finite element model of functional spinal unit (Objective 2)

For the functional spinal unit including growth plates and intervertebral disc modeled as poroelastic materials, static and low frequency conditions (i, ii) behaved similarly when individually comparing growth plates, nucleus and annulus results for the different stress components. However, condition (iii) showed slightly different results while condition (iv) exhibited quite distinct results which could be explained as follows: In the nucleus and annulus, the effective stresses were compressive for static, conditions (i) and (ii), meaning that the tissue was under compressive stress. For conditions with high frequency (1 Hz; conditions (iii) and (iv)), the effective stress was first compressive; it then gradually decreased to reach zero stress and eventually took positive values, which could be translated as tensile stress. However, considering the vertical deformation in the nucleus, it can be seen that tissue was still under compression (negative values) which refutes the hypothesis of tensile stress. From the soil consolidation theory, when there is an upward seepage in the tissue, pore pressure is built up at depth and effective stress is lessened. If the rate of seepage and therefore the hydraulic gradient are gradually augmented, a critical condition is reached, where effective stress is zero. This means that the solid phase carries out no force. Under this condition, the soil stability is lost. On the other hand, when there is a downward seepage, pore pressure is reduced with depth and effective stress is increased [128]. This phenomenon could explain the distinct behavior of the condition (iii, iv) in growth plates and disc as, after this critical situation happens, results become not reliable. Adding gravitational loads to the model might help avoiding this condition in the nucleus and annulus. It was hypothesized that this critical condition occurred in the nucleus and annulus and that it further influenced the stress distribution in the growth plates for the high frequency conditions (iii, iv). Hence, these two conditions were not compared and discussed with respect to the other conditions in the following sections.

For the functional spinal unit under static or low frequency cyclic compression, the compressive load was first taken by the fluid phase and then transferred to the solid matrix with time as the fluid drained out of the tissue. However, when comparing growth plates and disc, the rate of transfer directly depended on their poroelastic properties as well as the boundary pore pressure. The growth plates showed the highest level of fluid loss (6% at the time of 500 s) and consequently the highest rate of reduction in pore pressure compared to annulus and nucleus. The fluid loss was almost zero in the nucleus, which resulted in a very slow rate in the load transfer from the fluid phase to the solid matrix. Finally, the annulus showed a constant level of pore pressure because the fluid intake from adjacent parts was almost equal to the fluid loss from the outer surface (0.2 % fluid intake at the time of 500 s).

Although the nucleus and growth plates share very close material properties, they showed different levels of fluid loss and accordingly deformation and load distribution between two phases because of their different boundary conditions. Based on Darcy’s law, fluid flows from the higher pressure region to the lower pressure region. Hence, the nucleus fluid is supposed to flow out through its boundary regions, either to the adjacent growth plates (with higher permeability 3.4 $\times10^{-15}$ vs 0.3$\times10^{-15}$ m^4/Ns) or to the annulus (with lower permeability 0.11 $\times10^{-15}$ vs 0.3$\times10^{-15}$ m^4/Ns). At the same time, growth plates can exchange fluid with the nucleus, annulus and cancellous bone in the vertebral body. Since cancellous bone has a higher permeability compared to the growth plates, nucleus and annulus (Table 3.4), it then makes fluid exchange easier from growth plates to cancellous bone. As a result, growth plates experienced more fluid loss compared to the annulus and nucleus. The fluid content of disc varies with the amount and duration of applied load. Malko et al. performed an MRI study and reported a 7 % fluid loss after three hours of approximately 1 MPa compressive loading on the lumbar spine [129]. Cheung et al. predicted 5.3 % of fluid loss under one hour of 0.7 MPa static loading with his finite element model [3]. Our simulations showed a small amount of fluid intake in the disc (0.27 % fluid intake after 1000 hr), which could be explained by the following phenomena. First, the FE model comprises the growth plate, which has lower permeability compared to the end plates in the adult model; this would reduce the fluid drainage from the disc and mainly from the nucleus. Second, the magnitude of the applied load in our study is 0.2 MPa, which is lower than the aforementioned studies (0.7 and 1 MPa). Third, the duration of load in our study is about 1000 s (about 20 min.), which is less than the two other studies (one and three hour(s)).

In terms of effective stress, the load sustained by the solid matrix was very similar for the growth plates and annulus (0.04 MPa). However, the nucleus showed a lower level of the effective strain (0.02 MPa). The total stress was around 0.2 MPa in the growth plates, which allowed maintaining equilibrium with respect to the applied load. For the disc, the nucleus showed a total stress level of 0.22 MPa, while the annulus had a stress level of 0.18 MPa, suggesting that the nucleus has a more important role in sustaining the applied compressive load. The difference between stress levels mostly comes back to the confined fluid in the nucleus due to lower permeability of annulus, which acts like a barrier against the fluid flow from the nucleus to the annulus. This result is consistent with the finite element study of Cheung et al. who reported more total stress for nucleus compared to the annulus [3].

This model like every other model has its own limitations. First of all, the gravitational force was not included in this model and just a uniform compressive load representative of the modulating force was applied. The application of gravitational force can especially improve the results in annulus and nucleus where the upward seepage leads to a critical condition at high frequencies. Adding gravitational load will increase the compression level, which might lead to more representative results. The simulations in this study were preliminary simulations so the gravity was not integrated. Furthermore, the long simulation time did not give the chance to try different values for different parameters. Second, the dimensions of the model were the one of an adult spine which was larger than adolescent’s spine that are the target of interest. However, it would not change the general behaviour of the functional unit as the growth plates were integrated to the model. Third, posterior elements, such as transverse processes, spinous process, facet joints and ligaments, were not modeled in the functional spinal unit. Integrating these components could improve the model behavior, since posterior elements are important for the stability of spine and load distribution in the disc. Fourth, the growth plates were considered to be parallel which is different from reality and might influence the stress distribution in the disc and growth plates. Furthermore, the simulations results were aimed to be compared with the experimental results on the rat tail where the growth plates were parallel and wedging was not involved. Fifth, a more complex model, which can address the material behavior at the cell level could significantly improve the modeling approaches and make them more realistic. As it was shown in this study, this type of models could not predict the differences between cyclic and static loads seen in the experimental studies. Including the biochemical reactions in the tissue as mechanical stimuli in the model would provide more insights on the biomechanical behaviour of the growth plates interacted with external loads.

4.5 General discussion

These simulations were done in parallel of an experimental study, where the effects of loading frequency and amplitude were investigated on the growth modulation in a rat tail model. According to their results, cyclic loads are as effective as static loads for growth modulation but they cause less damage within the growth plate. However, when combining high frequency (1.0 Hz) and amplitude (70%), the rats had repetitive inflammations damaging tissues. Results of the present study, which mimicked the same compressive loading conditions, allowed investigating if damage at the tissue level could be correlated to any of stress components or deformation variables from simulation results. Simulations using the axisymmetric biphasic model did not allow to distinguish between static and cyclic loading conditions. However, they showed that the permeability properties and peripheral pore pressure directly influence the stresses distribution between the two phases as well as the tissue deformation level. From simulations with the functional spinal unit, no difference was neither found between static and low frequency cyclic compressive loadings (i, ii) in terms of stress components, strain and fluid loss. Accordingly, the thesis hypothesis was refuted in both studies (objective 1 and 2) as no significant difference was seen between stress components in cyclic and static compressions.

Put together, these findings may suggest that the distinction between cyclic and static loadings in terms of tissue damage in the experimental study [2] could be a result of nutritional changes in the tissue, which cannot be represented in the developed finite element models. Albro et. al in their experimental study concluded that cyclic loading (0.2 Hz) of immature epiphyseal cartilage pump solutes through the articular surface from the synovial fluid in addition to inducing transvascular pumping [130]. This finding could explain why vibrational loadings are less detrimental to the growth plates in the rat tail model. Ateshian et al. also developed a complex finite element platform for computational modeling of chemical reactions, interstitial growth and remodeling involving charged solutes and solid-bound molecules to model the mechanoelectrochemical behavior of biological tissues and cells [131, 132]. Having a more bio-representative model may help to broaden the insights into the interaction of mechanical loading and tissue metabolism.

In the study with a functional unit of the spine, besides growth plates, the results were investigated in the nucleus and annulus as they have direct interaction with growth plates. Our results do not agree with the ones of Cheung et al. who analysed the biomechanical behavior of intervertebral discs under static and vibrational loadings (0.5, 1, 2 and 4 HZ). They reported the same effective stress for both vibrational and static loading but higher pore pressure and thereby greater total stress for vibrational loading in the nucleus. It should be noted that their oscillation magnitude was 10% and the average compressive load was about 0.7 MPa, which are different from this study (10% versus 30% and 70%, 0.7 versus 0.2 MPa). Higher level of compressive load might result in more fluid loss in the disc and growth plates which would influence the deformation, stress levels and stress distribution between two phases. In addition, the posterior elements and ligaments were integrated in their model of a functional spinal unit, which could reduce the compressive load taken by the disc. Furthermore, the boundary conditions also differed; in their study the inferior surface of L5 was fixed at an angle of 30° to the horizontal plane and the gravitational loads were integrated to their model, which would improve the upward seepage [3]. Also, from experimental studies, loading frequencies below 0.5 Hz were found to be the best among the tested frequencies (0.5, 1.5 and 2.5 Hz) in preserving proteoglycan content within the disc a rat tail model [133]. In addition, with the same model, it was shown that the frequency of 0.2 Hz was the best frequency (among 0.01, 0.2 and 1 Hz) to preserve normal disc metabolism [134]. These findings could partly explain the infection in the rats at the combined high frequency and amplitude condition.

This finite element study for the first time has investigated the biomechanical response of growth plates to static and cyclic compressive loadings in terms of stress, strain and fluid loss, including an investigation of the effects of loading frequency and oscillation amplitude. Results revealed that boundary conditions and poroelastic properties considerably influence on these mechanical parameters. However, the results showed that this type of finite element models were unable to predict the difference between static and cyclic loading conditions with different loading frequencies and amplitudes.

CONCLUSION AND RECOMMENDATIONS

In this thesis, the biomechanical response of the growth plate under static and cyclic compressions was investigated using the finite element method. To achieve this objective, two specific objectives were defined. The first objective was to investigate the effects of compressive loading conditions (frequency and amplitude), peripheral pore pressure (0 and 0.1 MPa) and transversal permeability (*K*, 10% *K* and 1% *K*) on the developing stress components (pore pressure, effective stress and total stress) and deformation using a simplified axisymmetric growth plate model. The second objective was to study the influence of compressive loading frequency and amplitude on the resultant stress components (pore pressure, effective stress and total stress), principal strains and fluid loss in growth plates, nucleus and annulus, with a 3-D finite element model of a spinal functional unit.

In the first part, simulations showed no difference between static and cyclic compressive loadings in terms of stress components and displacement. Furthermore, results showed that transversal permeability and peripheral pore pressure directly influenced the stress distribution between the solid and fluid phases as well as the deformation in the tissue. For lower permeabilities and higher peripheral pore pressure, a higher volume of fluid was maintained in the tissue resulting in higher pore pressure and lower displacement levels compared to the more permeable conditions. The load transfer from the fluid to the solid phase consequently decreased, leading to reduced effective stresses.

In the second part, the effect of loading frequency and amplitude on the biomechanical response of the cartilaginous tissue was studied with a more realistic model. Results were very similar for low frequency conditions (i, ii) and static loading. However, the high frequency loading conditions (iii, iv) showed a distinct behavior. A critical state of zero effective stress was seen in the nucleus and annulus at high frequency compressive loadings because of the upward seepage in these components. This phenomenon made the comparison between high frequency and low frequency loading conditions impossible because after the critical state, tissue underwent an unstable situation leading to unreliable results. Integration of gravitational force to the model, in addition to the applied compression, might help to avoid this problem.

Fluid loss in growth plates was greater than in the nucleus while annulus part was taking in fluid with a very slow rate. Furthermore, it was found that the solid matrix had a more important role in sustaining the compressive load in the annulus part and growth plates (higher effective stress) compared to the nucleus. In addition, the nucleus took over a larger portion of applied compressive load comparing to the annulus (higher total stress in the nucleus). Nevertheless, the pumping effect of the vibrational loads, which would improve the nutrition in the tissue, could not be addressed in this model.

This study showed that the developed biphasic finite element models were not able to distinguish between static and cyclic (different loading frequencies and amplitudes) compressive loads. However, boundary conditions (peripheral pore pressure) and permeability properties influenced the strain and the load distribution between two phases in the material. To have more insights into the biomechanical response of the growth plate to applied compressive loads, the chemical reactions, such as the pumping effects of the vibrational loads, which could improve the nutrition in the tissue, should be reflected as mechanical stimuli in future finite element models. In addition, gravitational loadings should be integrated in the next models to avoid upward seepage effects in the modeled tissues. Furthermore, parametric studies on the effects of the peripheral pore pressure distribution, poroelastic properties and loading parameters should be done to explore in more details the biomechanical responses of spinal tissues to the compressive loadings.

REFERENCES

[1] B. Valteau, G. Grimard, I. Londono, F. Moldovan, and I. Villemure, "In vivo dynamic bone growth modulation is less detrimental but as effective as static growth modulation," *Bone,* vol. 49, pp. 996-1004, 2011.

[2] A. L. Menard, G. Grimard, B. Valteau, I. Londono, F. Moldovan, and I. Villemure, "In vivo dynamic loading reduces bone growth without histomorphometric changes of the growth plate," *J Orthop Res,* vol. 32, pp. 1129-36, 2014.

[3] J. T.-M. Cheung, M. Zhang, and D. H.-K. Chow, "Biomechanical responses of the intervertebral joints to static and vibrational loading: a finite element study," *Clinical Biomechanics,* vol. 18, pp. 790-799, 2003.

[4] R. Natarajan, J. Williams, S. Lavender, and G. Andersson, "Poro-elastic finite element model to predict the failure progression in a lumbar disc due to cyclic loading," *Computers & structures,* vol. 85, pp. 1142-1151, 2007.

[5] F. Montgomery and S. Willner, "The natural history of idiopathic scoliosis: Incidence of treatment in 15 cohorts of children born between 1963 and 1977," *Spine,* vol. 22, pp. 772-774, 1997.

[6] J. A. Janicki and B. Alman, "Scoliosis: Review of diagnosis and treatment," *Paediatrics & child health,* vol. 12, p. 771, 2007.

[7] L. E. Peterson and A. L. Nachemson, "Prediction of progression of the curve in girls who have adolescent idiopathic scoliosis of moderate severity. Logistic regression analysis based on data from The Brace Study of the Scoliosis Research Society," *The Journal of bone and joint surgery. American volume,* vol. 77, p. 823, 1995.

[8] J. E. Lonstein and J. M. Carlson, "The prediction of curve progression in untreated idiopathic scoliosis during growth," *J Bone Joint Surg Am,* vol. 66, pp. 1061-71, 1984.

[9] C. Hueter, "Anatomische studien an den extremitaetengelenken neugeborener und erwachsener," *Virchows Archiv,* vol. 25, pp. 572-599, 1862.

[10] D. R. von Volkmann, *Verletzungen und Krankheiten der Bewegungsorgane,* 1882.

[11] G. M. Y. Quan and M. J. Gibson, "Correction of Main Thoracic Adolescent Idiopathic Scoliosis Using Pedicle Screw Instrumentation Does Higher Implant Density Improve Correction?," *Spine,* vol. 35, pp. 562-567, Mar 1 2010.

[12] T. Maruyama, T. Kitagawa, K. Takeshita, A. Seichi, T. Kojima, K. Nakamura, *et al.*, "Fusionless surgery for scoliosis: 2-17 year radiographic and clinical follow-up," *Spine,* vol. 31, pp. 2310-2315, 2006.

[13] I. A. F. Stokes, H. Spence, D. D. Aronsson, and N. Kilmer, "Mechanical modulation of vertebral body growth: implications for scoliosis progression," *Spine,* vol. 21, pp. 1162-1167, 1996.

[14] I. A. F. Stokes, D. D. Aronsson, A. N. Dimock, V. Cortright, and S. Beck, "Endochondral growth in growth plates of three species at two anatomical locations modulated by mechanical compression and tension," *Journal of Orthopaedic Research,* vol. 24, pp. 1327-1334, 2006.

[15] A. Alberty, J. Peltonen, and V. RitsilÃ¤, "Effects of distraction and compression on proliferation of growth plate chondrocytes: a study in rabbits," *Acta Orthopaedica,* vol. 64, pp. 449-455, 1993.

[16] I. A. F. Stokes, K. C. Clark, C. E. Farnum, and D. D. Aronsson, "Alterations in the growth plate associated with growth modulation by sustained compression or distraction," *Bone,* vol. 41, pp. 197-205, 2007.

[17] E. Akyuz, J. T. Braun, N. A. T. Brown, and K. N. Bachus, "Static Versus Dynamic Loading in the Mechanical Modulation of Vertebral Growth," *Spine,* vol. 31, pp. E952-E958 10.1097/01.brs.0000248810.77151.22, 2006.

[18] A. G. Robling, K. M. Duijvelaar, J. V. Geevers, N. Ohashi, and C. H. Turner, "Modulation of appositional and longitudinal bone growth in the rat ulna by applied static and dynamic force," *Bone,* vol. 29, pp. 105-113, 2001.

[19] X. Wang and J. J. Mao, "Chondrocyte proliferation of the cranial base cartilage upon in vivo mechanical stresses," *Journal of dental research,* vol. 81, pp. 701-705, 2002.

[20] X. Wang and J. J. Mao, "Accelerated Chondrogenesis of the Rabbit Cranial Base Growth Plate by Oscillatory Mechanical Stimuli," *Journal of Bone and Mineral Research,* vol. 17, pp. 1843-1850, 2002.

[21] A. Chagnon, C.-E. Aubin, and I. Villemure, "Biomechanical Influence of Disk Properties on the Load Transfer of Healthy and Degenerated Disks Using a Poroelastic Finite Element Model," *Journal of biomechanical engineering,* vol. 132, pp. 111006-8, 2010.

[22] I. Villemure, C. Ã. Aubina, J. Dansereau, and H. Labelle, "Simulation of progressive deformities in adolescent idiopathic scoliosis using a biomechanical model integrating vertebral growth modulation," *Journal of biomechanical engineering,* vol. 124, p. 784, 2002.

[23] I. A. Stokes, R. G. Burwell, and P. H. Dangerfield, "Biomechanical spinal growth modulation and progressive adolescent scoliosis-a test of the'vicious cycle'pathogenetic hypothesis: Summary of an electronic focus group debate of the IBSE," *Scoliosis,* vol. 1, p. 16, 2006.

[24] M. Driscoll, C.-E. Aubin, A. Moreau, Y. Wakula, J. Sarwark, and S. Parent, "Spinal growth modulation using a novel intravertebral epiphyseal device in an immature porcine model," *European Spine Journal,* vol. 21, pp. 138-144, 2012.

[25] L. Shi, D. Wang, M. Driscoll, I. Villemure, W. C. W. Chu, J. C. Y. Cheng*, et al.*, "Biomechanical analysis and modeling of different vertebral growth patterns in adolescent idiopathic scoliosis and healthy subjects," *Scoliosis,* vol. 6, p. 11, 2011.

[26] J. Clin, C. E. Aubin, and H. Labelle, "Virtual prototyping of a brace design for the correction of scoliotic deformities," *Medical and Biological Engineering and Computing,* vol. 45, pp. 467-473, 2007.

[27] M. M. P. Augustus A. White III, "Physical Properties and Functional Biomechanics of the Spine," in *Clinical Biomechanics of the Spine*. vol. 1, ed Philadelphia, Pennsylvania: J.B. Lippincott Company, 1990.

[28] R. Drake, A. W. Vogl, and A. W. Mitchell, *Gray's basic anatomy*: Elsevier Health Sciences, 2012.

[29] I. Villemure and I. A. F. Stokes, "Growth plate mechanics and mechanobiology. A survey of present understanding," *Journal of Biomechanics,* vol. 42, pp. 1793-1803, 2009.

[30] C. T. Brighton, "Structure and function of the growth plate," *Clinical orthopaedics and related research,* vol. 136, pp. 22-32, 1978.

[31] N. Kember, "CELL DIVISION IN ENDOCHONDRAL OSSIFICATION A Study of Cell Proliferation in Rat Bones by the Method of Tritiated Thymidine Autoradiography," *Journal of Bone & Joint Surgery, British Volume,* vol. 42, pp. 824-839, 1960.

[32] E. Hunziker and R. Schenk, "Physiological mechanisms adopted by chondrocytes in regulating longitudinal bone growth in rats," *The Journal of physiology,* vol. 414, pp. 55-71, 1989.

[33] N. J. Wilsman, E. M. Leiferman, M. Fry, C. E. Farnum, and C. Barreto, "Differential growth by growth plates as a function of multiple parameters of chondrocytic kinetics," *Journal of Orthopaedic Research,* vol. 14, pp. 927-936, 1996.

[34] J. Trueta and A. Trias, "The vascular contribution to osteogenesis IV. The effect of pressure upon the epiphysial cartilage of the rabbit," *Journal of Bone & Joint Surgery, British Volume,* vol. 43, pp. 800-813, 1961.

[35] M. Driscoll, "Design, optimization, and evaluation of a fusionless device to induce growth modulation and correct spinal curvatures in adolescent idiopathic scoliosis," NR95218 Ph.D., Ecole Polytechnique, Montreal (Canada), Ann Arbor, 2011.

[36] A. A. White and M. M. Panjabi, *Clinical biomechanics of the spine* vol. 446: Lippincott Philadelphia, 1990.

[37] M. Y. Lu, W. C. Hutton, and V. M. Gharpuray, "Can variations in intervertebral disc height affect the mechanical function of the disc?," *Spine,* vol. 21, pp. 2208-2216, 1996.

[38] A. Mak, "The apparent viscoelastic behavior of articular cartilage—the contributions from the intrinsic matrix viscoelasticity and interstitial fluid flows," *Journal of Biomechanical Engineering,* vol. 108, pp. 123-130, 1986.

[39] V. C. Mow and R. Huiskes, *Basic orthopaedic biomechanics & mechano-biology*: Lippincott Williams & Wilkins, 2005.

[40] M. Nordin and V. H. Frankel, *Basic biomechanics of the musculoskeletal system*: Lippincott Williams & Wilkins, 2001.

[41] B. Cohen, W. Lai, and V. Mow, "A transversely isotropic biphasic model for unconfined compression of growth plate and chondroepiphysis," *Journal of biomechanical engineering,* vol. 120, p. 491, 1998.

[42] K. Sergerie, M.-O. Lacoursière, M. Lévesque, and I. Villemure, "Mechanical properties of the porcine growth plate and its three zones from unconfined compression tests," *Journal of Biomechanics,* vol. 42, pp. 510-516, 2009.

[43] J. L. Williams, P. D. Do, J. D. Eick, and T. L. Schmidt, "Tensile properties of the physis vary with anatomic location, thickness, strain rate and age," *Journal of orthopaedic research,* vol. 19, pp. 1043-1048, 2001.

[44] V. Mow, S. Kuei, W. Lai, and C. Armstrong, "Biphasic creep and stress relaxation of articular cartilage in compression: theory and experiments," *Journal of biomechanical engineering,* vol. 102, pp. 73-84, 1980.

[45] B. Cohen, G. S. Chorney, D. P. Phillips, H. M. Dick, and V. C. Mow, "Compressive stress-relaxation behavior of bovine growth plate may be described by the nonlinear biphasic theory," *Journal of orthopaedic research,* vol. 12, pp. 804-813, 1994.

[46] R. Wosu, K. Sergerie, M. Lévesque, and I. Villemure, "Mechanical properties of the porcine growth plate vary with developmental stage," *Biomechanics and modeling in mechanobiology,* vol. 11, pp. 303-312, 2012.

[47] J. Soulhat, M. Buschmann, and A. Shirazi-Adl, "A fibril-network-reinforced biphasic model of cartilage in unconfined compression," *Journal of biomechanical engineering,* vol. 121, pp. 340-347, 1999.

[48] M. Fortin, J. Soulhat, E. Hunziker, M. Buschmann, and A. Shirazi-Adl, "Unconfined compression of articular cartilage: nonlinear behavior and comparison with a fibril-reinforced biphasic model," *Journal of biomechanical engineering,* vol. 122, pp. 189-195, 2000.

[49] C.-Y. Huang, V. C. Mow, and G. A. Ateshian, "The role of flow-independent viscoelasticity in the biphasic tensile and compressive responses of articular cartilage," *Journal of biomechanical engineering,* vol. 123, pp. 410-417, 2001.

[50] W. Wilson, C. Van Donkelaar, B. Van Rietbergen, and R. Huiskes, "A fibril-reinforced poroviscoelastic swelling model for articular cartilage," *Journal of biomechanics,* vol. 38, pp. 1195-1204, 2005.

[51] B. F. LeVeau and D. B. Bernhardt, "Developmental biomechanics effect of forces on the growth, development, and maintenance of the human body," *Physical Therapy,* vol. 64, pp. 1874-1882, 1984.

[52] I. Stokes, "Mechanical effects on skeletal growth," *Journal of Musculoskeletal and Neuronal Interactions,* vol. 2, pp. 277-280, 2002.

[53] I. A. Stokes, R. G. Burwell, and P. H. Dangerfield, "Biomechanical spinal growth modulation and progressive adolescent scoliosis--a test of the 'vicious cycle' pathogenetic hypothesis: summary of an electronic focus group debate of the IBSE," *Scoliosis,* vol. 1, p. 16, 2006.

[54] M. Cancel, G. Grimard, D. Thuillard-Crisinel, F. Moldovan, and I. Villemure, "Effects of in vivo static compressive loading on aggrecan and type II and X collagens in the rat growth plate extracellular matrix," *Bone,* vol. 44, pp. 306-315, 2009.

[55] E. Akyuz, J. T. Braun, N. A. T. Brown, and K. N. Bachus, "Static versus dynamic loading in the mechanical modulation of vertebral growth," *Spine,* vol. 31, pp. E952-E958, 2006.

[56] J. Cobb, "Outline for the study of scoliosis," *Instr Course Lect,* vol. 5, pp. 261-275, 1948.

[57] K. L. Kesling and K. A. Reinker, "Scoliosis in Twins: A Meta-analysis of the Literature and Report of Six Cases," *Spine,* vol. 22, pp. 2009-2014, 1997.

[58] L. Taffs, "Experimental scoliosis in primates: a neurological cause," *Journal of Bone & Joint Surgery, British Volume,* vol. 64, pp. 503-507, 1982.

[59] M. Turgut, Ç. Yenisey, A. Uysal, M. Bozkurt, and M. E. Yurtseven, "The effects of pineal gland transplantation on the production of spinal deformity and serum melatonin level following pinealectomy in the chicken," *European Spine Journal,* vol. 12, pp. 487-494, 2003.

[60] I. A. Stokes and M. Gardner-Morse, "Muscle activation strategies and symmetry of spinal loading in the lumbar spine with scoliosis," *Spine,* vol. 29, pp. 2103-2107, 2004.

[61] T. G. Lowe, M. Edgar, J. Y. Margulies, N. H. Miller, V. J. Raso, K. A. Reinker*, et al.*, "Etiology of idiopathic scoliosis: Current trends in research*," *The Journal of Bone & Joint Surgery,* vol. 82, pp. 1157-1157, 2000.

[62] Y. P. Charles, J. P. Daures, V. de Rosa, and A. DimÃ©glio, "Progression risk of idiopathic juvenile scoliosis during pubertal growth," *Spine,* vol. 31, pp. 1933-1942, 2006.

[63] J. B. Emans. (2003). *REFERENCE MANUAL FOR THE BOSTON SCOLIOSIS BRACE*. Available: www.srs.org

[64] J. E. LONSTEIN, "Milwaukee brace treatment of scoliosis," *Scoliosis Research Society Bracing Manual (http://www. srs. org/professionals/education_materials/SRS_bracing_manual/index. htm.),* 2003.

[65] B. M. Charles d'Amato. (2003). *The Providence Scoliosis System* Available: www.srs.org

[66] F. E. R. C. Ralph Hooper, Charles Price. (2003). *THE CHARLESTON BENDING BRACE AN ORTHOTIST'S GUIDE TO SCOLIOSIS MANAGEMENT* Available: www.srs.org

[67] F. E. R. C. Ralph Hooper, Charles Price. (2003). *SpineCor System*. Available: www.srs.org

[68] A. Veldhuizen, J. Cheung, G. Bulthuis, and G. Nijenbanning, "A new orthotic device in the non-operative treatment of idiopathic scoliosis," *Medical engineering & physics*, vol. 24, pp. 209-218, 2002.

[69] L. A. Karol, "Effectiveness of bracing in male patients with idiopathic scoliosis," *Spine*, vol. 26, 2001.

[70] F. P. Castro Jr, "Adolescent idiopathic scoliosis, bracing, and the Hueter-Volkmann principle," *The Spine Journal*, vol. 3, pp. 180-185, 2003.

[71] P. J. O'Neill, L. A. Karol, M. K. Shindle, E. E. Elerson, K. M. Brintzenhofeszoc, D. E. Katz, *et al.*, "Decreased orthotic effectiveness in overweight patients with adolescent idiopathic scoliosis," *The Journal of Bone & Joint Surgery*, vol. 87, pp. 1069-1074, 2005.

[72] K. J. Noonan, L. A. Dolan, W. C. Jacobson, and S. L. Weinstein, "Long-term psychosocial characteristics of patients treated for idiopathic scoliosis," *Journal of Pediatric Orthopaedics*, vol. 17, pp. 712-717, 1997.

[73] C. Goldberg, D. Moore, E. Fogarty, and F. Dowling, "Adolescent idiopathic scoliosis: the effect of brace treatment on the incidence of surgery," *Spine*, vol. 26, pp. 42-47, 2001.

[74] J. Clin, C.-É. Aubin, S. Parent, and H. Labelle, "Biomechanical modeling of brace treatment of scoliosis: effects of gravitational loads," *Medical and Biological Engineering and Computing*, vol. 49, pp. 743-753, 2011.

[75] J. Clin, C. E. Aubin, S. Parent, A. Sangole, and H. Labelle, "Comparison of the biomechanical 3D efficiency of different brace designs for the treatment of scoliosis using a finite element model," *Eur Spine J*, vol. 19, pp. 1169-78, 2010.

[76] J. Clin, C. E. Aubin, A. Sangole, H. Labelle, and S. Parent, "Correlation between immediate in-brace correction and biomechanical effectiveness of brace treatment in adolescent idiopathic scoliosis," *Spine (Phila Pa 1976)*, vol. 35, pp. 1706-13, 2010.

[77] J. Clin, C. E. Aubin, S. Parent, J. Ronsky, and H. Labelle, "Biomechanical modeling of brace design," *Stud Health Technol Inform*, vol. 123, pp. 255-60, 2006.

[78] J. Dubousset, J. A. Herring, and H. Shufflebarger, "The crankshaft phenomenon," *J Pediatr Orthop*, vol. 9, pp. 541-50, 1989.

[79] E. R. Westrick and W. T. Ward, "Adolescent idiopathic scoliosis: 5-year to 20-year evidence-based surgical results," *J Pediatr Orthop*, vol. 31, pp. S61-8, 2011.

[80] B. A. Akbarnia, K. Cheung, H. Noordeen, H. Elsebaie, M. Yazici, Z. Dannawi, *et al.*, "Next Generation of Growth-Sparing Technique: Preliminary Clinical Results of a Magnetically Controlled Growing Rod (MCGR) in 14 Patients With Early Onset Scoliosis," *Spine*, 2012.

[81] M. Yazici and Z. D. Olgun, "Growing rod concepts: state of the art," *European Spine Journal*, pp. 1-13, 2012.

[82] M. Yazici and J. Emans, "Fusionless instrumentation systems for congenital scoliosis: expandable spinal rods and vertical expandable prosthetic titanium rib in the management of congenital spine deformities in the growing child," *Spine*, vol. 34, p. 1800, 2009.

[83] E. Luque and A. Cardosa, "Segmental spinal instrumentation in growing children," *Orthop Trans*, vol. 1, p. 37, 1977.

[84] R. E. McCarthy, D. Sucato, J. L. Turner, H. Zhang, M. L. A. W. Henson, and K. McCarthy, "Shilla growing rods in a caprine animal model: a pilot study," *Clinical Orthopaedics and Related ResearchÂ®*, vol. 468, pp. 705-710, 2010.

[85] P. O. Newton, F. D. Faro, C. L. Farnsworth, G. S. Shapiro, F. Mohamad, S. Parent, *et al.*, "Multilevel spinal growth modulation with an anterolateral flexible tether in an immature bovine model," *Spine,* vol. 30, pp. 2608-2613, 2005.

[86] R. R. Betz, A. Ranade, A. F. Samdani, R. Chafetz, L. P. D'Andrea, J. P. Gaughan, *et al.*, "Vertebral body stapling: A fusionless treatment option for a growing child with moderate idiopathic scoliosis," *Spine,* vol. 35, pp. 169-176, 2010.

[87] J. T. Braun, E. Akyuz, J. W. Ogilvie, and K. N. Bachus, "The efficacy and integrity of shape memory alloy staples and bone anchors with ligament tethers in the fusionless treatment of experimental scoliosis," *Journal of Bone and Joint Surgery-American Volume,* vol. 87A, pp. 2038-2051, 2005.

[88] L. Miladi and J. Dubousset, "Magnetic Powered Extensible Rod for Thorax or Spine," in *The Growing Spine,* B. Akbarnia, M. Yazici, and G. Thompson, Eds., ed: Springer Berlin Heidelberg, 2010, pp. 585-591.

[89] B. A. M. D. S. B.-A. O. T. A. G. A. M. A. Akbarnia, "Dual Growing Rod Technique for the Treatment of Progressive Early-Onset Scoliosis," *Spine Spine,* vol. 30, pp. S46-S57, 2005.

[90] J. T. Smith, "Bilateral rib-to-pelvis technique for managing early-onset scoliosis," *Clin Orthop Relat Res,* vol. 469, pp. 1349-55, May 2011.

[91] J. Ouellet, "Surgical technique: modern Luque trolley, a self-growing rod technique," *Clin Orthop Relat Res,* vol. 469, pp. 1356-67, 2011.

[92] R. McCarthy, "Growth Guided Instrumentation: Shilla Procedure," in *The Growing Spine,* B. Akbarnia, M. Yazici, and G. Thompson, Eds., ed: Springer Berlin Heidelberg, 2010, pp. 593-600.

[93] P.-L. Sylvestre, I. Villemure, and C.-É. Aubin, "Finite element modeling of the growth plate in a detailed spine model," *Medical and Biological Engineering and Computing,* vol. 45, pp. 977-988, 2007.

[94] I. Villemure, C. E. Aubin, J. Dansereau, and H. Labelle, "Simulation of progressive deformities in adolescent idiopathic scoliosis using a biomechanical model integrating vertebral growth modulation," *J Biomech Eng,* vol. 124, pp. 784-90, 2002.

[95] M. Driscoll, C.-E. Aubin, A. Moreau, I. Villemure, and S. Parent, "The role of spinal concave–convex biases in the progression of idiopathic scoliosis," *European Spine Journal,* vol. 18, pp. 180-187, 2009.

[96] J. Clin, C. E. Aubin, S. Parent, and H. Labelle, "A biomechanical study of the Charleston brace for the treatment of scoliosis," *Spine (Phila Pa 1976),* vol. 35, pp. E940-7, Sep 1 2010.

[97] A. Sevrain, C. E. Aubin, H. Gharbi, X. Wang, and H. Labelle, "Biomechanical evaluation of predictive parameters of progression in adolescent isthmic spondylolisthesis: a computer modeling and simulation study," *Scoliosis,* vol. 7, p. 2, 2012.

[98] M. Driscoll, C. E. Aubin, A. Moreau, and S. Parent, "Finite element comparison of different growth sparring instrumentation systems for the early treatment of idiopathic scoliosis," *Stud Health Technol Inform,* vol. 158, pp. 89-94, 2010.

[99] C. Driscoll, C. E. Aubin, H. Labelle, and J. Dansereau, "Optimized use of multi-functional positioning frame features for scoliosis surgeries," *Stud Health Technol Inform,* vol. 158, pp. 83-8, 2010.

[100] E. Wagnac, P.-J. Arnoux, A. Garo, and C.-E. Aubin, "Finite element analysis of the influence of loading rate on a model of the full lumbar spine under dynamic loading conditions," *Medical and Biological Engineering and Computing,* pp. 1-13, 2012.

[101] A. S. Liu and P. A. Laing, "Lunar gravity analysis from long-term effects," *Science,* vol. 173, pp. 1017-20, 1971.

[102] A. Nachemson and J. M. Morris, "In vivo measurements of intradiscal pressure discometry, a method for the determination of pressure in the lower lumbar discs," *The Journal of Bone and Joint Surgery (American),* vol. 46, pp. 1077-1092, 1964.

[103] A. Schultz, G. Andersson, R. Ortengren, K. Haderspeck, and A. Nachemson, "Loads on the lumbar spine. Validation of a biomechanical analysis by measurements of intradiscal pressures and myoelectric signals," *The Journal of bone and joint surgery. American volume,* vol. 64, p. 713, 1982.

[104] A. G. Patwardhan, R. M. Havey, K. P. Meade, B. Lee, and B. Dunlap, "A follower load increases the load-carrying capacity of the lumbar spine in compression," *Spine,* vol. 24, p. 1003, 1999.

[105] A. G. Patwardhan, K. P. Meade, and B. Lee, "A Frontal Plane Model of the Lumbar Spine Subjected to a Follower Load: Implications for the Role of Muscles," *Journal of biomechanical engineering,* vol. 123, pp. 212-217, 2001.

[106] A. Shirazi-Adl and M. Parnianpour, "Load-bearing and stress analysis of the human spine under a novel wrapping compression loading," *Clinical Biomechanics,* vol. 15, pp. 718-725, 2000.

[107] J. Clin, C.-É. Aubin, N. Lalonde, S. Parent, and H. Labelle, "A new method to include the gravitational forces in a finite element model of the scoliotic spine," *Medical and Biological Engineering and Computing,* vol. 49, pp. 967-977, 2011.

[108] M. Holmes, "Finite deformation of soft tissue: analysis of a mixture model in uni-axial compression," *Journal of biomechanical engineering,* vol. 108, pp. 372-381, 1986.

[109] M. K. Kwan, W. M. Lai, and V. C. Mow, "A finite deformation theory for cartilage and other soft hydrated connective tissues—I. Equilibrium results," *Journal of biomechanics,* vol. 23, pp. 145-155, 1990.

[110] W. Lai, V. C. Mow, and V. Roth, "Effects of nonlinear strain-dependent permeability and rate of compression on the stress behavior of articular cartilage," *Journal of Biomechanical Engineering,* vol. 103, pp. 61-66, 1981.

[111] M. Argoubi and A. Shirazi-Adl, "Poroelastic creep response analysis of a lumbar motion segment in compression," *Journal of biomechanics,* vol. 29, pp. 1331-1339, 1996.

[112] N. D. Broom and A. Oloyede, "The importance of physicochemical swelling in cartilage illustrated with a model hydrogel system," *Biomaterials*, vol. 19, pp. 1179-1188, 1998.

[113] A. Oloyede and N. Broom, "Is classical consolidation theory applicable to articular cartilage deformation?," *Clinical Biomechanics,* vol. 6, pp. 206-212, 1991.

[114] J. STYF, "Pressure in the erector spinae muscle during exercise," *Spine,* vol. 12, pp. 675-679, 1987.

[115] K. Takahashi, T. Miyazaki, T. Takino, T. Matsui, and K. Tomita, "Epidural pressure measurements: relationship between epidural pressure and posture in patients with lumbar spinal stenosis," *Spine*, vol. 20, pp. 650-653, 1995.

[116] J. P. Little, M. J. Pearcy, and G. J. Pettet, "Parametric equations to represent the profile of the human intervertebral disc in the transverse plane," *Medical & biological engineering & computing,* vol. 45, pp. 939-945, 2007.

[117] E. J. Chiu, "Characterization of the human intervertebral disc with magnetic resonance imaging," 9839470 Ph.D., University of California, San Francisco, Ann Arbor, 1998.

[118] Y. M. Lu, W. C. Hutton, and V. M. Gharpuray, "Can variations in intervertebral disc height affect the mechanical function of the disc?," *Spine (Phila Pa 1976),* vol. 21, pp. 2208-16; discussion 2217, 1996.

[119] N. L. Fazzalari, I. H. Parkinson, Q. A. Fogg, and P. Sutton-Smith, "Antero-postero differences in cortical thickness and cortical porosity of T12 to L5 vertebral bodies," *Joint Bone Spine,* vol. 73, pp. 293-7, 2006.

[120] S. J. Ferguson, K. Ito, and L. P. Nolte, "Fluid flow and convective transport of solutes within the intervertebral disc," *J Biomech,* vol. 37, pp. 213-21, 2004.

[121] Y. M. Lu, W. C. Hutton, and V. M. Gharpuray, "Do bending, twisting, and diurnal fluid changes in the disc affect the propensity to prolapse? A viscoelastic finite element model," *Spine (Phila Pa 1976),* vol. 21, pp. 2570-9, Nov 15 1996.

[122] L. J. Smith and N. L. Fazzalari, "The elastic fibre network of the human lumbar anulus fibrosus: architecture, mechanical function and potential role in the progression of intervertebral disc degeneration," *European Spine Journal,* vol. 18, pp. 439-448, 2009.

[123] K. Lee and E. Teo, "Poroelastic analysis of lumbar spinal stability in combined compression and anterior shear," *Journal of spinal disorders & techniques,* vol. 17, pp. 429-438, 2004.

[124] L. Yahia, J. Audet, and G. Drouin, "Rheological properties of the human lumbar spine ligaments," *Journal of Biomechanics,* vol. 25, p. 817, 1992.

[125] S. Aharinejad, R. Bertagnoli, K. Wicke, W. Firbas, and B. Schneider, "Morphometric analysis of vertebrae and intervertebral discs as a basis of disc replacement," *American Journal of Anatomy,* vol. 189, pp. 69-76, 1990.

[126] B. A. Best, F. Guilak, L. A. Setton, W. Zhu, F. Saed-Nejad, A. Ratcliffe, *et al.*, "Compressive mechanical properties of the human anulus fibrosus and their relationship to biochemical composition," *Spine,* vol. 19, pp. 212-221, 1994.

[127] J. C. Iatridis, M. Weidenbaum, L. A. Setton, and V. C. Mow, "Is the nucleus pulposus a solid or a fluid? Mechanical behaviors of the nucleus pulposus of the human intervertebral disc," *Spine,* vol. 21, pp. 1174-1184, 1996.

[128] S. Helwany, "Permeability and Seepage," in *Applied Soil Mechanics,* ed: John Wiley & Sons, Inc., 2007, pp. 332-376.

[129] J. A. Malko, W. C. Hutton, and W. A. Fajman, "An in vivo magnetic resonance imaging study of changes in the volume (and fluid content) of the lumbar intervertebral discs during a simulated diurnal load cycle," *Spine,* vol. 24, pp. 1015-1022, 1999.

[130] M. B. Albro, R. E. Banerjee, R. Li, S. R. Oungoulian, B. Chen, A. P. del Palomar, *et al.*, "Dynamic loading of immature epiphyseal cartilage pumps nutrients out of vascular canals," *Journal of Biomechanics,* vol. 44, pp. 1654-1659, 6/3/ 2011.

[131] G. Ateshian, R. Nims, S. Maas, and J. Weiss, "Computational modeling of chemical reactions and interstitial growth and remodeling involving charged solutes and solid-bound molecules," *Biomechanics and Modeling in Mechanobiology,* vol. 13, pp. 1105-1120, 2014/10/01 2014.

[132] G. A. Ateshian, S. Maas, and J. A. Weiss, "Multiphasic finite element framework for modeling hydrated mixtures with multiple neutral and charged solutes," *Journal of biomechanical engineering,* vol. 135, p. 111001, 2013.

[133] C. T. Ching, D. H. Chow, F. Y. Yao, and A. D. Holmes, "Changes in nuclear composition following cyclic compression of the intervertebral disc in an in vivo rat-tail model," *Med Eng Phys,* vol. 26, pp. 587-94, Sep 2004.

[134] J. J. Maclean, C. R. Lee, M. Alini, and J. C. Iatridis, "Anabolic and catabolic mRNA levels of the intervertebral disc vary with the magnitude and frequency of in vivo dynamic compression," *J Orthop Res,* vol. 22, pp. 1193-200, Nov 2004.